Performance of Cold Formed Welded Tubular Steel Joints under Moment Loading

By

Kenny Mudenda

Supervisor

Prof. Alphose Zingoni

Department of Civil Engineering

University of Cape Town

P/Bag Rondebosch 7701

Cape Town

This thesis is submitted in partial fulfillment of the requirements for award of the Master of Science Degree in Engineering at the University of Cape Town.

March 2008

DECLARATION

I know the meaning of plagiarism and declare that all the work in the document, save for that which is properly acknowledged, is my own.

ACKNOWLEDGEMENTS

My deepest gratitude goes to the following:

The University of Cape Town through the Department of Civil Engineering as well as the Canon Collins Educational Trust for southern Africa (CCETSA) for the generous financial support.

Prof. Alphose Zingoni for the guidance and support in all aspects of my studies and for believing in my abilities.

To the staff of The Civil Engineering Department for making the postgraduate experience a truly rewarding one. The technicians in the workshop and concrete lab, in particular the two Charles' Mr. Nicholas and Mr. May for the assistance with joint tests.

To my fiancé, Chitaba M. Chama, I reserve special gratitude. Your love and support has lifted me through challenging times and seasons.

To my parents for always believing in me and covering me in that warm blanket of prayer. To God is the glory.

ABSTRACT

[Kenny Mudenda. Performance of Cold Formed Welded Tubular Steel Joints under Moment Loading. March 2008]

Although exhibiting many superior properties to open sections structural hollow sections (SHS) have seen limited application in structures where joints resist moments. Their application has remained largely in truss type and lattice type structures where pinned joints are assumed. However, SHS have wide potential for use in structures with moment resisting joints. Much still needs to be done, however, to develop an understanding of joint behaviour under moment loads. It is also desirable to come up with means of developing design tables that can simply the design process.

The purpose of the research was to investigate the behavior of SHS joints under moment loading through experimental tests as well as using finite element modeling. In the finite element analysis various models were studied in order to come up with one that would give fairly accurate results in order for a parametric analysis to be carried out. Results generated from the parametric analysis were used to develop simple design tables with the important joint parameters with regards to moment-rotation behavior.

The structural hollow sections studied predominantly exhibited a semi-rigid joint behavior under moment loading with most of them attaining the ultimate moment before reaching the adopted deformation limit. Brace to chord ratio, member thickness and ratio of brace to chord thickness were found to affect the behavior of the joints.

TABLE OF CONTENTS

1 INTRODUCTION 1

1.1 Background 1

1.2 Research Aim 3

1.3 Conclusion 3

2 REVIEW OF LITERATURE 4

2.1 Introduction 4

2.2 Welded Connection Profiles 5

2.3 Material Properties of Steel 6

2.4 Manufacture of SHS 8

2.5 Welding 9

2.6 Residual stress 13

2.7 Joints 14

2.8 Analytical Models 15

2.8.1 Analytical Models based on failure mode for CHS 16

2.8.2 Analytical models based on failure modes for RHS 20

2.8.3 Analytical models for joint moment-rotation behaviour 26

2.9 Experimental Testing of hollow section joints 29

2.9.1 Test Set-up 31

2.10 Numerical studies on hollow section joints 34

2.11 Design Codes 37

2.11.1 Hollow Section Design Codes 37

2.11.2 Welding Standards 39

3 Moment Rotation Behaviour 48

3.1 Introduction 48

3.2 Joint Classification 49

3.3 Classification schemes 51

3.3.1 Eurocode 3 52

3.3.2 Bjorhovde Scheme 53

3.4 Ultimate strength 54

3.5 Conclusion 54

4 Experimental Tests 57

4.1 Introduction 57

4.3 Test specimens 58

4.4 Test set-up 60

4.5 Failure modes 61

4.6 Moment-rotation plots 64

4.7 Conclusion 68

5. Finite Element Modelling 70

5.1 Introduction 70

5.2 FE Modelling 70

5.3 FE Models 71

5.3.1 Post processing 74

5.4 Calibration of model 75

5.5 Parametric Study 80

5.5.1 Moment-Rotation plots from parametric study 82

5.5.2 Design Tables 85

5.6 Conclusion 88

6 DISCUSSION 90

6.1 Introduction 90

6.2 Experimental results 90

6.3 Finite Element results 91

6.4 Conclusion 91

7 CONCLUSION AND RECOMMENDATION 92

7.1 Introduction 92

7.2 Conclusion 92

7.3 Recommendations 93

7.4 Summary 93

LIST OF FIGURES

Fig. 1Types of hollow section joint configurations 5
Fig. 2 Iron-Carbon phase diagram 8
Fig. 3 Fillet weld *Fig. 4 Butt weld* 11
Fig. 5 Fillet weld details *Fig. 6 Butt weld details* 11
Fig. 7 Heat affected zone of a welded metal 12
Fig. 8 *Schematic diagram of a fusion weld, showing temperature distribution and corresponding changes in grain structure in the heat affected-zone (HAZ) in the parent metal* 13
Fig. 9 Ring model for a CHS cross joint 17
Fig. 10 Punching shear model for a CHS joint 18
Fig. 11 Model for shear load of the chord 19
Fig. 12 Yield line model for a T, Y and X joint (chord face failure) 21
Fig. 13 Punching shear model 22
Fig. 14 Physical interpretation of effective width terms 23
Fig. 15 Shear failure model of the chord 24
Fig. 16 Chord side wall bearing model for full width joints 25
Fig. 17 Basic concept of the Multi-linear equation 27
Fig. 18 Influence of shape factor 27
Fig. 19 Determination of initial stiffness and design moment using the component method 28
Fig. 20 Test set-up for an X-joint moment *Fig. 21 Displacement transducer* 32
Fig. 22 Schematic details for knee joint test (Wilkinson, 2000) 33
Fig. 23 joint geometric parameters 33
Fig. 24 Correlation between FE model and experimental test results (Christitsas et al, 2007) 36
Fig. 25 Classification of joints according to moment-rotation behavior 49
Fig. 26 A plot of applied moment vs relative opening of joint 50
Fig. 27 Classification of joints according to stiffness and strength 51
Fig. 28 CHS T-joint *Fig. 29 RHS T-joint* *Fig. 30 BB X-joint* 57

Fig. 31 Experimental test configuration for T-joint tests 60
Fig. 32 Experimental test configuration for X-joint tests 61
Fig. 33 Brace deflection at failure in a CHS member *Fig. 34 Weld failure in a CHS member* 62
Fig. 35 Brace deflection at failure in a RHS member *Fig. 36 Weld failure in a RHS member* 62
Fig. 37 Weld failure in CHS X-joint *Fig. 38 Bird beak X-joint at failure* 63
Fig. 39 Weld failure in a RHS X-joint 63
Fig. 40 Results for CHS X-joint tests 64
Fig. 41 Results for RHS X-joint tests 64
Fig. 42 Results for birdbeak X-joint tests 65
Fig. 43 Results for CHS T-joint tests 65
Fig. 44 Results for RHS T-joint tests 66
Fig. 45 C3D8 and C3D20 Solid elements 73
Fig. 46 Four node shell element representation showing nodes 73
Fig. 47 Four node discrete rigid quadrilateral element 73
Fig. 48 RHS shell model *Fig. 49 Solid CHS model* 74
Fig. 50 CHS joint showing results in the post-processing 'visualization' module of ABAQUS 75
Fig. 51 Calibration of RHS T-joint using a half model employing solid elements 76
Fig. 52 Calibration of RHS T-joint using a full model employing solid elements 76
Fig. 53 Calibration of CHS T-joints using solid elements 77
Fig. 54 Calibration of RHS T-joints using a full model employing shell elements 77
Fig. 55 Calibration of CHS T-joints using shell elements 78
Fig. 56 Calibration of Bird beak X-joint using shell elements 79
Fig. 57 Calibration against results obtained by Jubran & Cofer (1995) for CHS T-joints 80
Fig. 58 M-Φ plots from finite element analysis for CHS T-joints with β =0.22 and τ *=1* 82
Fig. 59 M-Φ plots from finite element analysis for CHS T-joints with β =1 and τ *=1* 83
Fig. 60 M-Φ plots for comparison between 2.5mm and 5mm CHS T-joints with β=1 and τ*=1* 83

Fig. 61 M-Φ plots for comparison for 5mm CHS T-joints between τ *=1and* τ *=0.833*.... 84
Fig. 62 M-Φ plots for comparison of 5mm CHS T-joints between τ *=1and* τ *=1.2* 84

LIST OF TABLES

Table 1: Steel Material Properties 7
Table 2: Comparison of Cold formed and Hot rolled sections 9
Table 3: Codes of practice for hollow sections 37
Table 4: Design codes/guides listed under design basis 38
Table 5: South African structural design standards based on limit states design 39
Table 6: Examples of application codes and standards and related welding procedure and welder approval standards 40
Table 7: Joint test specimens 58
Table 8: Material property of the joint components from tensile test 59
Table 9: Geometric properties of test specimens 59
Table 10: Joint characteristics obtained from experimental tests 67
Table 11: Plastic material properties used in FE models 72
Table 12: Table of joint properties employed in the FE study 81
Table 13: Design table 1 based on calibration in Table 12 (1) 85
Table 14: Design table 2 based on Table 12 (2(a)) 86
Table 15: Design table 3 based on Table 12 (2(b)) 86
Table 16: Design table 4 based on Table 12 (2(c)) 86
Table 17: Design table 5 based on Table 12 (2(d)) 87
Table 18: Design table 6 based on Table 12 (2(e)) 87

1 INTRODUCTION

1.1 Background

Structural hollow sections (SHS), also known as Hollow structural sections (HSS) in some countries, are structural steel sections of varying geometrical profile that are characterised by a hollow core and usually a thin member thickness. The available member thicknesses vary from country to country and tables of available sizes are usually given in design standards or by the manufacturers. The most common types of SHS are the circular hollow sections (CHS) and the rectangular hollow sections (RHS). Square hollow sections are considered to fall under the umbrella of the RHS. Other shapes may be formed with material, strength and geometrical properties being specified for the particular section. These may be custom made for clients or may be incorporated in national standards. For instance the South African Institute of Steel Construction (SAISC) design handbook includes a special shape in its tables known as a bunton or a flattened hollow section that is used extensively in mine shaft steelwork (SAISC, 1989).Special shapes available in Europe include triangular, hexagonal, octagonal, flat-oval, elliptical and half-elliptical shapes (Wardenier 2001).

SHS have found use in many different structures. These include roof and bridge trusses, frames, space trusses, offshore platforms, towers and masts. They are also used in mechanical equipment such as lifting platforms at airports, framing for motor vehicles as well as agricultural equipment like plough supports. They are also used as columns particularly with concrete infill. In structural applications they are most commonly used with lattice and truss type structures because joint behaviour is most favourable for this type of construction in these structures (ESDEP WG 13a, n.d.).

The SHS are said to be the latest in the family of structural sections (Dutta, 2002) and over the last century the structural behaviour of SHS has been extensively investigated. A lot is now known about the structural properties of the sections. The initial concern on the use of SHS was on the structural joints and this continues to be an area of attention from researchers even today. Although a lot of work was done in SHS research much of it had not been compiled in a systematic form until sometime in the 1960s when the International Committee for the Development and study of Tubular Structures or Comité International pour le Développement et l'Etude de la Construction Tubulaire (CIDECT) commissioned a

coordinated research programme with the aim of incorporating findings into national and international standards (Wardenier, 2001). A number of investigations culminated in a publication by Wardenier (1982) giving design formulae for joints under static loading, based on the CIDECT sponsored research. A list of the other research publications available from CIDECT is available online at (www.cidect.com/en/Research_Projects/welded_joints.php) covering the period 1970-2004. CIDECT has also published design handbooks for SHS design. It must be mentioned that as the CIDECT sponsored research was going on a lot of researchers from other institutions around the world were working on various aspects of hollow section structural performance/behaviour. For instance Kurobane et al (1984) developed simple predictive equations for CHS based on regression models and test specimens. This led to later development of simple analytical models for various joint configurations. Results obtained from the vast amount of research carried out at the time led to Australia, Japan, Canada, USA, the European Union (EU) and the International Standards Organisation (ISO) incorporating design guidelines into their standards.

A challenge with hollow section joints arises in the analysis of the stresses at the joints because of the nature of the stress interactions. Apart from predicting joint behaviour another big challenge with hollow section construction has been that of joint fabrication particularly for the CHS as end profiling is needed for joints to fit into each other. RHS joints on the other hand are cut flat making their fabrication easier. Also, because welding is the predominant method of connecting unstiffened members there is a considerable alteration of the material properties of the weld zone as well as the welded components resulting in complex stress responses from the welded joint.

SHS construction is particularly appealing because of the following advantages (SAISC, 1989):

Aesthetics - The SHS are closed sections having no hidden corners or edges and thus provide a good appearance. Also, compared to other steel members their joints are usually neat.

Strength - For the same unit weight class CHS and square RHS have a greater buckling resistance than open sections. In situations of bi-axial bending they perform better as they possess one radius of gyration, unlike the open sections that usually have a stronger and weaker axis.

Wind Drag - SHS have low wind drag coefficients and hence are less likely to suffer from wind loading effects in frame structures such as towers. This also applies to their drag characteristics in water hence making them suitable for offshore structures as well.

Maintenance - Because they don't have hidden edges they are easy to paint and apply corrosion resistant measures.

Torsional Resistance - Torsional stiffness is enhanced by the closed periphery.

Girder Action - SHS have a larger critical buckling load than open sections hence they can span longer with slender members than the open sections.

Because most current research was based mainly on axial static loads, a lot still remains to be investigated on moment loaded joints particularly with respect to application in semi-rigid design. Previous research on moment loading has focused more on the T and L joints which are used in Vierendeel trusses. Recent research has also focused on the fatigue strength of SHS joints, crack modelling using finite element methods (FEM), composite columns as well as performance of high strength and stainless steels.

1.2 Research Aim

The objective of the research is to investigate the moment-rotation behaviour of welded hollow section joints through experimental testing and then use finite element methods to develop models that will facilitate parametric analyses of the tested joint profiles. Design tables will be developed based on current findings and the existing literature.

1.3 Conclusion

Despite the advantages of using hollow sections outlined, their application has largely been limited to truss and lattice type structures where joints are assumed to carry no moments. Application in moment resisting structures such as sway frames has been limited. This could be attributed to lack of simple, easy-to-use design guides, a lack of software that could accurately model semi-rigid joints and in some cases lack of a thorough understanding of the joint behaviour under moment loading.

2 REVIEW OF LITERATURE

2.1 Introduction

Over the years an evolution in the form and appearance of structures has been slowly taking place and engineering practice as well as materials must keep up with these changes. The drive for aesthetically appealing and innovative structures as well as functional requirements have been at the fore in encouraging the development of tubular structures and the promotion of use of these members. It is no surprise that structures made of hollow sections continue to win various prizes around the world for both aesthetics and functionality.

Functionality plays a big role in selection of structural materials. The discovery of offshore oil deposits, for instance, required the erection of robust structures at sea that could take up operational loads as well as the forces from wave and wind action at sea. A material such as hollow sections with low drag characteristics renders an obvious advantage. This led to the extensive application of hollow section members, particularly CHS members, in the construction of offshore platforms. Problems encountered by open sections such as buckling and instability phenomenon are in many cases not a problem with SHS owing to their geometry. Application of SHS in areas not previously used such as moment frames need be investigated and developed provided good aesthetics, functionality and economy can be achieved.

Many of the challenges facing the widespread use of hollow sections have much to do with joints; either on the methods of achieving good connection or simply understanding the behaviour of the joints. Once the behaviour is understood the next step would then be to develop ways of simplified analysis and design.

Despite the various challenges facing the development of SHS, with continued research a clear understanding of their behaviour can be achieved and simple design rules formulated for use by designers.

2.2 Welded Connection Profiles

Although finding use in multi-planar structures, SHS are predominantly used in uni-planar structures mostly with lattice and truss type construction. They are used to a lesser extent in frame structures. The most common joint configurations for welded joints are shown in Fig.1:

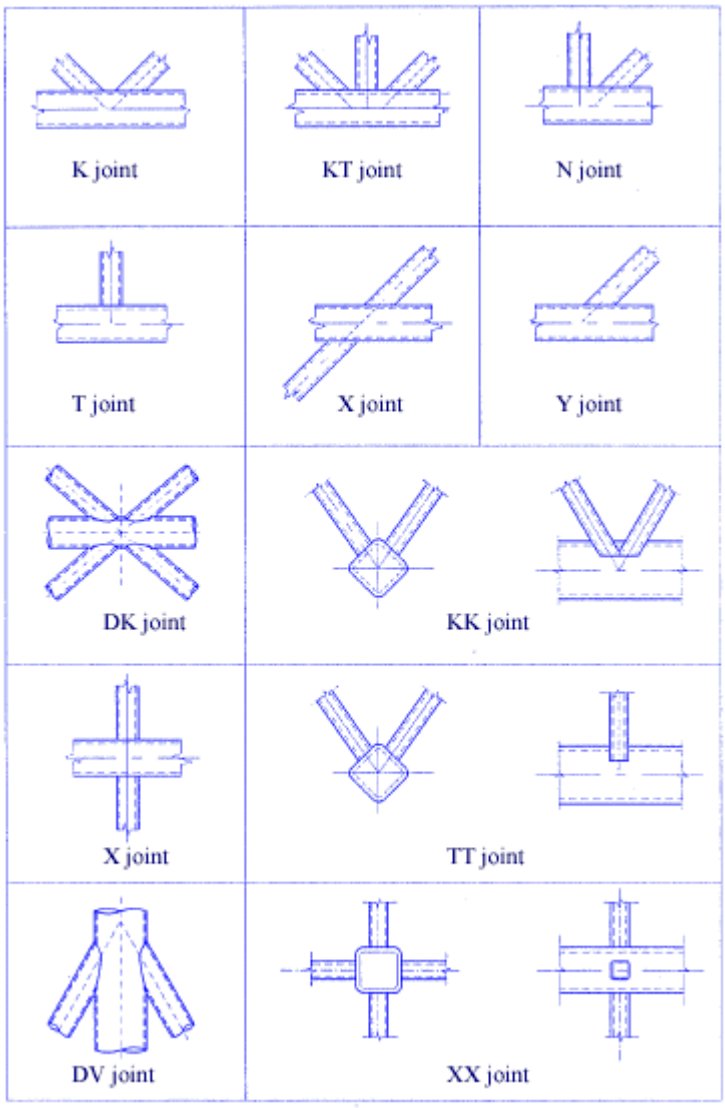

Fig. 1 Types of hollow section joint configurations
Adapted from (Eurocode 3, 2003)

The most common loadings on the members are axial loads, in-plane bending moments and out-of-plane bending moments. Shear loads exist in the members as effects from the loading types mentioned. In truss type construction effort is made to design the joints in such a way as to avoid joint eccentricities so that secondary moments are eliminated. Because the predominant loads in trusses are axial loads the joints are assumed not to carry any moments i.e. pinned joints and joint moments are neglected. Saidani (1998) carried out investigations

on effect of joint eccentricity on force distribution in RHS lattice girders and found that eccentricities can, at worst, have significant bending moments especially in gapped joints. He further discovered that they affect axial forces in the brace members. For SHS joints, truss theory that assumes pinned joints at connections with no effects from eccentricity of joints holds true as long as certain conditions specified in design codes and books are met (Dutta 2002). Moment connections such as are present in a Vierendeel truss which has vertical bracing members were studied by Packer (1993). This truss is statically indeterminate and carries moments at the joints hence they are designed specifically to carry moment loading in addition to axial and shear forces. In-plane and out-of-plane moment loading occurs in other structures hence the studies into behaviour under this loading type.

The main parameters affecting joint strength in welded joints are

(a) Chord and brace geometry
(b) Type and quality of weld
(c) Stiffness and rotational capacity of the joint
(d) Orientation of connecting members

2.3 Material Properties of Steel

Steel is an alloy of Iron with Carbon being the primary alloying material. Steel that has only Carbon as an alloying material is known as Carbon steel or plain Carbon steel. Steels are further classified according to the amounts of Carbon present in solution. With time all engineering materials will either be replaced with better performing alternatives or will be constantly improved in order to get better performing variants to improve in-service performance. The same applies to steel. Many new and stronger forms on steel are being produced with various new properties. Many of these new variants have other elements (in addition to Carbon) as alloying materials. Varying the amounts of these alloying elements alters the physical and mechanical properties of the steel. Sometimes the alloying materials in the steel are present as impurities as there may be limits to which these elements may be effectively removed from the mixture with iron during the steel production phase.

Steel is manufactured from Iron through a multi-step process. Iron is extracted from its ores through a method of extractive metallurgy known as smelting. The iron is extracted in the

first stage in an impure form known as pig Iron. It is from this material that cast Iron, wrought Iron and Steel are produced; the final product being dependent on the amount of Carbon contained in solid solution as an alloying material. A good understanding of the material properties of steel and what happens to it at elevated temperatures is essential to understanding the behaviour not only of the in-service behaviour of steel sections but also the performance of welded joints between steel members. The material properties of steel can be broken into two groups depending on whether they are affected by working on the steel either in the hot or cold form or not (ESDEP WG 2, n.d.). Those that are affected by working conditions are the structure sensitive properties whereas those not affected or only slightly affected by working conditions are the structure insensitive properties. Table 1 shows the two different types of material properties.

Table 1: Steel Material Properties

Structure Sensitive Properties	**Structure Insensitive Properties**
▪ Yield Strength ▪ Ductility ▪ Hardness ▪ Toughness	▪ Bulk density ▪ Coefficient of Thermal Expansion ▪ Young's Modulus

Therefore when steel is heated and cooled there is a possibility of the structure sensitive properties being altered depending on the work carried out on the piece and the cooling conditions imposed. The structure sensitive properties are also the mechanical properties of the material whereas the structure insensitive properties are the physical properties of steel (ESDEP WG 2, n.d.). The characteristic behaviour of steel as it is heated or cooled from elevated temperature or the molten state is best understood by its phase diagram which is a representation of the phases that it goes though as it cools. The phase diagram can also be used to illustrate what happens when the metal is given any form of heat treatment up to the liquid or molten state. As the metal moves from solid to liquid and vice versa its crystalline structure changes at given temperature and Carbon content from face centred cubic (FCC) to body centred cubic (BCC). There is a characteristic phase diagram for each type of steel. The most important range for Carbon content is the one between 0 and 6.67% hence this is usually the only part of the phase diagram used for commercial steels. The Iron – Carbon phase diagram is shown in Fig.2

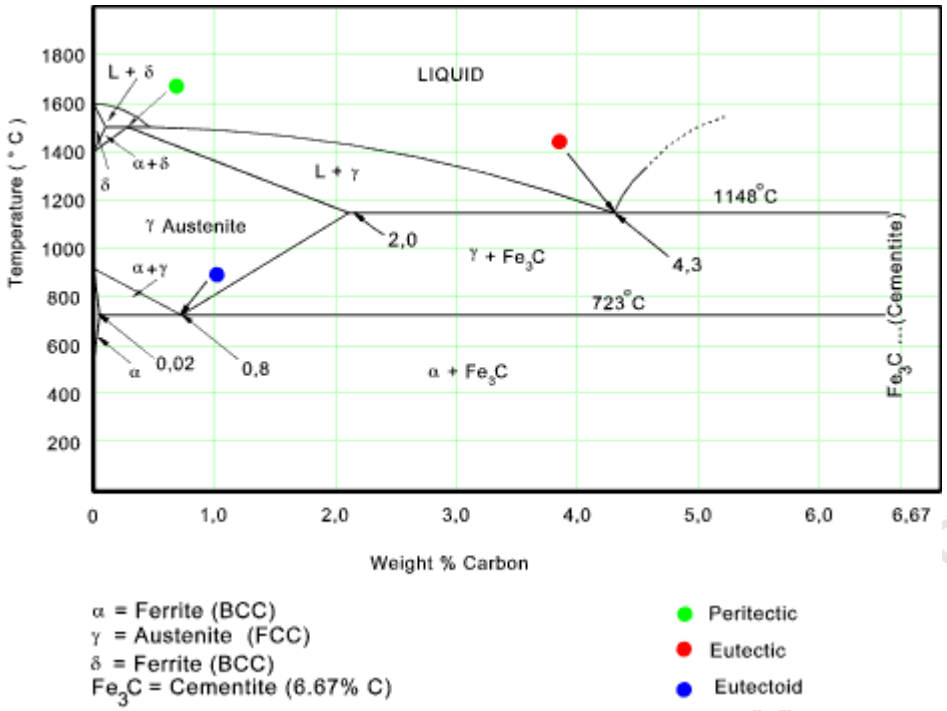

Fig. 2 Iron-Carbon phase diagram
Source: (www.roymech.co.uk/useful_tables/phase_diagram.html)

2.4 Manufacture of SHS

Hollow sections may either be made by cold forming process or by a hot drawing/rolling process. Those produced by the former method are known as cold formed sections while those by the latter are known as hot rolled sections or seamless tubes. Both can be manufactured to similar geometric sizes but they are treated separate as they have different properties such as dimensional tolerances and residual stress characteristics. Cold formed sections have more residual stresses inherent to the cold forming process. Characteristics of the two methods (Dutta 2002) are shown in Table 2

Table 2: Comparison of Cold formed and Hot rolled sections

Cold formed sections	**Hot rolled section**
1. Manufactured from steel sheets which are rolled into shape and welded or fused together at the seams. 2. The size of tube diameter that can be achieved is limited only by transportability of finished tubes 3. Maximum wall thickness that is practical is characteristically less than that for hot rolled tubes	1. Manufactured in the hot state through a two stage hot rolling process 2. Tubes up to a maximum diameter of 800mm can be produced using this method 3. Wall thickness of 270mm can be achieved

Rectangular hollow sections are produced from the CHS through a forming process that may be carried out at hot or cold temperature. In this forming process the CHS tubes are passed through a series of rollers that gradually shape the tube from a circular profile to a rectangular profile.

2.5 Welding

Although bolted and other connection types have been investigated for SHS (Dutta 2002) welding remains the most preferred method for joint fabrication with SHS joints. Due to a rise in labour and material costs it has become economical to avoid as much as possible joints with stiffeners and gusset plates. This view has been supported by Seward (1994). The preferences for welding are due therefore, in no small way, to the economical and ease of fabrication aspects of welded joints. The most widely used method for most structural welding is the electric-arc method where a welding rod or electrode is fused to the parent metal by means of the heat generated by high current electricity (Seward 1994) and (Dutta 2002). The most common types of arc welding are:

(i) Shielded metal arc welding (SMAW)
(ii) Gas metal arc welding (GMAW)
(iii) Flux-cored arc welding (FCAW)
(iv) Tungsten inert gas arc welding (TIG) and,
(v) Submerged arc welding (SAW)

Nakashima et al (2000) showed that GMAW which is predominantly used in Japan produces stronger welds than FCAW which is predominantly used in the USA. However FCAW proved to be more economical. Because different countries produce steel with different properties according to their preferred standards (whether National or International) it is important to pay attention to the grade of steel used for the structural sections when selecting the welding type to be employed. The grade is determined by the chemical composition of the steel i.e. the quantities of the alloying materials in the steel. The grade also determines the material properties of the steel. The property of weldability is used to define the welding properties of a metal. According to Illston et al (1979) 'weldability may be defined as the capacity of a metal to be joined by welding into a structure that can perform in a satisfactory manner for an intended service'. Generally the weldability of steel is determined by its Carbon Equivalent Value (CEV) which is given by formula (2.1) and expressed as a percentage composition of the alloying materials.

$$C + \frac{Mn}{6} + \frac{Cr + Mo + V}{5} + \frac{Ni + Cu}{15} \qquad (2.1)$$

According to CORUS (n.d) 'to maintain weldability the maximum CEV for steel sections should not exceed 0.54%'. A lower CEV implies better weldability properties. The welded joint can be fabricated either in a fabrication shop or on site. Dutta (2002) outlines some guidelines to be followed on how to decide which members to be welded in the shop and which ones need be welded on site as the structure is assembled. This takes into consideration the limitations imposed by the need to move the different parts of a structure from the fabrication shop to site.

The two types of welds that are made from electric-arc welding (also known simply as arc welding) are fillet and butt welds. Fillet welds are the most economic of the two and are generally triangular in shape. Both welds are essentially made with a convex outer surface in order to meet the minimum requirement of thickness as specified in welding standards. The throat thickness is usually the most important property to be specified by the designer. For fillet welds the leg length is also important. In order to ensure optimal performance of the joint the usual practice is to use a weld material/metal that has strength greater than the base material. Because they are cheaper, fillet welds are the most commonly use for fabrication of SHS joints. Butt welds are usually used for end to end connections as they develop the full

strength due to complete penetration of the joint. They are also used for the common joint configurations when they are at certain predetermined critical angles. Design guides for welding outline strict measures for welding workmanship as well as inspection of completed work. The design guides are discussed in further detail in section (2.11.2). The two weld types are shown in Fig. 3 and Fig. 4

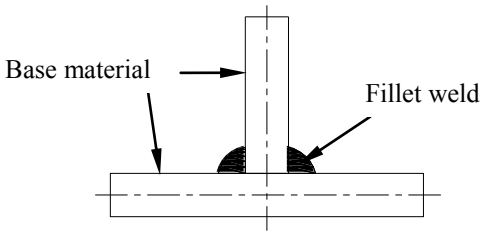

Fig. 3 Fillet weld

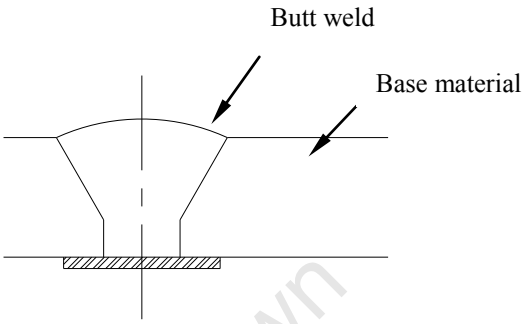

Fig. 4 Butt weld

The throat thickness as is it determined for both welds is shown in Figures 5 and 6. Throat thicknesses for both fillet and butt welds are shown in these Figures. For the fillet weld the leg length is also specified as shown in Fig.5

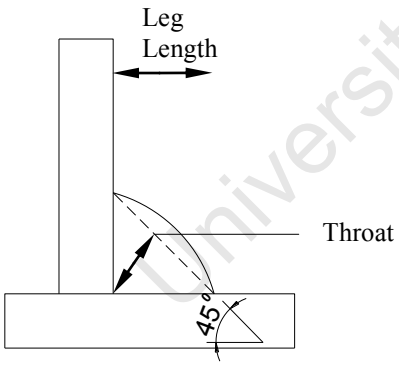

Fig. 5 Fillet weld details

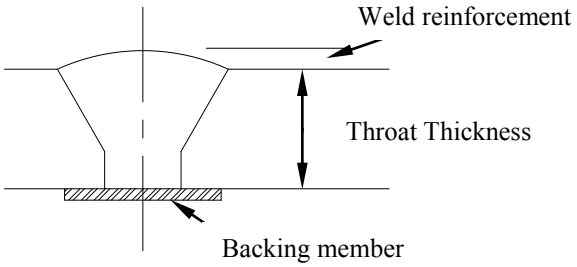

Fig. 6 Butt weld details

Welding is a complex process that involves a localised melting of the parent material (also known as the base metal) as the welding is taking place at a particular location/point. Because iron easily dissolves carbon at high temperatures and this would alter the material properties (see section) the molten metal has to be protected from Carbon and other gaseous impurities that may dissolve in the base metal. The protection is provided by means of an inert gas or combination of inert and other gases or a flux material. However, despite the protection from

the gas the material adjacent to the weld still goes through some metallurgical changes primarily due to the uncontrolled cooling rates particularly with on-site welding where welding environment cannot easily be controlled. Therefore after welding operation there exists three distinct zones which are; the base metal, heat affected zone (HAZ) and the weld metal deposited from the consumable electrode. The HAZ and residual stresses induced by the weld are the main negative effects of the welding process. The HAZ is just adjacent to the weld metal and symbolises the part of the metal that has been affected by the heat and subsequent cooling during the welding process. This is illustrated in Fig.7

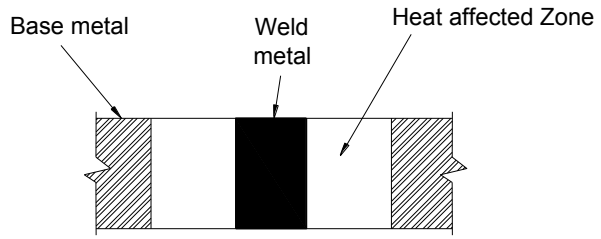

Fig. 7 Heat affected zone of a welded metal

The metal in the HAZ has material properties significantly different from those of the parent and weld metals. The major effect of the cooling is the loss of ductility hence it is more susceptible to brittle failure.

Illston et al (1979) states that 'during welding, a temperature gradient is established which varies from the fusion temperature at the weld metal to room temperature at some point in the parent metal away from the weld'. This is illustrated in Fig. 8. Illston et al (1979) further states that 'this produces changes in the metallurgical condition and properties of the parent metal in the vicinity of the weld, the so-called heat-affected-zone (HAZ). The micro-structural changes in this region can be considerable and are generally accompanied by a deterioration of its mechanical properties. These changes depend on (1) the composition of the parent metal, (2) its original condition, and, possibly, (3) the cooling rate after the weld'.

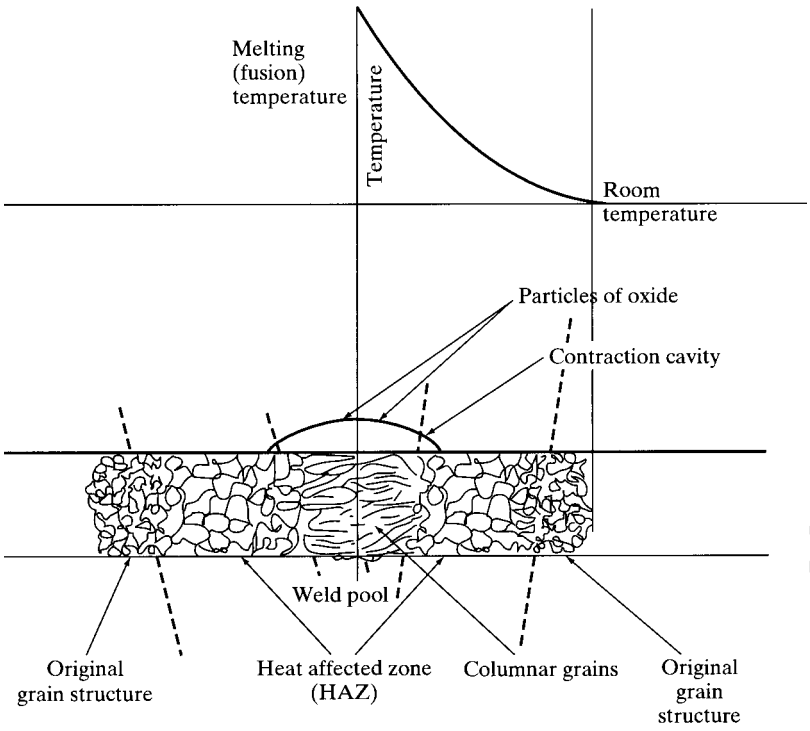

Fig. 8 *Schematic diagram of a fusion weld, showing temperature distribution and corresponding changes in grain structure in the heat affected-zone (HAZ) in the parent metal*
Source: (Illston, J. M. et al, 1979)

In their test on wear behaviour of a steel weld joint Krishnan et al (2006) citing Easterling (1993) noted that the HAZ is characterised by 4 sub-zones; Sub – critical (SCHAZ), Inter-critical (ICHAZ), Fine grain (FGHAZ) and Course grain (CGHAZ) heat affected zones, each exhibiting different microstructures. The four sub zones are listed in their order from the base metal to the weld metal. The progression from the SCHAZ to CGHAZ is a fine grain to course grain structure. The steel is thus progressively losing strength as it moves to the course grain structure.

2.6 Residual stress

Residual stresses in steel are considered to be part of a set of parameters contributing to imperfections in the steel members. They create non-uniform behaviour in the steel due to their localised nature in steel members. Residual stresses are pre-stresses locked in the steel member. They develop as the steel is cooling from the molten state, when it is cold-worked and as a residual effect of the welding process. Dwight and Young (1970) studied the residual stresses that arise out of the welding process. They found that welding induces a high residual

tension in the vicinity of a longitudinal weld. The rest of the member compensates for this with a resulting decrease in buckling strength. They came up with simple predictive formulas based on MIG-welded plates but concluded that prediction of residual stress in welded members cannot hope to be precise. According to Dutta (2002) residual stresses in welds can be primarily reduced through the selection of appropriate welding sequences. Other factors affecting development of residual stresses in welding process are weld thickness, number of weld passes, rigidity of structural elements in a weld structure and the welding process used. The effect on SHS of residual stresses is to induce different stress distributions than those determined from formulae. Residual stresses also have an effect on the fatigue life of a structure. Where necessary the cold formed profiles are stress relief annealed at 530-580°C or given other appropriate heat treatment to reduce residual stresses.

2.7 Joints

The stability of a structure will in many cases depend not only on the members making up the structure but also how the members or components are joined. As Seward (1994) has observed, many structural failures are caused by defects related to joints. The method of joining determines the behaviour and performance of the joint and structure as a whole. Therefore the importance of sound design cannot be overstated. Joints in structural engineering can be classified in three groups based on how they transfer loads:

(vi) Rigid joints
(vii) Semi-rigid joints
(viii) Pinned joints

The difference between these types of load transfer mechanisms is mainly determined by the way the joint transmits a moment from the loaded member to the supports or secondary members. The moment characteristic is established by means of a plot of the applied moment versus the rotation between the connected members. This characteristic plot is known as the moment-rotation curve or M-Φ curve.

SHS joint behaviour was first established by studying the limit states (both serviceability and ultimate) experimentally, seven of which have become universally accepted on account of being the most predominant failure modes. These are:

i. Chord face plastic failure
ii. Overall shear failure of the chord
iii. Chord punching shear failure of top face
iv. Brace effective width/weld failure
v. Local buckling of braces or chord
vi. Local buckling of chord face or sides

The failure modes are common to both cases of axial and moment loading. Kozy (2004) and, Lee and Wilmshurst (1995) support the view that behaviour of welded joints is very complex and their analysis difficult. There are four ways in which the joint characterisation can be mathematically carried out; curve fitting, simple analytical models, mechanical models and finite element analysis. This view is supported by Jaspart (2000). Both Jaspart (2000) and Kozy (2004) are of the view that experimental testing is essential in validating mathematical models and remains the most accurate way of determining the behaviour of SHS joints. It would seem that the only disadvantage with experimental testing is that it may be more costly than most forms of mathematical modelling. Lee and Wilmshurst (1995) suggest that elastic-plastic finite element analysis is gradually replacing experimental testing as the foremost tool in SHS joint analysis. They attributed this to 'availability of sophisticated software and high speed computers at relatively low cost'. However, Dutta (2002) is of the view that due to non-uniformity of stress distribution in these joints the kind of finite element analysis that can be carried out on them has to be applied on a case-by-case basis and is very expensive. Since the analytical models, finite element analysis, and experimental testing have been the foremost tools used in SHS joint analysis they are detailed further. The essence in all this is to determine joint behaviour as well as develop simple formulae for the design strength of the joint based on their behaviour and defined failure modes.

2.8 Analytical Models

Analytical models for ultimate strength are usually based on the failure modes given in 2.7. (i.) – (vi.) and are common to both axial load and pure bending. Whereas this ultimate strength approach is sufficient for axially loaded joints it may not be the case for moment resisting joints. For instance in the semi-rigid analysis and design of moment resisting joints, such as in sway frames, the ultimate failure moment alone is not enough to aid the designer.

The initial joint stiffness as well as the moment capacity at a predefined limit is required. A predefined limit for the moment capacity is required because most tubular joints typically exhibit a large rotation capacity before ultimate failure, hence the need to impose a limit on the joint rotation for rational design. Some analytical models based on joint behaviour for moment resisting joints are presented in 2.8.3.

Because for SHS different joint configurations and types exhibit different behaviour, analytical models that have been used based on the failure modes are different for CHS and RHS sections. These models serve to describe the joint behaviour and give information on the influencing parameters. Models that take into account all influencing parameters are, in general, too complicated. This view is supported by (ESDEP WG 13b, n.d. and Kozy, 2004). Researchers have therefore tended to use more simplified models with assumptions and incorporating only the critical governing parameters to predict joint strength. The common analytical models for both CHS and RHS based on failure mode are adapted from (*ESDEP WG13, n.d. and Wardenier, 2001*) and presented in 2.8.1 and 2.8.2 respectively. Figures 9 to 16 are adapted from (*ESDEP WG13b and ESDEP WG13c, n.d.).*

2.8.1 Analytical Models based on failure mode for CHS

The models for CHS joints are; ring model, punching shear and the chord shear models.

2.8.1.1 Ring Model

The ring model is shown in Fig. 9. This model is commonly applied to the analysis of T, Y and X joint configurations, the chord being idealised as a two-dimensional ring with an effective length B_e which is determined experimentally. This model was first presented by Togo (1967 cited by Wardenier 2001). In this model only the force normal to the chord is assumed to cause plastification of the chord with two-line loads equal to half the bracing loads representing the loading system. Influence of axial and shear stress is neglected in the model.

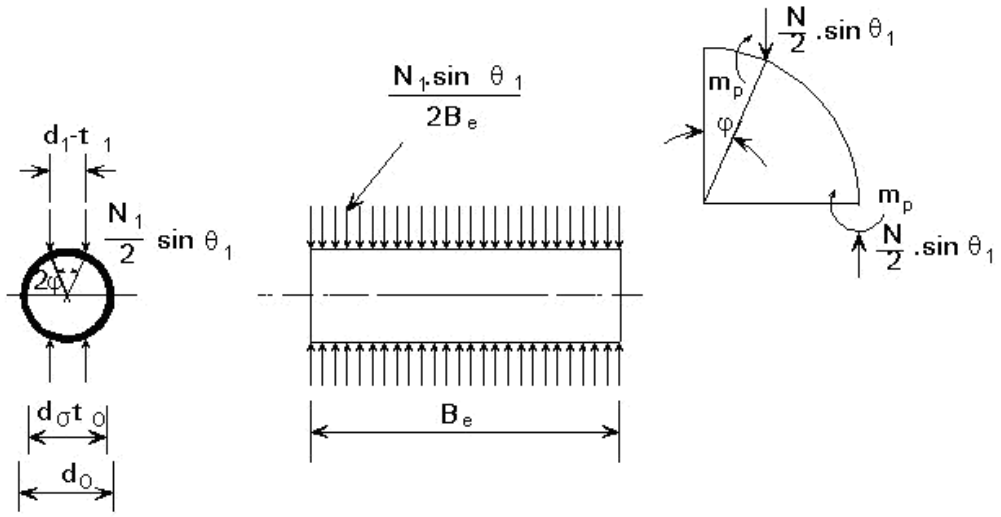

Fig. 9 Ring model for a CHS cross joint

The plastic moment m_p can be calculated using equation (2.2):

$$m_p = \frac{N_{1y} \sin\theta_1}{4}.(1-\sin\varphi)\left(\frac{d_o - t_o}{2}\right) \qquad (2.2)$$

Taking account of the effective length B_e of the ring, the plastic moment is given by:

$$m_p = \frac{B_e . t_o^2}{4}.f_{yo} \qquad (2.3)$$

Substituting Equation (2.3) in Equation (2.2) and assuming $\sin\varphi \approx \beta$ and $\frac{d_o - t_o}{2} \approx \frac{d_o}{2}$ gives:

$$N_{1y} = \frac{2B_e}{d_o}.\frac{1}{1-\beta}\frac{f_{yo}.t_o^2}{\sin\theta_1} \qquad (2.4)$$

To avoid infinity strength for the case where $\beta = 1$ a correction to the formula is proposed by (ESDEP WG 13b), which also states that for T, Y and X-joints reasonable agreement between test results and the semi-analytical ring model can be obtained. This is supported by Choo *et al* (2003) who carried out numerical models on X-joints with elliptical hollow sections. They compared findings from their numerical models with the ring model formulae and found a good prediction of the joint behaviour from the ring model.

In the other types of joints such as K and N type this model is not able to predict the joint strength. Other factors such as the gap between braces as well as membrane action tend to have effects on the joint not adequately accounted for by this model. Effects of membrane action are assumed not to play a significant role in T, Y and X joints.

2.8.1.2 Punching Shear Model

The model was proposed for a brace in full contact with the chord and experiencing a tensile axial load. As is the case with the chord plastification model, only the force component acting normal to the chord has the effect; in this case causing shear that leads to the brace member separating away from the chord. It is assumed that the shear force acts equally over the entire contact area of the brace and chord, neglecting curvature effects. The model is shown in Fig. 10

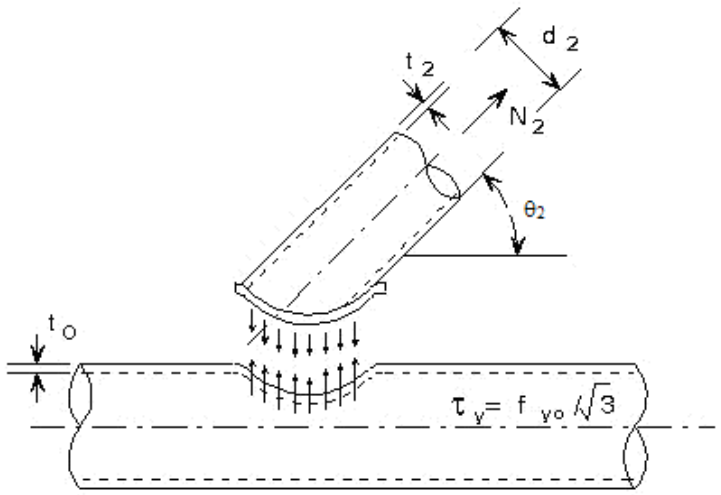

Fig. 10 Punching shear model for a CHS joint

For joints with $\theta_2 = 90°$, the theoretical uniformly distributed punching shear stress at its limiting value $f_{yo}/\sqrt{3}$ can be calculated as follows:

$$\frac{N_2}{\pi . d_2 . t_o} = \frac{f_{yo}}{\sqrt{3}} \qquad (2.5)$$

For joints with bracings with $\theta_2 < 90°$, the punching shear area is increased by the factor shown in equation (2.6).

$$\frac{1+\sin\theta_2}{2\sin\theta_2} \tag{2.6}$$

Taking into consideration that only the normal force has the shear effect, N_2 is multiplied by $\sin\theta_2$ which finally gives:

$$N_2 = \frac{f_{yo}}{\sqrt{3}}.\pi.d_2.t_o.\frac{1+\sin\theta_2}{2\sin^2\theta_2} \tag{2.7}$$

Generally the validity of this formula is for small values of β. As the value of β increases, the applied load will be transferred by hoop stress to the chord.

2.8.1.3 Chord Shear Model

For K or N joints configurations with a gap, the chord can fail at the gap due to shear or a combination of shear, axial and moment loads. When the chord section is compact, the following formulae for the plastic design can be applied:

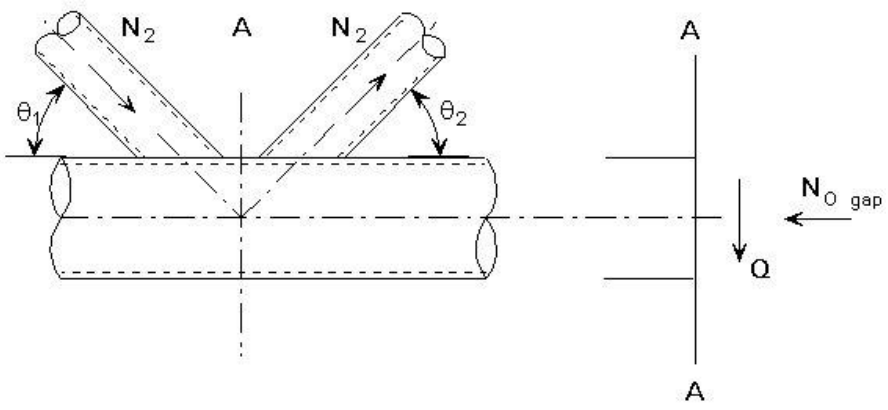

Fig. 11 Model for shear load of the chord

$$N_i \sin\theta_i \le 2\frac{f_{yo}}{\sqrt{3}}.(d_o - t_o).t_o \tag{2.8}$$

$$N_{o\,gap} \le \pi.(d_o - t_o).t_o.f_{yo} \tag{2.9}$$

$$M_{o\,gap} \le (d_o - t_o)^2.t_o.f_{yo} \tag{2.10}$$

Generally, the moments are small and only the interaction between axial load and shear load has to be considered:

$$\left(\frac{N_{o\ gap}}{\pi.(d_o - t_o).t_o.f_{yo}}\right)^2 + \left(\frac{N_i \sin\theta_i}{\frac{2.f_{yo}}{\sqrt{3}}(d_o - t_o).t_o}\right)^2 \leq 1.0 \qquad (2.11)$$

Some stiffening of the gap from bracings is achieved for small gaps in these joints and this adds to the shear resistance.

In the design codes a partial safety factor is usually factored into the ultimate load resistance to get the design capacity/resistance.

According to ESDEP WG 13b (n.d.) Eurocode 3 (Eurocode, 1992), Table 1b has a range of validity for welded joints between circular hollow sections. The validity of the resulting semi-empirical design resistance formulae is restricted to the parametrical ranges of the experimental tests. Design recommendations presented in the code for uni-planar axially loaded T, Y, X and K-joints of circular hollow sections have been derived from the research by the international institute of welding (IIW) and CIDECT.

2.8.2 Analytical models based on failure modes for RHS

Five models have been developed for the different failure modes and geometries of connecting members used for RHS joints. The models are; the yield line model, punching shear model, effective bracing width model, chord shear failure model and the local buckling model.

2.8.2.1 Yield Line Model

Yield line analysis involves determination of the most likely failure pattern at which a collapse mechanism is formed in the system due to formation of plastic hinges. The process is an energy balancing one which involves determining the work done by an external force over a displacement and internal work by the plastic moments. A mathematical expression is then obtained at which plastic failure will take place. For RHS the method is particularly accurate with medium-low values of β. The yield line model is shown in Fig. 12

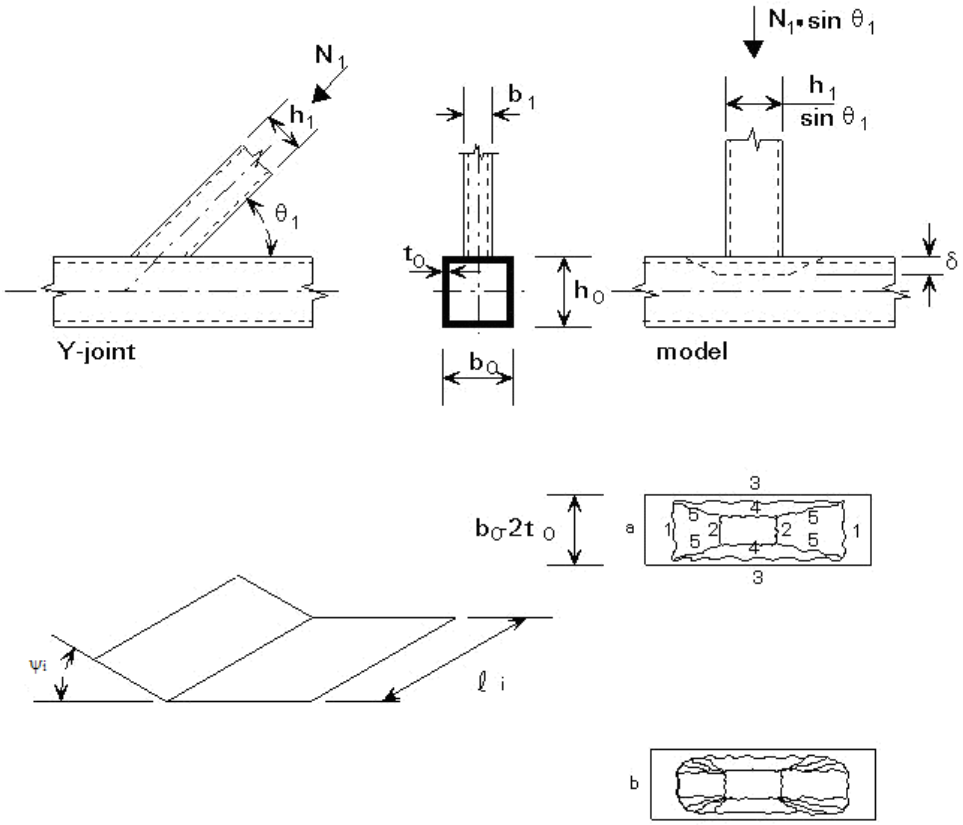

Fig. 12 Yield line model for a T, Y and X joint (chord face failure)

Equating external work done by the force N_1 internal work done at the plastic hinge gives:

$$N_1 . \sin\theta_1 . \delta = \sum l_i \psi_i m_{pl} \qquad (2.12)$$

Where, $m_{pl} = \dfrac{t^2_o f_{yo}}{4}$

Differentiating equation (2.12), substituting for m_{pl} and solving then gives:

$$N_1 = \frac{f_{yo}.t^2_o}{1-\beta}\left[\frac{2h_1}{b_o.\sin\theta_1} + 4\sqrt{1-\beta}\right]\frac{1}{\sin\theta_1} \qquad (2.14)$$

According to Kosteski *et al* (2003) the formula in (2.14) was first derived as shown in formula (2.15) by Jubb and Redwood (1966) for a T-joint at a right angle to the chord.

$$P_Y = \frac{F_{yo}.t^2_o}{(1-\beta)}\left[2\frac{h_1}{b_o} + 4\sqrt{1-\beta}\right] \qquad (2.15)$$

Cao *et al* (1998) accounted for the influence of an axial load present in the chord member resulting in the following formula (2.16).

$$P_Y \sin\theta = \frac{F_{yo}.t^2{}_o}{(1-\beta)}\left[2\frac{h'_1}{b'_o} + 4\sqrt{1-\beta}'\sqrt{1-n^2}\right] \qquad (2.16)$$

2.8.2.2 Punching Shear Model

Just as the case for the CHS model this is modelled with a tensile load causing the brace member to separate from the chord by a fracturing of the chord member face. For this model, unlike the CHS model, an effective punching shear width b_{ep} is used. This effective width is determined experimentally. The full perimeter is not considered fully effective due to the non-uniform stiffness along the section perimeter.

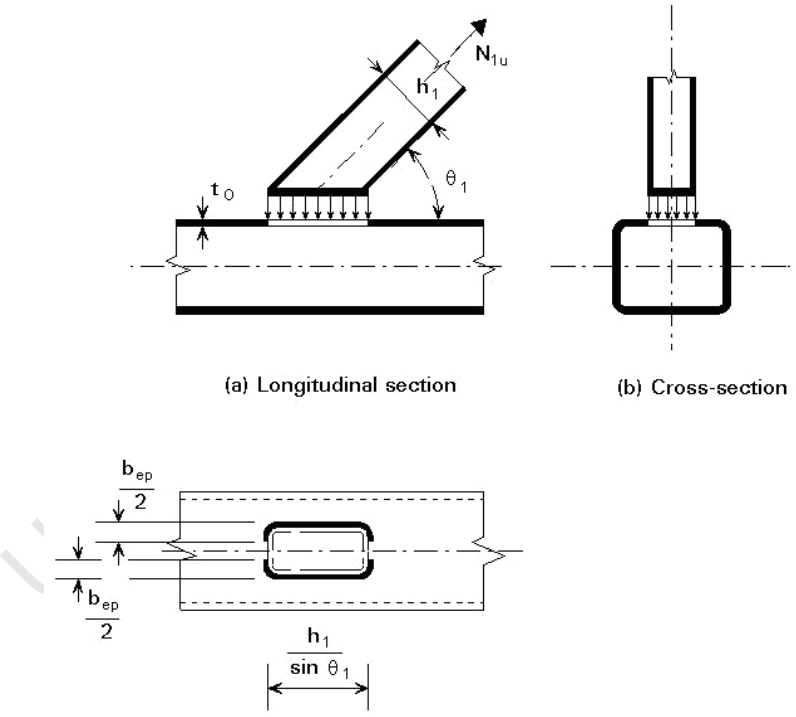

Fig. 13 Punching shear model

This model is applied to T, Y and X joints and the shear strength is determined from (2.17)

$$N_1 = \frac{f_{yo}}{\sqrt{3}}.t_o\left(\frac{2h_1}{\sin\theta_1} + 2b_{ep}\right)\frac{1}{\sin\theta_1} \qquad (2.17)$$

2.8.2.3 Effective Bracing Width Model

Whereas the punching shear phenomenon may be critical for brace members with thick walls the case may be different for thin walled members. Therefore for thin walled bracing members the strength is related to the geometries of the braces. A concept of effective width is used as shown in Fig. 14. For the T, Y and X joints the load at ultimate failure is determined from:

$$N_1 = f_{y1}.t_1\left(2h_1 - 4t_1 + 2b_{eff}\right) \qquad (2.18)$$

The effective width b_{eff} being determined experimentally.

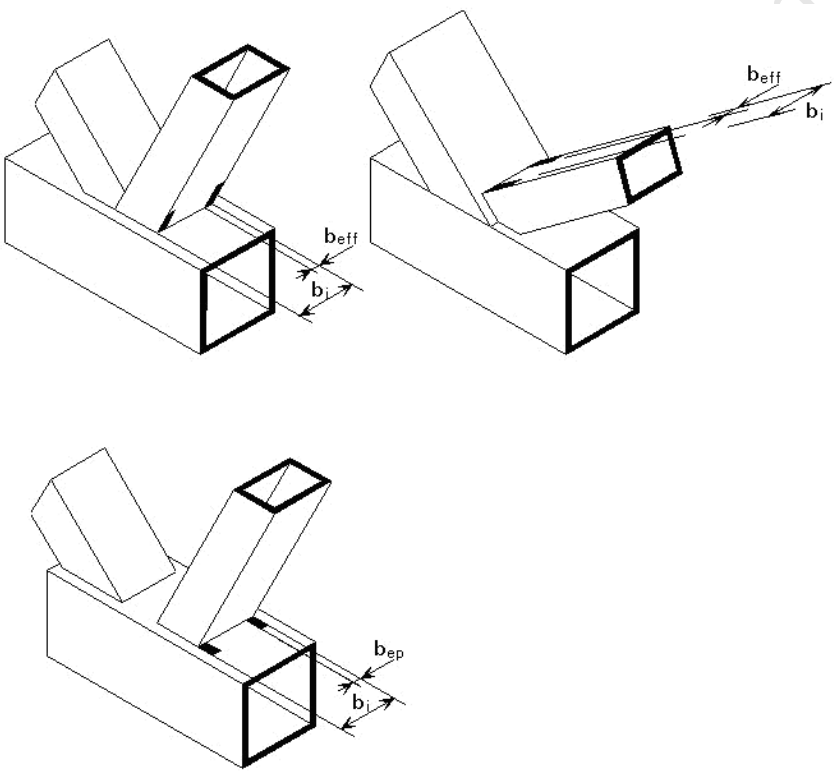

Fig. 14 Physical interpretation of effective width terms

2.8.2.4 Shear Failure Model of the Chord

For gap joints it is possible for failure to take place in the gap region by shear failure of the chord. This is most likely when the bracings meeting at the chord are subjected to a compressive and tensile load respectively. The plastic shear load is used in this model and is given by:

$$V_p = \frac{f_{yo}}{\sqrt{3}}.A_v \qquad (2.19)$$

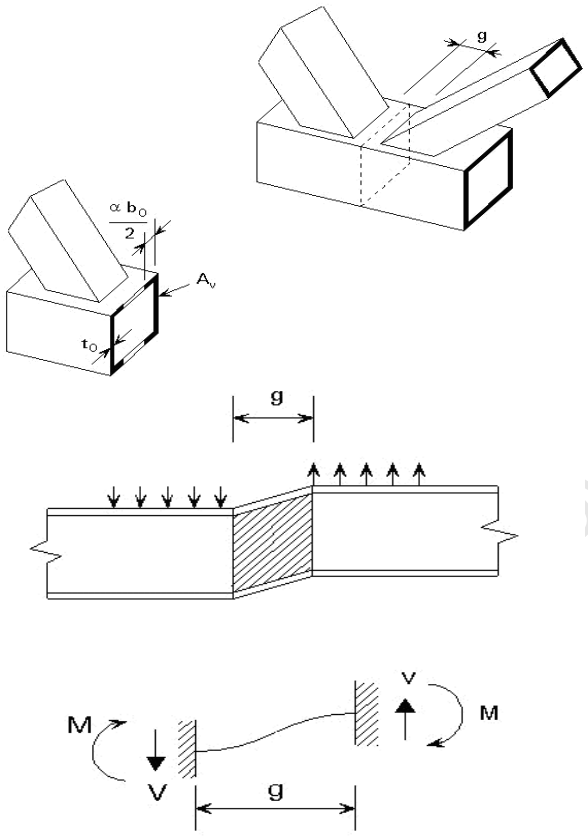

Fig. 15 Shear failure model of the chord

The shear area A_v is given by 2 $h_o.b_o.t_o$. However, tests have shown that for small gaps only part of the top flange is effective for shear transfer. Thus an effective shear area is used as shown in (2.20).

$$A_v = (2h_o + \alpha b_o)t_o \qquad (2.20)$$

Where α is a function of g/t_o

The remaining chord cross-section area transmits the axial force.

2.8.2.5 Chord Wall Bearing or Local Buckling Model

The model for buckling of the chord side walls is shown in Fig. 16. This model is applicable to T, Y and X joint configurations. Local buckling of the chord is likely to happen when the bracing size is close or equal to that of the chord i.e. with high β values.

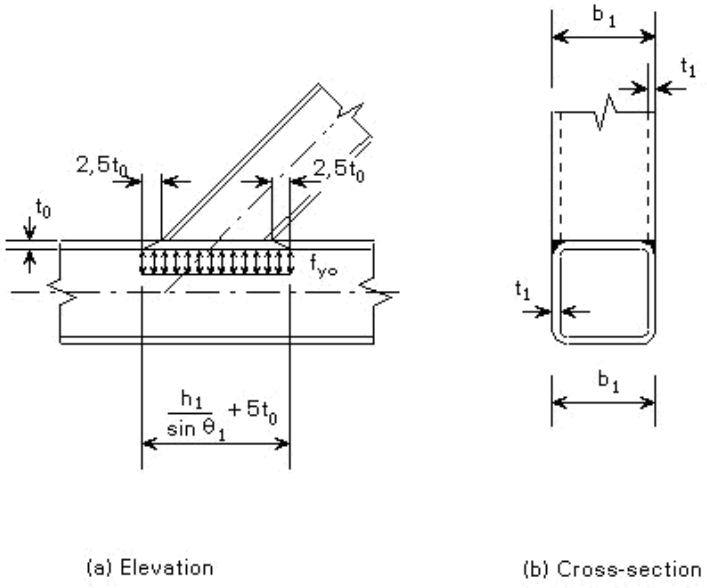

(a) Elevation (b) Cross-section

Fig. 16 Chord side wall bearing model for full width joints

For a value of β = 1 the formula becomes:

$$N_1 = 2 f_{yo} . t_o \left(\frac{h_1}{\sin \theta_1} + 5t_o \right) . \frac{1}{\sin \theta_1} \qquad (2.21)$$

For slender walls and compression loads, f_{yo} is replaced by a critical buckling stress f_k, which is a function of the chord web slenderness h_o/t_o (ESDEP WG 13c, n.d.).

The models discussed have looked at the cases of CHS-CHS and RHS-RHS connections and although derivations are based on axial load, analytical ultimate formulas for moment loaded joints are derived in a similar manner as failure modes are similar.

As regards joints between CHS and RHS members, Mashiri and Zhao (2004) tested a T-joint between a CHS brace and RHS chord. The obvious advantage of this arrangement is that there is no need for profiling the CHS as it can be cut flat to fit on the RHS chord. The joint

was loaded with an in-plane moment and the load versus chord flange indentation curve determined in order to find the ultimate strength. Plastic yield analysis was used to develop a predictive formula for ultimate strength which agreed with the experimental results, hence showing that analytical models can be developed for joints incorporating different member types.

2.8.3 Analytical models for joint moment-rotation behaviour

In semi-rigid design the initial joint stiffness (K or $S_{j,ini}$) as well as ultimate joint moment are required. The challenge with developing an analytical model for the moment-rotation behaviour of a joint is to establish a relationship between mechanical properties of the joint components and mathematical parameters of an equation. Several researchers have come up with analytical models that can be used to predict the M-Φ curves for various joints in order to determine the two required parameters $S_{j,ini}$ and M_{ult}. Examples of models are the polynomial model, power model, three parameter exponential model and the four power parameter model. Eurocode 3 (1993) also presents an analytical model based on what is known as the component method. The resulting M-Φ curve can either be idealised as a bi-linear, tri-linear or fully non-linear representation.

The shortcomings of most models that have been developed are that they appear to each be applicable only to certain joint configurations particularly those against which they where calibrated. For instance Yang and Lee (2006) proposed an improved analytical model for the prediction of initial stiffness and ultimate moment of double angle connections. This would suggest that this model cannot be used for other connection types. The tri-linear model from Eurocode 3 has come to be widely used due to its ease of application and the fact that it is applicable to many joint types, although Premthamkorn and Chomchuen (2005) observed that it gives a crude approximation. The two authors further proposed an improvement to the Eurocode tri-linear model by developing a multi-linear equation. The multi-linear equation showed close correlation with experimental test results which gave a more accurate prediction than the one presented by the tri-linear model. The multi-linear equation (2.22) assumes a diminishing slope as the moment increases, finally reaching zero at plastic moment.

$$\theta_j = \sum_{i=1}^{j} \frac{\left[M_i - M_{i-1}\right]}{K\left[1 - \left(\frac{M_i}{M_p}\right)^n\right]} \qquad (2.22)$$

Where K is the initial stiffness of connection, M_p is the plastic moment of the connection and n is the shape factor.

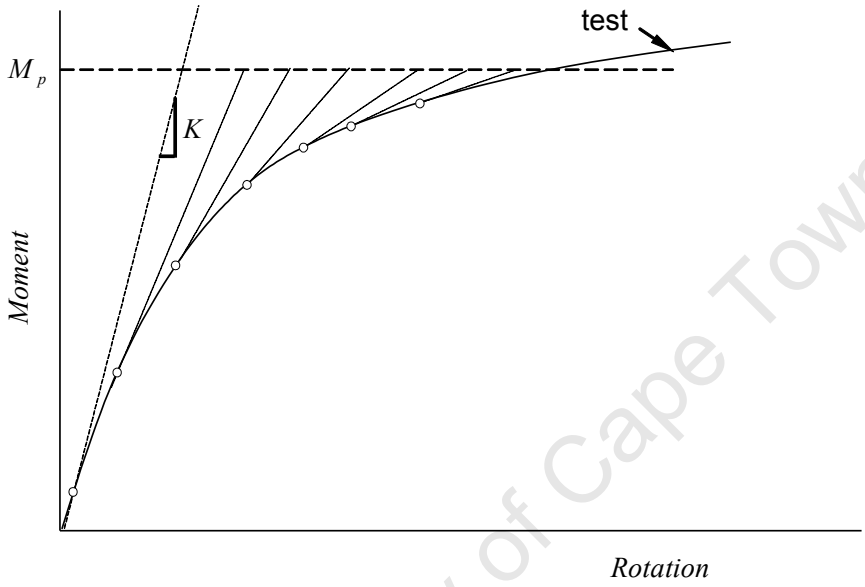

Fig. 17 Basic concept of the Multi-linear equation

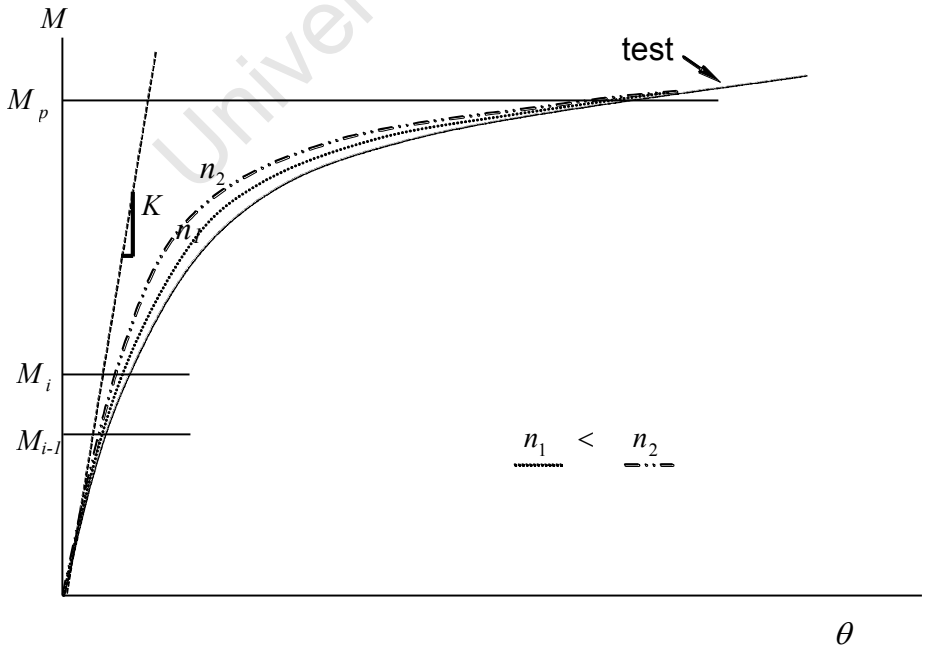

Fig. 18 Influence of shape factor

K and M_p are determined from Eurocodes component method. The authors developed equations for the shape factor n for bolted connections with angles, bolted end-plate connections and welded connections of open sections using regression analysis.

All the models discussed have been calibrated against test data from experiments carried out on open steel sections hence they need to be verified for validity with regards to hollow section joints.

Fig. 19 shows the steps employed in applying the Component Method.

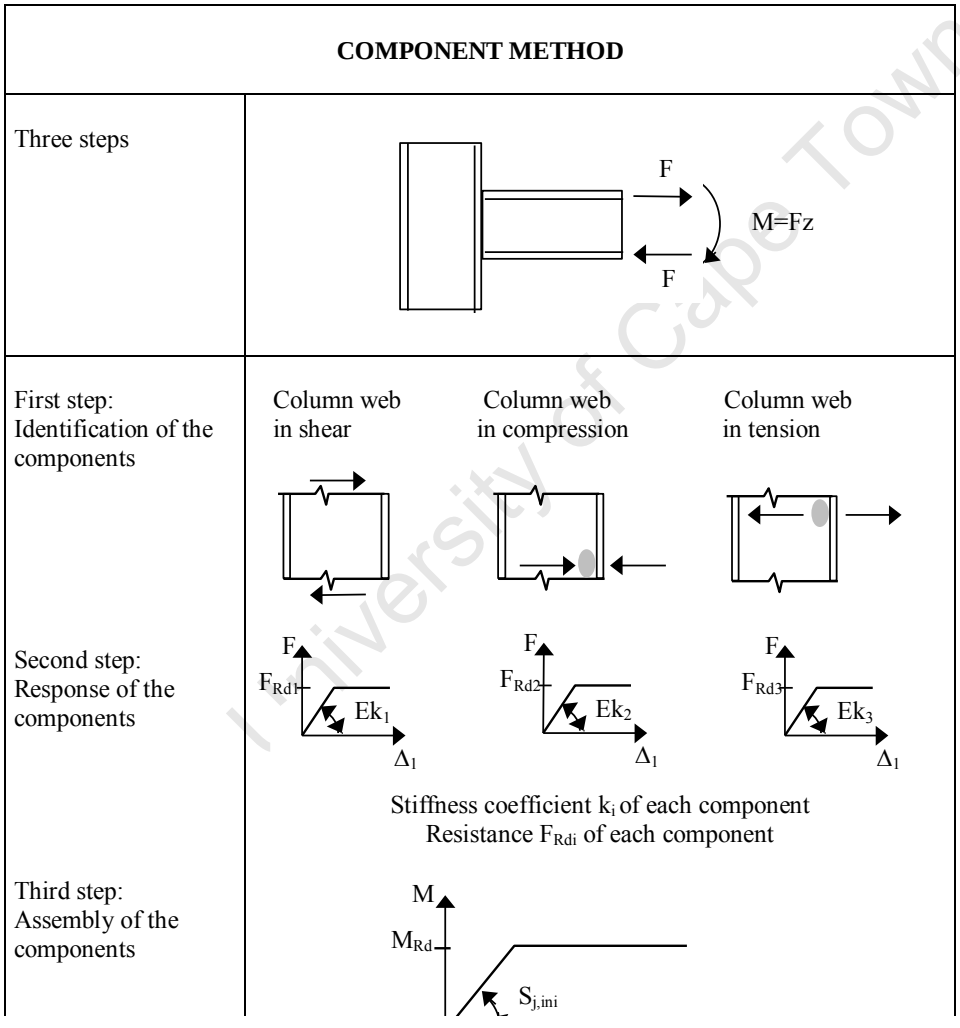

Fig. 19 Determination of initial stiffness and design moment using the component method

2.9 Experimental Testing of hollow section joints

Experimental testing involves a physical study of specimens subjected to certain conditions so as to ascertain the behaviour or response as would happen in service. In experimental testing procedure the joints may be tested as a single unit i.e. isolated case or as part of a whole structural assembly. The choice is usually limited only by economic considerations. When tested as an isolated unit care must be taken to ensure that the conditions imposed on the specimen are close as possible to what would happen if the joint was in-service in a structure. This means that boundary conditions, loading rates and load types are accurately and correctly applied. An accurate way of capturing a measured output must be devised as well. Even though Lee & Wilmshurst (1995) suggest that elastic-plastic finite element analysis is gradually replacing experimental testing as the foremost tool in SHS joint analysis they too used experimental data from (Makino et al 1984) to calibrate their finite element models. This is because experimental testing still serves as a primary source of information for making valid conclusions on joint behaviour and hence for calibrating FE and other models. Joint strength incorporated in the codes such as Eurocode (Eurocode, 1999) is based on semi empirical design formulas derived from analytical models and experimental evidence (Wardenier 2001, ESDEP WG13b, n.d. and ESDEP WG13c, n.d.). According to Lee and Gazzola (2006) three design codes; ISO 19902 (ISO 2001), API RP2A (API 1993) and HSE Guidance Notes (HSE 1990) do not have design formulas for overlap K-joints due to a lack of test data. This would suggest why validity tables are included in design codes. The validity is thus for cases where experimental tests have been used to confirm or calibrate analytical and numerical models. According to Wardenier (2001) most joint tests have been carried out on isolated joints and rarely in complete frames. With correct application, experimental testing still remains the most accurate method of obtaining joint behaviour of SHS joints.

It would appear that much of the early research into tubular joints was initially focused on rectangular hollow sections presumably due to their ease of fabrication. Most studies have focused on the T-, Y-, X- and K- configurations or combinations of these. Early research in moment connections for tubular sections was carried out by Lazar and Fang (1971), Brockenbough (1972) and Korol et al (1977). Kanatani et al (1982) were among the early CIDECT sponsored researchers. They carried out experimental tests on un-reinforced RHS T-joints subjected to in-plane bending. They documented failure modes and studied fillet weld

size effects on the joint behaviour. Studies were carried out on cold formed sections. Overall displacements and local deformations were recorded using dial gauges. Weld size was found to affect stiffness, strength and deformation capacity as well as failure mode. Yura et al (1981) carried out work aimed at improving on the ultimate capacity equations for design and made recommendations to that effect based on their findings. Stamenkovic and Sparrow (1983) carried out experimental tests on CHS T-joints to determine ultimate strength under combined axial and moment loads. Their results showed a linear relationship between axial load and moment capacity of the joints. Test specimens were hot-rolled CHS sections. As with Yura et al (1981) they reported no sudden failure of the tested specimens but rather a failure due to excessive deformation of the chord. Packer (1993) presented a compilation of comprehensive design equations for T-, X- and knee RHS joints based on CIDECT sponsored and other research, and these equations are in predominant use today. Most of the researchers have presented the moment loaded behavior of the joints in form of a moment-rotation (M-Φ) curve and in all cases the joint exhibits elastic behavior with low rotations followed by large rotations in the plastic range. This suggests that tubular section joints have a considerable post yield capacity as they can sustain large rotation before ultimate failure.

Circular tubular members have found wide application in offshore structures due to their low drag characteristics. The response of tubular joints to both in-plane and out-of-plane bending (OPB) moments was presented by the Society of Steel Construction of Japan (1972) and cited by (Yura and Zettlemoyer, 1981) who presented results from bending tests on T- and K- CHS joints. The out of plane bending stiffness, and moment capacity, is in all cases less than that for the in-plane case. Since out-of-plane bending is prevalent in offshore structures in addition to other structural loading it too has been an area of focus for researchers. Lee et al (1995) carried out a study of circular tubular T/Y-joints loaded by OPB moment. They discovered that, as in the case of in-plane (IP) bending, there was a large post yield capacity and concluded that a design based on the elastic behaviour of the joint would be over-conservative.

Another joint configuration that is used mostly in frames is the L-joint. Findings reported by Packer (1993) indicate that the unreinforced L-joint has limited moment capacity and several proposals to reinforce it have been made albeit at the expense of economy. These limits may explain why so little is reported on research into this type of joint configuration. A comprehensive test program was carried out by Mang et al (1996) to study the behaviour of

CHS reinforced and unreinforced L-joints subjected to a closing moment effect. In most cases the reinforced joint was found to have twice as much strength as the corresponding unreinforced joint. A research on the plastic behaviour of knee (L-) joints was carried out by Wilkinson and Hancock (2000) and in that study the stiffened connection was able to attain the plastic moment whereas as the unstiffened joint failed at less than the plastic moment.

The search for innovation coupled with the desire for aesthetic enhancement has led to research in the bird-beak joint. In this type of joint the RHS or SHS chord or brace is rotated through an angle and then fixed in the normal way to the other member or members. Early research on this type of joint was focused on the performance under axial loads. Christitsas et al (2007) carried out an experimental study of conventional and bird-beak SHS X-joints subjected to in-plane bending in order to compare performance of the two types. The bird-beak joint studied was one where the chord member is rotated through 45^0 compared to the normal chord orientation. Tests showed that chord orientation has significant effect on joint strength as well as rotational stiffness for ratios of $\beta < 0.85$, with bird-beak showing higher strength than the conventional joint. The experimental results were further used to calibrate a FE model for a parametric study.

2.9.1 Test Set-up

Two challenges with experimental testing are simulating performance in real life i.e. simulating the behavior as it would be in service and developing a way of accurately measuring the requisite parameters. Measurements have to be accurate and, where necessary, taken at appropriate intervals so as to allow the researcher make accurate inferences from the data. In the case of joint tests such factors as how the joint is held in position, how the loads are applied and how the displacement or angular measurements are taken play an important role in accurately describing the performance of the joint under given loading conditions. Different fixity conditions for hollow sections can be achieved mainly by welding, bolting or employment of other clamping mechanisms. Supports can usually be easily fabricated as well. In some instances these mechanisms may come inherent with testing machines hence eliminating the need for fabrication.

Measurements can be taken using different devices and instruments. Loading machines come with dials or displays that show the load levels and even a manual loading tool such as a jack can have a load cell attached so as to give a reading of applied load. Displacement measurements can be made using such instruments as dial gauges and LVDT displacement transducers while angular measurements can be taken by protractors and angular transducers.

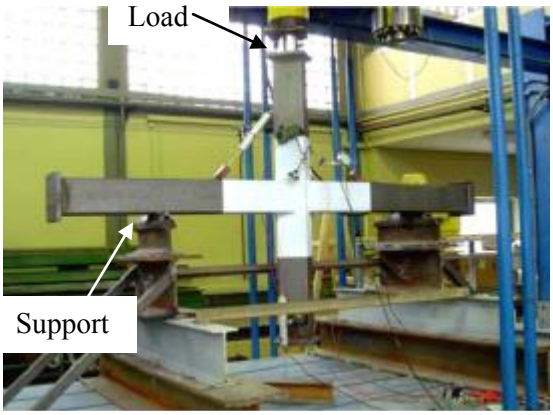

Fig. 20 Test set-up for an X-joint moment experiment (Christitsas et al, 2007)

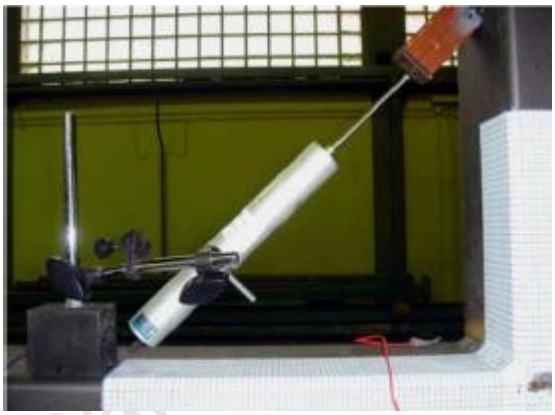

Fig. 21 Displacement transducer (Christitsas et al, 2007)

Due to the varying types of hollows section connection geometries and the different material strengths there is not one particular way of experimental set-up. The choice will largely depend on the parameter under investigation and to some extent the materials available to the researcher in the test workshop. Wilkinson and Hancock (2000) used the test set-up shown in Fig.22 for in-plane bending moment tests on cold-formed RHS knee joints.

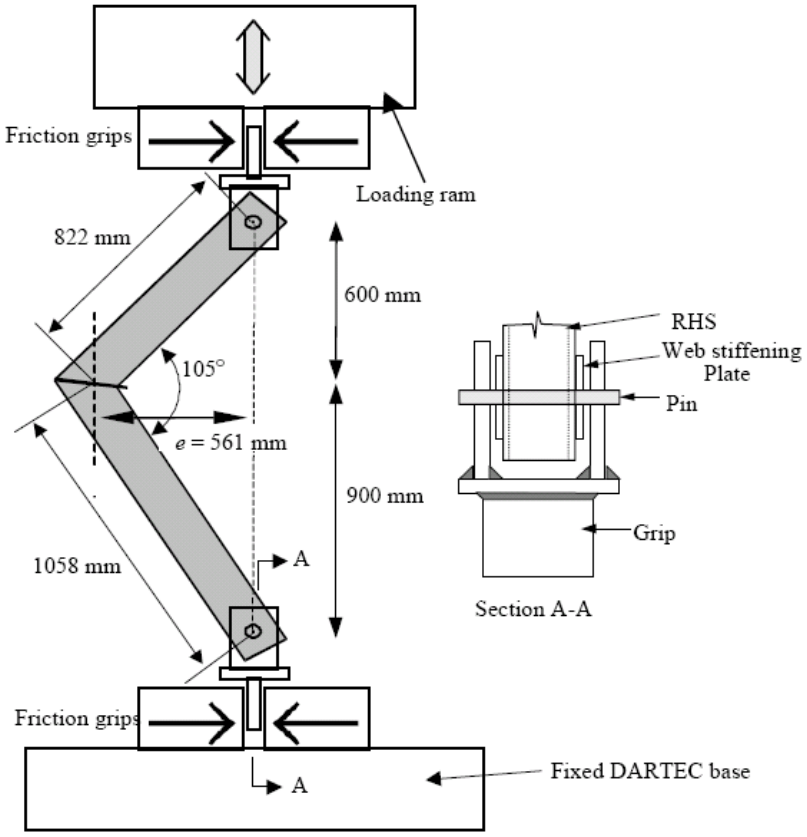

Fig. 22 Schematic details for knee joint test (Wilkinson, 2000)

Researchers usually present the geometric parameters of the test specimens in terms of non-dimensional parameters described in Fig.23

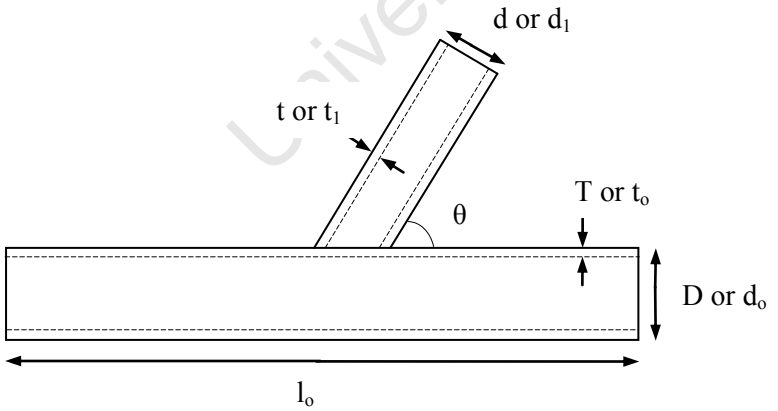

$$\tau = \frac{t_1}{t_o}$$

$$\beta = \frac{d_1}{d_o}$$

$$2\gamma = \frac{d_o}{t_o}$$

$$\alpha = \frac{2l_o}{d_o}$$

Fig. 23 joint geometric parameters

Note that for RHS the symbol ‘d’ would be replaced by ‘h’. Generally the subscript ‘1’ would be for brace parameters while ‘o’ is for chord parameters. Lee et al (1995) carried out tests for OPB moment with geometric parameters of $\alpha = 17$, $\beta = 0.375$, $\gamma = 18$ and $\tau = 0.42$. Some

researchers also use (l_1) to describe the length of the brace member. Some researchers like Stamenkovic and Sparrow (1983) do not present their data in terms of the dimensionless parameters but rather by the actual dimensions. In this case they were presented as l_o=815.5mm (≈ $7d_o$), d_o=114.3mm, l_1=298.5mm and d_1 ranging from 48.3 – 114.3mm. The parameters presented in Fig.23 are also frequently used to describe FE model geometry.

Having carried out experimental testing it becomes easy to develop good and accurate FE models for large scale numerical parametric studies in wide ranges not covered by the tests hence saving on cost.

2.10 Numerical studies on hollow section joints

The numerical method of analysis primarily involves the employment of the finite element method (FEM). Owing to the development of the microcomputer hand calculations have been all but replaced with the use of computers. The early finite element models were based on 2D models (Korol and Mirza, 1982) but most modern analysis is carried out using 3D models, made possible by more powerful and faster computers as well as software with high capabilities for modeling and analysis. Some of the common FE modeling software in use today are ABAQUS, ANSYS, PATRAN, NASTRAN and ADINA. A lot more others have been developed for both commercial and research use.

A comprehensive discussion on the use of the finite element method for strength, stress and fracture analyses of CHS joints is presented by Lee (1999). Though focused mainly on CHS joints the discussion is in many respects applicable to RHS joints as well. A detailed look at model and mesh generation, choice of elements, material definition, analysis approaches and modeling limitations is presented. The view of many researchers is summed in the statement that "numerical simulation using finite elements, with judicious calibration against reliable test results, has been found to adequately model the required behavioural characteristics of steel tubular joints, including initial stiffness, mode(s) of failure, ultimate load and complete load-deformation response" (Lee 1999, pp.266). It is essential to note that although modeling these joints is an attainable goal, producing a good model can be complex, if not arduous, and therefore has to be well thought out. This is particularly true for tubular sections as they exhibit non-uniform stress distribution as well as geometric and material nonlinearity.

Optimal meshing of the model, choice of elements, material definitions, analysis approach and a good understanding of the software being employed help produce good models. The two most widely used element types for modeling tubular joints are the brick (solid) elements as well as shell elements (which can either use a thin or thick formulation) (Lee, *ibid*). In many cases where there is symmetry in the joint only a part of the joint along the line of symmetry is modeled thus saving on computing time. This is prudent practice.

Modeling of the weld at the joint is omitted by many researchers owing to its complexity. Although researchers like Choo et al (2004), Lee and Gazzola (2006), Jubran and Cofer (1995) and Mang et al (1996) have modeled the welds at joint intersections, Lee et al (1995) discarded the modeling of the weld as it was found not to have much effect on the outcome of the analysis as was shown by Van der Valk (1988) who obtained good correlation of results without having to model the welds. This view is supported by Lee (1999) while making an exception for K-joints with significant gaps which develop added stiffness in the gap area due to the welds. In modeling the welds both solid and shell elements have been used. Shell elements, which essentially model the mid-plane of the tubular members, are thought to produce models which are more accurate as the solid elements are liable to produce stiff models if not enough elements are provided through the member thickness.

Jubran and Cofer (1995) used a combination of shell and solid elements for their models. The tubular members were modeled with shell elements and solid elements were used in the weld region. The choice of solid elements was aimed at modeling the tri axial stresses in the weld region. The model showed good correlation with experimental data for in-plane bending. Lee et al (1995) carried out a study on CHS T/Y-joints for offshore structures subjected to OPB moment load. Results from the experimental tests were used to calibrate a FE model. Four and eight nodded shell elements were used and a convergence study was carried out to refine the model. The model gave moment-rotation characteristics similar to what was obtained from the experiments, however, strain and displacement correlation was poor. Karamanos and Anagnostou (2004) carried out FE analysis on CHS joints under static loads and subjected to pressure, with particular focus on underwater structures. Due to insufficient test data, the model was calibrated against joints tested under normal conditions. Nonlinear analysis was carried out on X- and T- joints and results showed a significant effect of pressure on joint strength and deformation capacity. This study was an extension to a previous study by Conelly and Zettlemoyer (1991) whose study on X-joints also showed

reduced ultimate capacity with increasing hydrostatic pressure. The two studies show just how versatile and invaluable the FE modeling can be as simulating a test under pressure conditions would be a difficult and presumably expensive undertaking. Lee and Gazzola (2006) endeavoured to develop a design equation for overlap tubular K-joints using results from a FE parametric analysis. The model was calibrated against data for gap K-joints due to a lack of test data for the overlap joint. Four node thin shell elements were employed and the model was used to determine geometric effects on joint performance as well as associated failure modes. Owing to the lack of test data a characteristic design equation could not be derived but a capacity prediction formula is presented.

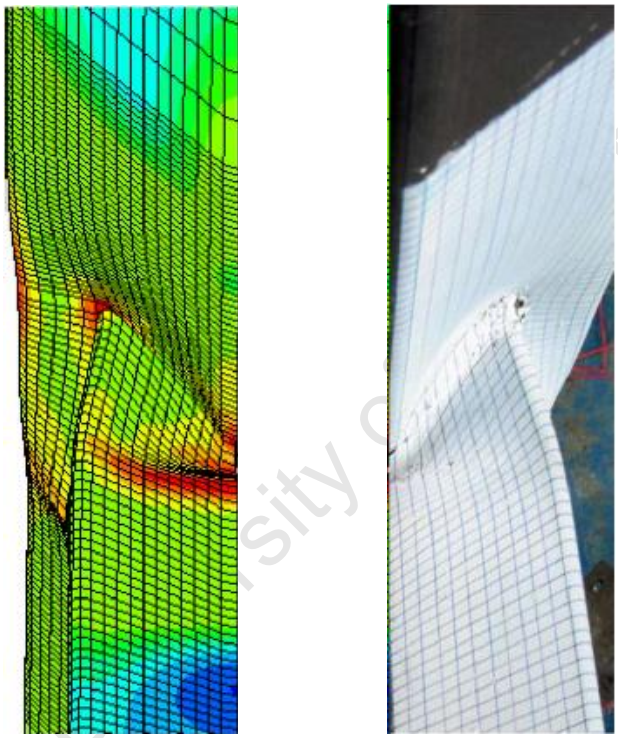

Fig. 24 Correlation between FE model and experimental test results (Christitsas et al, 2007)

The primary objective of carrying out FE modeling as well as experimental joint testing is to come up with an understanding of joint behaviour and develop easy and practical means of carrying out the analysis and design of structures employing these joints. Thus the results of FE analysis and experimental tests need to undergo a process of refinement and simplification in order to be effectively used in design codes and guidelines.

2.11 Design Codes

2.11.1 Hollow Section Design Codes

Designers are usually provided with quick and easy ways for obtaining requisite information for carrying out the structural design without having to perform complex and repeated calculations. Also, knowledge obtained from research as well as past experience can be made available to guide the designer in an easy-to-use form. This is done through the use of design codes or design standards as well as design guides. Design codes also have the added attribute of ensuring consistency and providing a regulatory framework based on well researched information. Countries like Australia have carried out extensive research and the results have been used to develop appropriate design rules for cold-formed SHS and RHS for use in their limit states steel design specification (Wilkinson 1999). Much of the European standard has been developed from research carried out by CIDECT and IIW. There are only a few countries that have incorporated design standards for hollow sections in their design codes of practice. Table 3 gives the list of current national codes of practice in use and the respective countries that have incorporated design standards for hollow sections.

Table 3: Codes of practice for hollow sections

Country	Cold Formed	Hot Finished
Australia	AS 1163-1991	AS 1163-1991
Canada	CAN/CSA-G40.20-M92	CAN/CSA-G40.20-M92
USA	ASTM A500-93	ASTM A501-89
Europe (CEN countries)	EN 10219-1 & 2	EN 10210-1 & 2
Japan	JIS G3466-1988 JSS II-10-1998 JASS 6	JIS G3444-1988

Adapted from: CIDECT [Internet] Available at (http://www.cidect.org/en/Standards.php)

Apart from the national codes of practice there are other design codes as well as design guides that have been developed for the design of CHS tubular structures particularly for offshore applications. These design codes and guides are based on either the working stress design or limit states design approaches. They are presented in Table 4.

Table 4: Design codes/guides listed under design basis

Working stress design	Limit states design
API RP2A – WSD (1993)	API RP2A – LRFD (1993)
AWS (1994)	AWS (1994)
DnV (1993)	CIDECT (1991)
HSE (1990)	CSA (1992)
	DnV (1993)
	NPD (1990)

Source: BOMEL, 1996

The API, AWS and DnV codes allow the designer to choose between working stress and limit states design approaches. A comparison of design equations for in-plane bending (IPB) among the codes listed in Table 4 is presented by (BOMEL, 1996). The comparison indicates that API, CIDECT, HSE and NPD give one strength formula irrespective of the joint type, the DnV formula is restricted to T-joints and the CSA is said not to be applicable to K-joints. HSE (2002) also provides a comparison of four offshore design codes. Both documents also list some of the sources of research for the design strength equations presented in the design guides. The International organization of standardization (ISO) has also developed design guidelines for hollow section joints (ISO 2001). In South Africa the SAISC handbook on hollow sections presents monographs from CIDECT as well as the European code tables for the design of hollow sections in its Appendix (SAISC 1989). It also has member tables for section properties of the hollow sections.

Retief et al (2005) observed that the South African (SA) structural design codes are fragmented and are in many cases referenced to other standards. The only standards that are developed purely from local research are those for timber and masonry. The fragmented nature of the codes is made apparent when designing with concrete and steel for instance. Because these two codes are referenced to the British and Canadian standards respectively inconsistencies arise when the two materials are used in one structure. Table 5 summarises the main South African structural design standards.

Table 5: South African structural design standards based on limit states design

Standard	Title	Comments	Date
SABS 0160	**The general procedure and loadings to be adopted in the design of buildings**	**Locally developed References** (Retief et al citing Kemp et al 1987 and Milford 1988)	1993
SANS 10100	**The structural use of concrete Part 1 Design Part 2 Materials and execution of work**	**Based on British code BS 8110**	2005
SANS 10162	**The structural use of steel Part 1 LS Design of hot rolled steelwork Part 2 LS Design of cold formed steelwork**	**Based on Canadian code CAN3-S16-01**	2005
SANS 10163-1	**The structural use of timber Part 1: Limit states design**	**Locally developed**	2001
SANS 10164	**The structural use of masonry Part 1: Unreinforced masonry walling Part 2: Structural design and requirements for reinforced and prestressed masonry**	**Locally developed**	1987 2003
TMH-7	**Code of practice for the design of highway bridges and culverts in South Africa Part 1 General Part 2 Specification of loads Part 3 Structural concrete**	**Specifications for structural concrete are based on the CEB-*fip* Model Code**	1989

Adapted from: Retief et al (2005)

Although the SAISC handbook for structural hollow sections (SAISC, 1989) provides design guidelines for ultimate axial and moment loads on statically loaded SHS it does not address semi-rigid design.

2.11.2 Welding Standards

Application standards and codes of practice ensure that a structure or component will have an acceptable level of quality and be fit for the intended purpose (TWI, n.d.). Most fabricators use company or industry specific, British (BS), European (BS EN), US AWS (American Welding Society) and ASME (American Society of Mechanical Engineers) or International ISO Standards. Examples of application codes and standards and related welding procedure and welder approval standards are listed in Table 6.

Table 6: Examples of application codes and standards and related welding procedure and welder approval standards

		Welding Standard	
Application	**Application code/standard**	**Procedure approval**	**Welder approval**
Pressure Vessels	PD 5500 ASME VIII	BS EN 15614 ASME IX	BS EN 287 ASME IX
Process Pipework	BS 2633 BS 4677 ANSI/ASME B311 ANSI/ASME B31.3 BS 2971	BS EN 15614-1 BS EN 15614-2 ASME IX ASME IX BS EN 15614-1 (if required)	BS EN 287 (Part 1) BS EN 9606-2 ASME IX ASME IX BS 4872/BS EN 287
Structural Fabrication	AWS D1.1 AWS D1.2 BS EN 1011 BS 8118	AWS D1.1 AWS D1.2 BS EN 15614-1 BS EN 15614-2	AWS D1.1 AWS D1.2 BS EN 287 BS EN 9606-2 BS 4872
Storage Tanks	BS 2654 BS 2594 API 620/650	BS EN 15614-1, -2 BS EN 15614-1, -2 ASME IX	BS EN 287 BS EN 9606-2 ASME IX

Adapted from: http://www.twi.co.uk/j32k/protected/band_3/jk38.html [Internet]

2.11.2.1 List of Relevant Standards for Welding

- American Welding Society, Structural Welding Code, AWS D1.1
- ASME Boiler and Pressure Vessel Code, Section IX: Welding Qualifications
- BS 4872 Approval Testing of Welders when Welding Procedure Approval is not Required
- BS EN 287:1998 Approval Testing of welders for fusion welding
- BS EN 9606-2: 2004 Approval testing of welders. Fusion welding. Aluminium and aluminium alloys.
- BS EN 15614-1: 2004 Specification and qualification of welding procedures for metallic materials. Welding procedure test.
- BS EN ISO 5817:2003 Welding - fusion-welded joints in steel, nickel, titanium and their alloys (beam welding excluded) - Quality levels for imperfections
- BS EN ISO 6520-1:1998 Welding and allied processes - Classification of geometric imperfections in metallic materials
- BS EN 30042:1994 Arc-welded joints in aluminium and its weldable alloys. Guidance on quality levels for imperfections.

(Source: http://www.twi.co.uk/j32k/protected/band_3/jk38.html)

REFERENCES

American Welding Society (AWS), 1994. *ANSI/AWS D1.1-94 Structural Welding Code – Steel*.

American Petroleum Institute (API). (1993). *API RP2A Recommended Practice for Planning, Design and Constructing Fixed Offshore Platforms – Working Stress Design* 20th Edition (1993); and *Load and Resistance Factor Design (LRFD)* First Edition (1993).

BOMEL. (1996). *Design and reassessment of tubular joints for offshore structures. Chapter3: Static Strength. C6060R07.21 REV A*. Berkshire, UK.

Brockenbough, R., L., 1972. Strength of square tube connections under combined loads. *Journal of the Structural* Division, ASCE, **98** (ST12), pp.2753-2768.

Canadian Standards Association (CSA). (1992). Steel Structures – Offshore Structures.

Cao, J.J. Packer, J.A. & Yang, G.J. 1998. Yield line analysis of RHS connections with axial loads. *Journal of Constructional Steel Research*. **48** (1), pp.1–25.

CEN. (1993). *Eurocode 3 (Annex J)*. Draft for Development. Comite Europeen de Normalisation.

CIDECT. (1991). *Design Guide for Circular Hollow Section (CHS) Joints under Predominantly Static Loading.*

CORUS. (2005). *Corus Tubes, SHS Welding, Structural & Conveyance Business*. [Online] Available: http://www.corusgroup.com/file_source/StaticFiles/Business%20Units/Corus%20Tubes/CT15-SHS%20Welding%2009-05-05.pdf. [Cited 20 July 2006].

CIDECT., n.d.. Research Projects, Welded joints (statics). [Online] Available: www.cidect.com/en/Research_Projects/welded_joints.php. [Cited 21 July 2006].

CIDECT., n.d.. *Standards and Codes, Product standard references for steel hollow sections in the world*. [Online]. Available from: http://www.cidect.org/en/Standards.php. [Cited 20 July 2006].

Connelly, Z. M. Zettlemoyer, N. (1991). Hydrostatic effects on the capacity of DT tubular joints. *Offshore technology conference*, OTC 6574, Houston, Texas, pp.119-130.

Choo, Y. S. Liang, J. X. van der Vegte, G. J. Liew, J. Y. R. 2004. Static strength of doubler plate reinforced CHS X-joints loaded by in-plane bending. *Journal of Constructional Steel Research.* **60** (12), pp.1725-1744.

Choo, Y.S. Liang, J.X. Lim, L.V. 2003. Static strength of elliptical hollow section X-joint under brace compression. In *Proceedings of the 10th International Symposium on Tubular Structures, 18-20 September. Madrid, Spain.*

Christitsas, A.D., Pachoumis, D.T., Galoussis, E.G., 2007. FEM analysis of conventional and square bird-beak SHS joint subject to in-plane bending moment – experimental study. *Journal of Constructional Steel Research.* **63** (10), pp. 1361 – 1372.

DnV. (1993). *Rules for Design, Construction and Inspection of Offshore Structures.*

Dutta, D. 2002. *Structures with Hollow Sections.* Berlin: Ernst & Sohn Verlag für Architektur und technische Wissenschaften GmbH.

Dwight J.B. Young B.W. 1970. Residual Stress due to Welding. *Conference on Joints in Structures* 1970, Session B, Paper 3, Institute of Structural Engineers, University of Sheffield.

Easterling K. 1993. *Introduction to Physical Metallurgy of Welding*. Oxford: Butterworths Heinemann, p.126.

ESDEP WG 2, n.d. *APPLIED METALLURGY: Lecture 2.3.1: Introduction to the Engineering Properties of Steel.* [Online]. Available: http://www.fgg.uni-lj.si/kmk/ESDEP/master/wg02/l0310.htm. [Cited 20 July 2006]

ESDEP WG 13a, n.d. *TUBULAR STRUCTURES: Lecture 13.1: Application of Hollow Sections in Steel Structures.* [Online].
Available: http://www.kuleuven.ac.be/bwk/materials/Teaching/master/wg13/l0100.htm
[Cited 20 July 2006].

ESDEP WG 13b, n.d. *TUBULAR STRUCTURES: Lecture 13.2: The Behaviour and Design of Welded Connections between Circular Hollow Sections under Predominantly Static Loading.* [Online]. Available:
http://www.kuleuven.ac.be/bwk/materials/Teaching/master/wg13/l0200.htm
[Cited 20 July 2006]

ESDEP WG 13c, n.d. *TUBULAR STRUCTURES: Lecture 13.3: The Behaviour and Design of Welded Connections between Rectangular Hollow Sections Under Predominantly Static Loading.* [Online]
Available: http://www.fgg.uni-lj.si/kmk/ESDEP/master/wg13/l0300.htm. [Cited 20 July 2006]

Eurocode 3. (1992). *ENV 993-1-1: Annex K: Hollow Section Lattice Girder Connections*. CEN.

Eurocode 3. (2003). *Design of Steel Structures – Part 1-8: Design of Joints*. Final Draft: PrEN 1993-1-8. CEN. Rue de stassart,36 B-1050. Brussels.

Health and Safety Executive (HSE). (1990). *Offshore Installations – Guidance on Design, Construction and Certification*. Fourth Edition. (Withdrawn in Oct. 1998).

HSE. (2002). Comparison of tubular joint strength provisions in codes and standards. *Offshore Technology Report,* 2001/082.

Illston, J.M. Dinwoodie, J.M. Smith, A.A. (1979). *Concrete, Timber, and Metals, the Nature and Behaviour of Structural Materials.* Van Nostrand Reinhold Co. Ltd.

ISO. (2001). *ISO 19902 – Fixed Steel Structures. Draft ISO/TC67/SC7N288*, Geneva, Switzerland.

Jaspart, J.P. 2000. General report: session on connections. *Journal of Constructional Steel Research.* **55** (1-3), pp.69–89.

Jubb, J.E.M. Redwood R.G. 1966. Design of joints to box sections. *Conference on Industrial Building and the Structural Engineer*. Institution of Structural Engineers, UK.

Jubran, J. S. Cofer, W. F. 1995. Finite-element modeling of tubular joints. I: Numerical results. *Journal of Structural Engineerin*g. **121** (3), pp.496-508.

Kanatani, H. Fujiwara, K. Tabuchi, M. Kamba, T. (1982). Bending tests on T joints of RHS chord and RHS branch. CIDECT Report: 5AF2-82/2

Karamanos, S. A. Anagnostou, G. 2004. Pressure effects on the static response of offshore tubular connections. *Marine Structures.* **17** (6), pp.455-474.

Kemp, A.R. Milford, R.V. Laurie, J.A.P. 1987. Proposals for a comprehensive limit states formulation for South African structural codes. *The Civil Engineer in South Africa*. **29** (9), pp. 351-360.

Korol, R. M. Mirza, F. A. 1982. Finite element analysis of RHS T-joints. *Journal of the Structural Division, ASCE.* **108** (9), pp.2081-2098.

Korol, R. M. El-Zanaty, M. Brady, F. J. 1977. Unequal width connections of square hollow sections in vierendeel trusses. *Canadian Journal of Civil Engineering*. **4** (2), pp.190-201.

Kosteski, N. Packer, J.A. Puthli, R.S. 2003. A finite element method based yield load determination procedure for hollow structural section connections. *Journal of Constructional Steel Research.* **59** (4), pp.453-471.

Kozy, B. 2004. Chord bearing capacity in long-span tubular trusses. Ph.D. dissertation, Dept. of Civil and Environmental Engineering, University of Pittsburgh, Pittsburgh.

Krishnan, S.N. Toppo, V. Basak, A. Ray, K.K. 2006. Wear behaviour of a steel weld joint. *Wear*. **260** (11-12), pp.1285-1294.
Kurobane Y. Makino Y. Kenshi O. 1984. Ultimate Resistance of Unstiffened Tubular Joints. *Journal of Structural Engineering*. **110** (2), pp. 385 – 400.

Lazar, B.E. Fang, P.J. (1971). *T-type moment connections between rectangular tubular sections*. Research Report. Sir George Williams University, Montreal.

Lee, M. M. K. 1999. Strength, stress and fracture analysis of offshore tubular joints using finite elements. *Journal of Constructional Steel Research.* **51** (1999), pp.265-286.

Lee, M. M. K. Gazzola, F. 2006. Design equations for offshore overlap tubular K-joints under in-plane bending. *Journal of Structural Engineering.* **132** (7), pp.1087-1095.

Lee, M. M. K. Dexter, E. M. Kirkwood, M. G. 1995. Strength of moment-loaded tubular T/Y-joints in offshore platforms. *The Structural Engineer. Journal of the Institution of structural Engineers*. **73** (15), pp.239-246.

Lee, M.M.K. Wilmshurst, S.R. 1995. Numerical Modelling of CHS Joints with Multiplanar Double-K configuration. *Journal of Constructional Steel Research*. **32** (3), pp. 281-301.

Makino, Y. et al. 1984. Ultimate capacity of tubular double K-joints. In *Proceedings of 2nd International Institute of Welding Conference on Welding of Tubular Structures.* Boston: Pergamon Press. P. 451-458.

Mang, F. Herion, S. Karcher, D. (1996). *L-joints made of circular hollow sections*. Final Report. Research programme CIDECT 5 BE. University of Karlsruhe, Germany.

Milford, R.V. 1988. Target safety and SABS 0160 load factors. *The Civil Engineer in South Africa*. **30** (10), pp.475 – 481.

Nakashima, M. Roeder, C.W. and Maruoka, Y. 2000. Steel moment frames for earthquakes in United States and Japan. *Journal of Structural Engineering, ASCE.* **126** (8), pp. 861–868

Norwegian Petroleum Directorate (NPD). (1990). *Guidelines on the Design and Analysis of Steel Structures.*

Packer A.J. 1993. Moment Connections between Rectangular Hollow Sections. *Journal of Constructional Steel Research*. **25** (1-2), pp.63 – 81.

Premthamkorn, P., Chomchuen, P. 2005. Modelling of semi-rigid steel connections by multi-linear equation. *Proceedings of the Fifth Workshop on Stability of Infrastructure Against Environmental Impacts, December 5-6, 2005, Manila, Philippines.*

Rasmussen, K.J.R. Young, B. 2001. Tests of X- and K- Joints in SHS Stainless Steel Tubes. *Journal of Structural Engineering.* **127** (10), pp.1173-1182.

Retief J.V. Dunaiski P.E. Wium, J.A. 2005. South African Structural Design Standards an Overview of Development. *African Concrete Code Symposium-2005.*

Saidani, M. 1998. The effect of joint eccentricity on the distribution of forces in RHS lattice girders. *Journal of Constructional Steel Research*. **47** (3), pp.211-221.

Seward, D. (1994). *Understanding Structures, Analysis, materials, design.* Hong Kong: THE MACMILLAN PRESS LTD.

Society of Steel Construction of Japan. (1972). *Study on tubular joints used for marine structures*. March 1972

South African Institute of Steel Construction (SAISC). (1989). *South African Structural Hollow Sections Handbook.* Cape Town. SAISC.

Stamenkovic, A. Sparrow, D.K. 1983. Load interaction in T-joints of steel circular hollow sections. *Journal of Structural Engineering.* **109** (9), pp.2192-2204.

Togo, T. 1967. Experimental study on mechanical behaviour of tubular joints. PhD thesis, Osaka University, Japan.

TWI. TWI WORLD CENTER FOR MATERIALS JOINING TECHNOLOGY. [Online] Available: *http://www.twi.co.uk/j32k/protected/band_3/jk38.html*. [Cited 24 July 2006].

van der Valk, C. A.C. 1988. *Factors controlling the static strength of tubular T-joints*. Shell Research Publication 829, Rijswijk. The Netherlands.

van der Vegte, G. J. de Koning, C. H. M. Puthli, R. S. Wardenier, J. 1991. The static strength and stiffness of multiplanar steel X-joints. *International Journal of Offshore Polar Engineering.* **1**(1), pp.42–52.

Wardenier J. 1982. *Hollow Section Joints*. Delft: Delft University Press, The Netherlands.

Wardenier, J. 2001. *Hollow Sections In Structural Applications.* [e-book]. CIDECT. Available: http://www.cidect.org/en/Publications/HPPraxis.php. [Cited July 2006].

Wilkinson, T. 1999. The Plastic Behaviour of Cold-Formed Rectangular Hollow Sections. PhD Thesis. University of Sydney, Australia.

Wilkinson, T. Hancock, J. G. 2000. Tests to examine plastic behaviour of knee joints in cold formed RHS. *Journal of Structural Engineering.* **126** (3), pp.297-305.

Yang, J.G. Lee, G.Y. 2007. Analytical models for the elliptical stiffness and ultimate moment of a double angle connection. *Engineering Structures.* **29** (4), pp.542-551

Yura, J.A. Zettlemoyer, N. Edwards, I.F. 1981. Ultimate capacity of circular tubular joints. ASCE, *Journal of the Structural Division.* **107** (ST10), pp.1965-1984.

3 Moment Rotation Behaviour

3.1 Introduction

In many steel structures, as indeed is the case with other materials, members have to be assembled with various types of connections at joints. A unified nature of classifying these joints is required and this could be either based on connection type or on joint behavior. Even though the former influences the latter, joint behavior is the most pertinent parameter for the analysis and design of structures and therefore a classification based on the joint behavior rather than the connection type has become a widely accepted way of classifying joints in steel structures. The fact that there are so many different types of connections also makes it difficult to use it as a basis for classification. Joint behavior is regarded as the response of the joint to actions imposed on it. The response to a moment load on the joint has come to be widely accepted as a method of classifying joints. Having established that, the connections can then also be classed in accordance with the type of joint response they yield. A rigid joint is associated with a fixed connection whereas connections that result in semi-rigid and pinned joints are correspondingly termed as semi-rigid and pinned connections respectively.

It is important to correctly predict the joint behavior in the analysis and design of steel structures as it influences global behavior of a structure. Failure to establish correctly the behaviour of joints may lead to incorrect design and ultimately joint failure. As Seward (1994) observes, failure of joints accounts for up to 30% of all construction failures in steel structures. In structures such as trusses and some braced frames where joints are assumed not to carry moments care must be taken to ensure that the joints exhibit enough ductility as to behave like a pinned joint. In structures such as sway frames where joints support moment transfer between connected members correct classification of the joints may lead to greater economy in member selection as well as correct analysis of the overall behavior of the structure. The choice of connection method will determine structural response at the joint and hence the type of analysis that must be carried out on the structure. Eurocode 3 (SSEDTA, 2002), for example, has three different analysis approaches based on the joint classification and these are: simple, semi-continuous and continuous analysis.

3.2 Joint Classification

Classification of joints is carried out based on the mechanism of moment transfer as well as relative movement of the connected members i.e. opening or closing under applied moment. Joints can be classified as rigid, semi-rigid or pinned (Jaspart 2000). With regards to moment transfer rigid joints are assumed to transfer the full moment between connected members, semi-rigid joints transfer only part of the moment while pinned joints are incapable of transferring any moments. Using the example of a beam column connection as shown in Fig.23 nominally rigid joints exhibit little or no relative movement between the connected members and thus transfer the full moment, semi-rigid joints exhibit a measurable opening or closing of the angle between the connected members hence transferring only part of the moment, while nominally pinned connections on the other hand exhibit an infinite opening of the angle between connected members. Fig.25 (i)-(iii) below illustrates the three types of joint behavior.

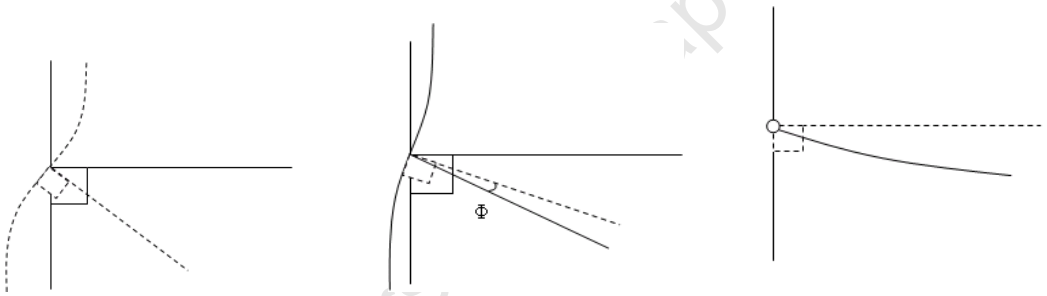

(i) Rigid joint (ii) Semi-rigid joint (iii) pinned joint

Fig. 25 Classification of joints according to moment-rotation behavior
Adapted from Jaspart (2000)

The word 'nominally' has been used for rigid and pinned joints because in reality rigid joints usually exhibit some relative rotation and pinned joints transfer some of the applied moments. However, the magnitudes are so low that they can be ignored without loss of accuracy in the analysis.

A typical plot of applied moment and relative opening of the joint is used to determine the class of the joint and is shown in Fig.26. This typical plot of applied moment (M or M_j) on a joint and the relative opening up of the connected members (Φ) is also called the moment-

rotation or M-Φ curve. The slope of the linear part of the moment-rotation, curve gives the initial stiffness of the joint ($S_{j,ini}$).

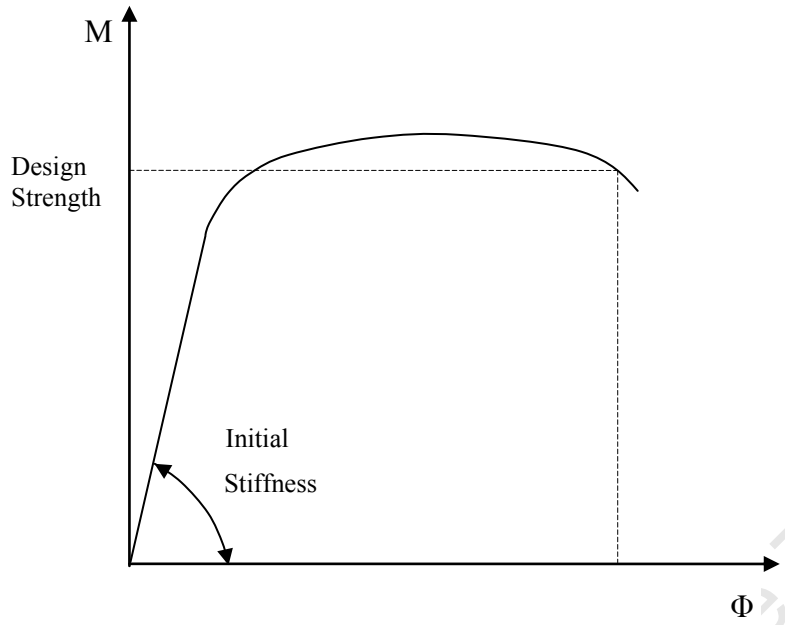

Fig. 26 A plot of applied moment vs relative opening of joint

The initial stiffness of the joint is a measure of how much the joint resists the relative rotation under loading in the elastic regime. When the stiffness is low the joint exhibits large rotations at low loading and tends towards the behavior of a pinned connection. On the other hand, when the stiffness is high the joint exhibits low rotations at high loading and tends towards the behavior of a fully fixed connection. Many joints in hollow sections exhibit a behavior intermediate between the rigid and the pinned cases (Packer, 1993) and hence are said to exhibit semi-rigid behavior.

Another important characteristic of the joint has to do with the yield moment of the joint in relation to the yield moment of the connected parts. When the yield moment (M_{Rd}) of the joint is less that that of the connected members the joint is termed as a partial-strength joint. It cannot develop the plastic moment (M_p) of the connected parts and in this case the joint would fail before the connected members. When the yield moment of the joint is higher than the yield moment of the connected members the joint is termed as a full-strength joint. In this case the connected members achieve the full plastic moment before the joint and hence are deemed to fail before the joint. The Joint classification based on stiffness and strength is shown in Fig.27.

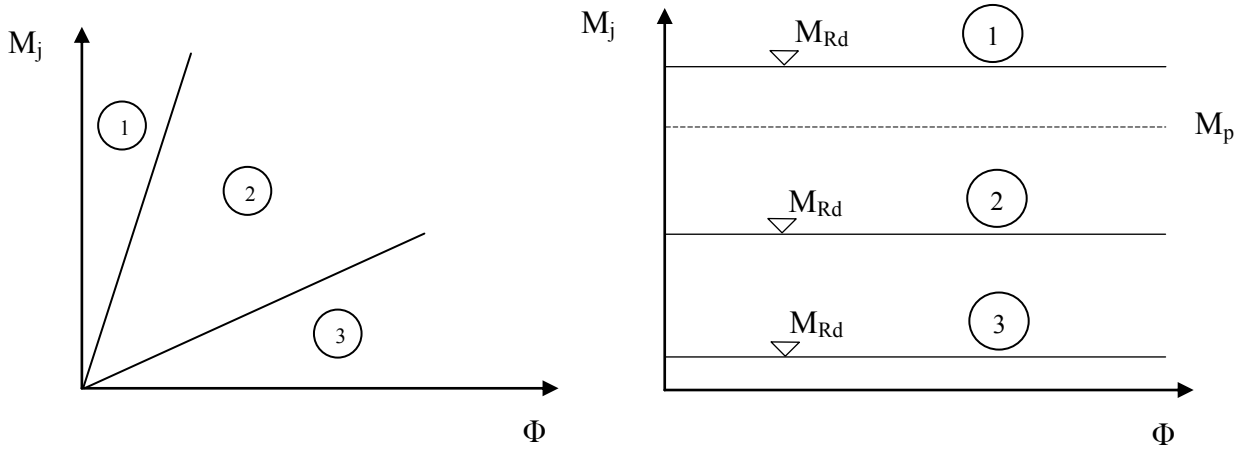

(i) Stiffness (ii) Resistance

Fig. 27 Classification of joints according to stiffness and strength adapted from (Grotmann and Sedlacek, 1998)

1. **Stiffness:**	rigid (1)	semi-rigid (2)	nominally pinned (3)
2. **Strength:**	full strength (1)	partial strength (2)	nominally pinned (3)

Another important characteristic of joints has to do with the extent of deformation the joint can sustain before ultimate failure. This is called its deformation capacity. The joints can fall broadly into the categories of 'ductile' and 'brittle' and these two will generally exhibit different deformation behavior and to some extent govern modes of failure.

It is therefore clear that from a structural point of view the three most important parameters defining the performance of a joint are strength, initial stiffness and deformation capacity (Jaspart 2000). Chisala (1999) suggests that all three parameters can be obtained from a typical plot of the M-Φ curve of a joint. He further states that the M-Φ curve is sensitive, for any given joint, to material properties as well as dimensional properties of the connected members. This observation is quite evident from the design codes which have different moment resistance formulae for the different classes based on parametric ranges of hollow section joint configurations.

3.3 Classification schemes

Two of the most widely used classification schemes are the EC3 or Eurocode 3 (SEEDTA, 2002) approach as well as the Bjorhovde approach proposed by Bjorhovde *et al* (1990) for

beam-column joints. Though particularly developed for beam-column joints these approaches may be extended to other moment resisting joints, albeit with some care. Both approaches make use of the three classifications based on joint behaviour presented in 3.2. In both approaches the classification is based on the initial stiffness of the joint as well as its moment resistance in relation to that of a connected member. With the Bjorhovde approach the connected member would be the beam whereas as with EC3 it would be the connected part with the least design resistance (SEEDTA, 2002: Lecture 15, pp17). A more detailed look at each approach is presented.

3.3.1 Eurocode 3

Eurocode 3 pre-supposes that the designer is aware of or has already decided on the beam member lengths for the frame to be designed. A further distinction is made between joints in braced frames and those in unbraced frames.

Classification by stiffness:

Rigid joint $S_{j,ini} \geq 25\frac{EI}{L}$ (unbraced frame)

(3.1)

$S_{j,ini} \geq 8\frac{EI}{L}$ (braced frames)

(3.2)

Semi-rigid joint $0.5\frac{EI}{L} < S_{j,ini} < 25\frac{EI}{L}$ (unbraced frame)

(3.3)

$0.5\frac{EI}{L} < Sj,ini < 8\frac{EI}{L}$ (braced frames)

(3.4)

Pinned joint $Sj,ini \leq 0.5\frac{EI}{L}$

(3.5)

Classification by strength:

Full-strength joint $M_{j,Rd} \geq M_{full-strength}$

(3.6)

Partial strength joint $0.25M_{full-strength} < M_{j,Rd} < M_{full-strength}$

(3.7)

Pinned joint $M_{j,Rd} \leq 0.25M_{full-strength}$

(3.8)

$\frac{EI}{L}$ = flexural stiffness of the connected beam

$M_{full-strength}$ = design resistance of the weaker of the connected member

3.3.2 Bjorhovde Scheme

Unlike the EC3 approach, with the Bjorhovde scheme the length of the beam need not be known in advance in order for the classification to be made. A member size does however need to be known or assumed. This is because the Bjorhovde approach uses the beam depth rather than its length in the classification scheme. This is particularly useful for researchers who investigate isolated joints as well as for designers when the actual size of the structure is not yet known. The scheme further has an advantage of taking ductility into consideration. The classification scheme is presented below:

Classification by stiffness:

Semi-Rigid Joint $0.5 \leq \frac{\overline{m}}{\overline{\theta}} \leq 2.5$

(3.9)

where, $\overline{m} = \frac{M}{M_p}$ and $\overline{\theta} = \frac{\theta_c}{\left(5M_p d / EI_b \right)}$

M_p, d and I_b are the plastic capacity, depth and moment of inertia of the connected beam respectively while θ_c is the connection rotation associated with the moment M.

Classification by strength:

Full-strength joint	$M_{j,Rd} \geq 0.7M_{full-strength}$	(3.10)
Partial strength joint	$0.2M_{full-strength} < M_{j,Rd} < 0.7M_{full-strength}$	(3.11)
Pinned joint	$M_{j,Rd} \leq 0.2M_{full-strength}$	(3.12)

This therefore means the Bjorhovde approach is less stringent in its classification of a rigid joint based on strength by placing the cut-off at 70% of the full strength. EC3, in contrast, defines a rigid joint as one that achieves the full-strength.

3.4 Ultimate strength

Most experimental tests for moment-rotation carried out on hollow sections joints yield M-Φ curves that show non-linear behaviour characterised by ultimate yield at large rotations. As such large rotations cannot be tolerated in most structures this ultimate yield load cannot be used in a design context. A unified definition of the ultimate strength for hollow section joints becomes important to define for design purposes. In cases where the curve shows peaks the first peak is taken as the ultimate strength. The challenge arises when the relationship shows no peaks at all. In such a case two approaches are currently used to determine the ultimate strength of hollow section joints. Lu *et al* (1994) define the ultimate strength based on chord flange indentation deformation of $0.3\%d_o$. This approach has been adopted widely. Another approach developed by Yura *et al* (1981) is based on a strain approach. The deformation limit proposed is defined by a rotation of $80f_y/E$ for the ultimate strength.

It is worth noting that for design purposes the strength values obtained from the methods outlined above are not directly used as the design values. Appropriate factors are applied in order to come up with the design values.

3.5 Conclusion

Although a detailed review on the merits of using semi-rigid joints has not been given; other researchers have covered the topic in great detail. However, a clear approach to determining

the class of joint has been given. Once the classification is done insight into the behaviour of hollow section joints under moment loading can be obtained making the route to a simplified design approach much clearer.

REFERENCES

Bjorhovde, R. Brozzetti, J. and Colson A. 1990. A Classification System for beam to column connections. *Journal of Structural Engineering*, ASCE. **116** (11), pp.3059-76.

Chisala, M.L. 1999. Modelling M-Φ curves for standard beam-to-column connections. *Engineering Structures.* **21** (12), pp.1066 – 1075.

Grotmann, D. Sedlacek, G. (1998). *Rotational stiffness of welded RHS beam-to-column joints. Final Report – Project 5BB-8/98*. Institute of Steel Construction. RWTH – Aachen.

Jaspart, J.P. 2000. General Report: session on connections. *Journal of Constructional Steel Research.* **55** (1-3), pp.69 – 89.

L.H. Lu, G.D. de Winkel, Y. Yu and Wardenier, J. (1994). *Deformation limit for the ultimate strength of hollow section joints.* In: Grundy, P. Holgate, A. and Wong, M.B. Editors, Tubular structures VI, Balkema, Rotterdam. pp. 341–347.

Packer, A.J. 1993. Moment Connections between Rectangular Hollow Sections. *Journal of Constructional Steel Research*. **25** (1-2), pp.63 – 81.

Seward, D. 1994. *Understanding Structures, Analysis, materials, design.* Hong Kong: THE MACMILLAN PRESS LTD.

Structural Steel Eurocodes – Development of a Trans-national Approach (SSEDTA). 2002. *A Training package for the teaching of Eurocodes 3, 4* [CD].

Yura, J.A. Zettlemoyer, N. Edwards, I.F. 1981. Ultimate capacity of circular tubular joints. ASCE, *Journal of The Structural Division.* **107** (ST10), pp.1965-1984.

4 Experimental Tests

4.1 Introduction

The experimental procedure to determine the moment-rotation joint behaviour was carried out for both CHS and RHS specimens. The RHS specimens include a 'bird beak' (BB) configuration. In a bird beak joint configuration either the brace or chord is rotated through an angle. In this case the brace was rotated through 45^0 as shown in Fig.30.Tests were carried out on three (3) joint configurations:

Welded T-joints
Welded X-joints and,
Welded X Bird beak joints

T- and X-joint configurations are shown in Fig.28 to Fig.30

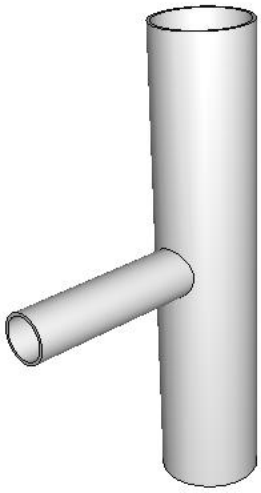

Fig. 28 CHS T-joint

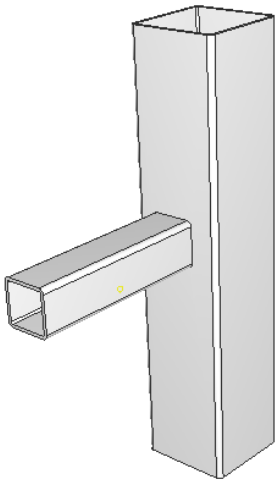

Fig. 29 RHS T-joint

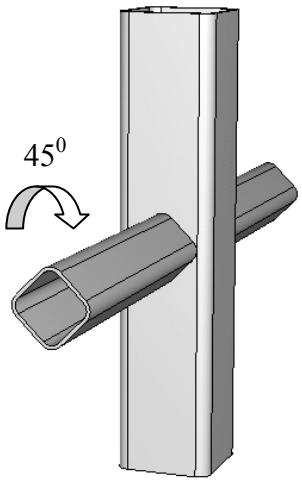

Fig. 30 BB X-joint

With the birdbeak joint, it is very similar in configuration to the ordinary RHS joint except either the connecting or the main member is rotated through an angle. The tests were carried out in order to determine the M-Φ behaviour of the specimens.

4.2 Test specimens

A total of fifteen (15) specimens were tested. The main member, also called the chord, onto which the secondary or brace members were welded was kept at constant cross-section dimension of 76.2mm x 76.2mm for RHS and diameter of 76.2mm for CHS. The sizes of the brace members were varied with three sizes being employed for both the RHS and CHS. All main and secondary members had a thickness of 2.5mm.

For the joint nomenclature a system of defining the joint based on the size of the connecting member was adopted. This is because, as mentioned earlier, the main member size was kept constant. Therefore in the nomenclature adopted a letter defining the joint type is followed by a two-digit number which gives the nominal size of the connected member. For instance, an RHS X-joint with a connected member size of 38.1mm x 38.1mm is labelled as an RHS X-38 joint. A list of all the specimens investigated is presented in Table 7.

Table 7: Joint test specimens

Joint Label	Brace Dimension (mm)	Chord Dimension (mm)
RHS		
X38	38.1 x 38.1 x 152	76.2 x 76.2 x 360
X65	63.5 x 63.5 x 220	76.2 x 76.2 x 360
X76	76.2 x 76.2 x 220	76.2 x 76.2 x 360
T38	38.1 x 38.1 x 152	76.2 x 76.2 x 360
T65	63.5 x 63.5 x 220	76.2 x 76.2 x 360
T76	76.2 x 76.2 x220	76.2 x 76.2 x 360
CHS		
X38	38.1 x 152	76.2 x 360
X50	50.8 x 220	76.2 x 360
X76	76.2 x220	76.2 x 360
T38	38.1 x 152	76.2 x 360
T50	50.8 x 220	76.2 x 360
T76	76.2 x220	76.2 x 360
BIRDBEAK		
BB X38	38.1 x 38.1 x 152	76.2 x 76.2 x 360
BB X65	63.5 x 63.5 x 220	76.2 x 76.2 x 360

Mechanical properties for the test specimens were determined through a tensile test. The test was carried out using a Zwick 1484 machine fitted with a 200kN capacity load cell. The specimens for the test coupons were standard size for both curved and flat profile; prepared according to British Standard (BS) 18 specification. Key material properties obtained from the tensile test are presented in Table 8.

Table 8: Material property of the joint components from tensile test

Component	$\sigma_{0.2\%}$ **(MPa)**	σ_u **(MPa)**	**Elongation**
CHS specimen	338	366	33%
RHS specimen	344	380	33%

Having determined the material properties the specimens were then fabricated by welding the members with a 5mm fillet weld using MIG welding technique. Profiling was required for the CHS joints in order for the members to fit together.

The geometrical joint properties of the specimens are presented in Table 9 below and the symbols are defined in accordance with Fig.23. Effort was made to keep the brace lengths to a minimum so that the moment effect would be carried by the joint and not be partially lost in flexure of the brace. The thickness of both brace and chord members was the same as can be seen from a value of τ equal to 1.

Table 9: Geometric properties of test specimens

		Joint Parameters					
Label	β	γ	τ	α	l_o *(mm)*	l_1 *(mm)*	d_o/h_o *(mm)*
T38	0.5	15.24	1	9.45	360	154.2	76.2
T50	0.66	15.24	1	9.45	360	218	76.2
T65	0.83	15.24	1	9.45	360	220	76.2
T76	1	15.24	1	9.45	360	195	76.2

The geometrical properties are similar for X-joint specimens as well.

4.3 Test set-up

The test set-up used for T-joints is shown in Fig.31. A Denison general purpose testing machine was used for the test. A test rig was designed to ensure that the vertical member was held rigidly so that only the brace member was able to move. The brace member was also kept short in order to have movement only at the joint and eliminate effects from flexure in the brace member.

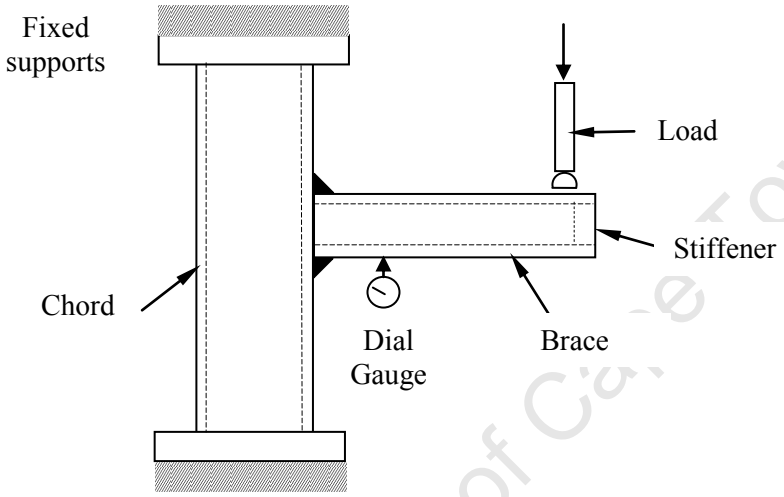

Fig. 31 Experimental test configuration for T-joint tests

For the X-joint specimen a different scheme was employed in order to ensure simultaneous loading of both brace members. An Amsler general purpose testing machine was used. Loading rams equidistant from the opposite faces of the chord were used to load the brace members. Dial gauge readings for one brace member were taken and used to determine the vertical deflection, and subsequently angular deflection, of the brace member. The test set-up employed is shown in Fig.32.

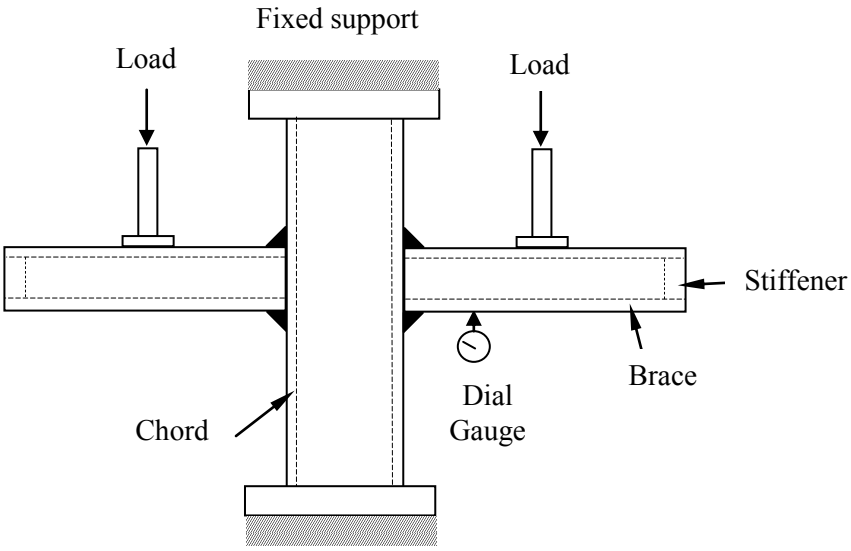

Fig. 32 Experimental test configuration for X-joint tests

Vertical deflection in both cases was measured using a dial gauge and the values then converted to angular rotation. The bottom part of the brace member is therefore used as the reference for determining the change in angle of the brace member. The joints were loaded to failure in both cases so that both the initial stiffness and ultimate moment could be determined. Readings were taken at regular interval during the loading. The intervals were adjusted depending on the size of the chord member. Since the smaller brace members were anticipated to fail at lower load a finer interval was employed for them. Loading rate was kept the same in all cases. The failure modes were noted for all specimens.

4.4 Failure modes

The most prevalent failure modes observed were local buckling failure of the chord and weld failure at the joint, modes (i) and (ii) respectively presented in Chapter 2.7. Observed failure modes for T-joints are shown in Fig.33 to Fig.36.

Fig. 33 Brace deflection at failure in a CHS member

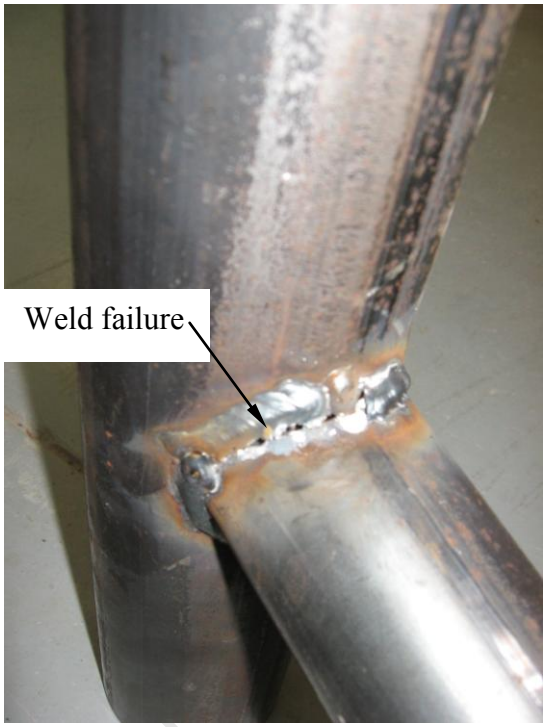

Fig. 34 Weld failure in a CHS member

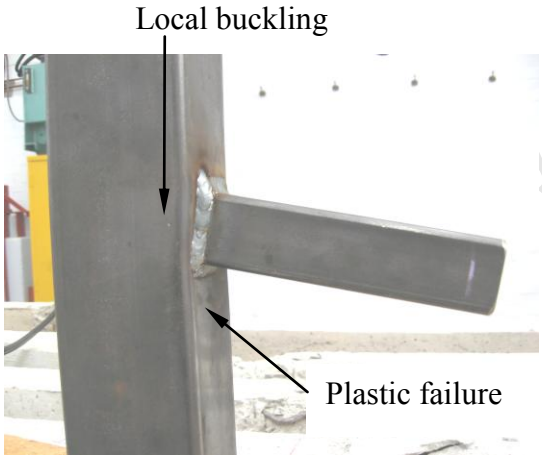

Fig. 35 Brace deflection at failure in a RHS member

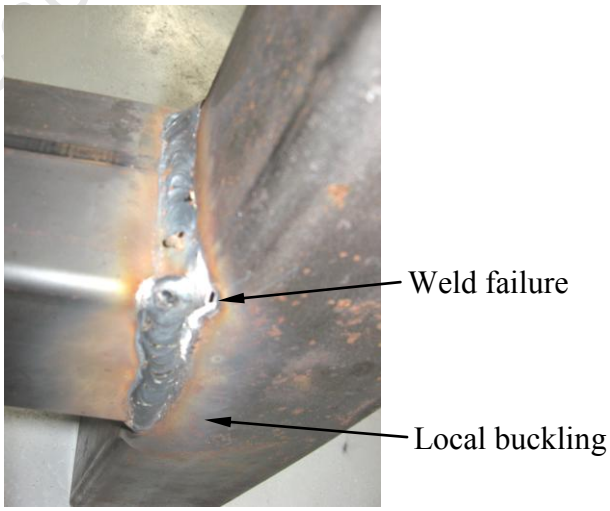

Fig. 36 Weld failure in a RHS member

Observed failure modes for X-joints are shown in Fig.37 to 39.

Fig. 37 Weld failure in CHS X-joint

Fig. 38 Bird beak X-joint at failure

Fig. 39 Weld failure in a RHS X-joint

4.5 Moment-rotation plots

A plot of the results obtained from the experiments is shown from Fig.40 to Fig.44.

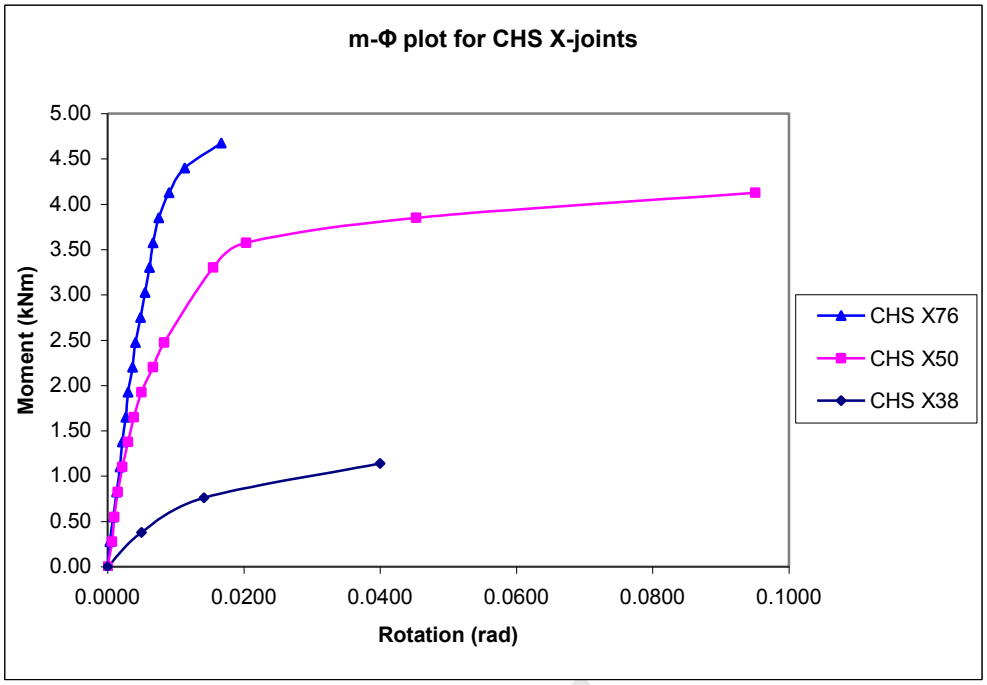

Fig. 40 Results for CHS X-joint tests

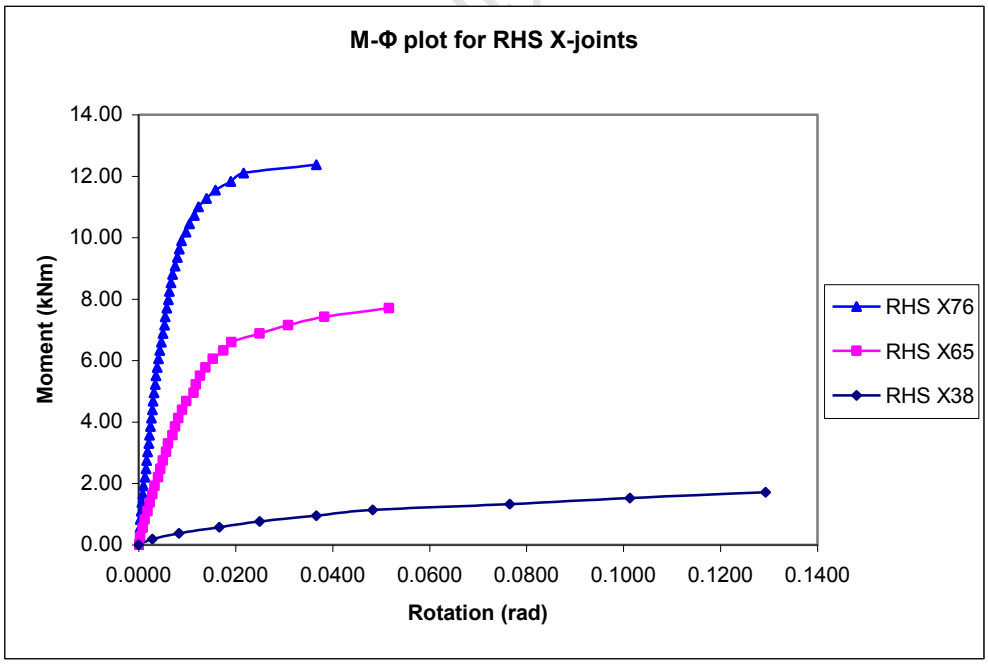

Fig. 41 Results for RHS X-joint tests

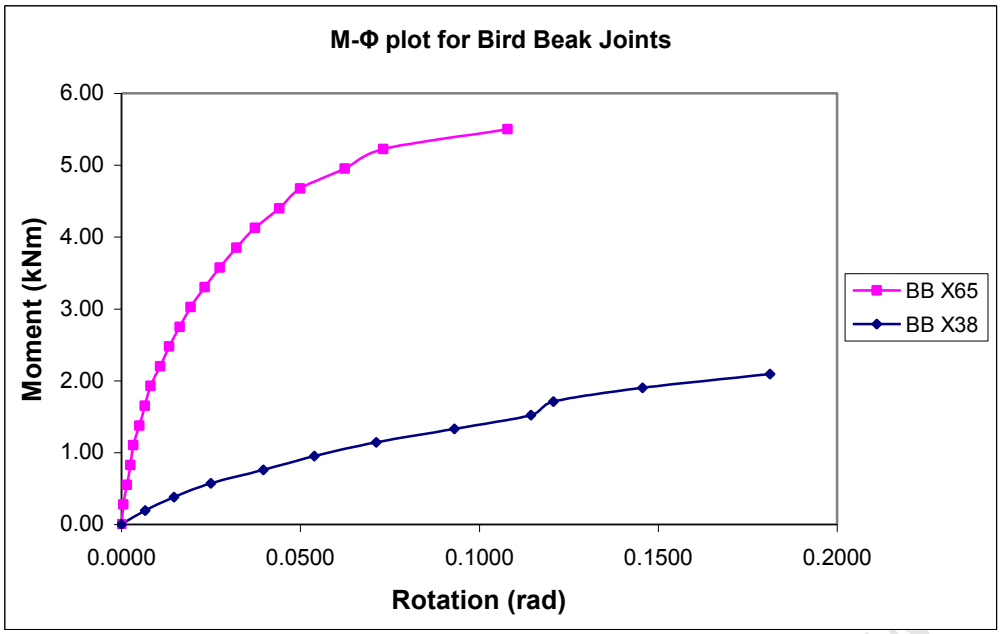

Fig. 42 Results for bird beak X-joint tests

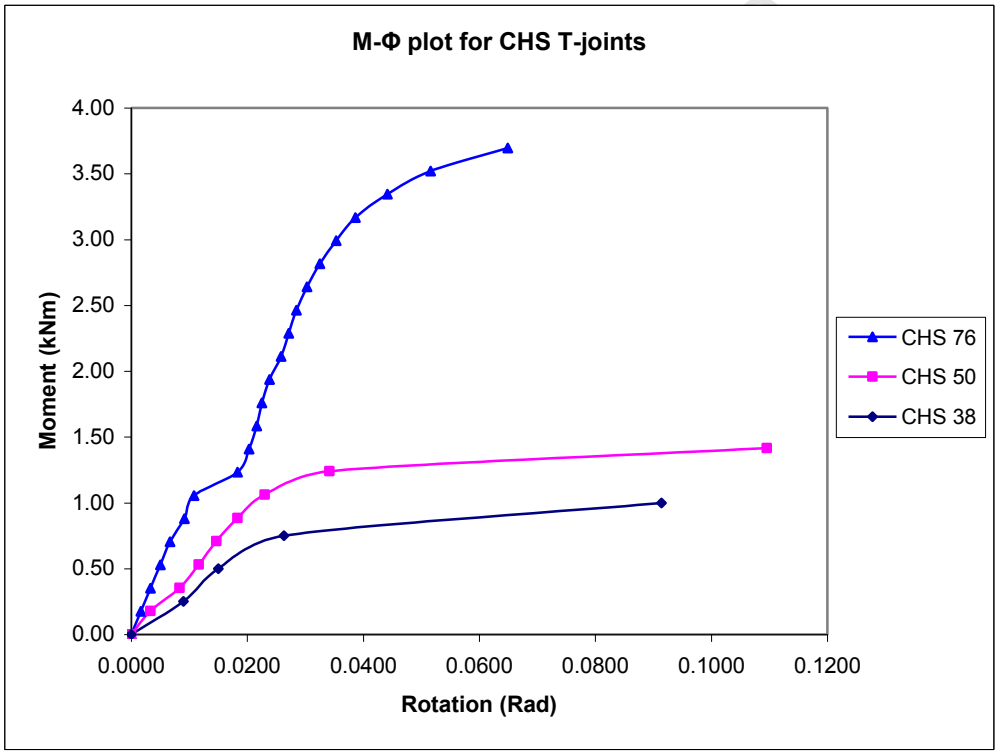

Fig. 43 Results for CHS T-joint tests

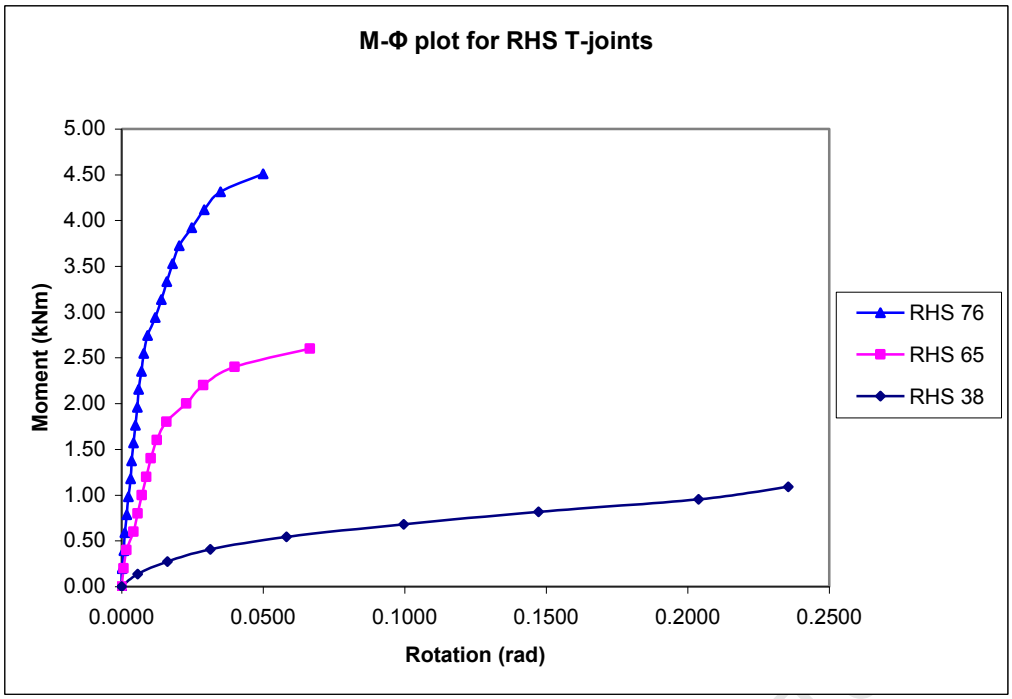

Fig. 44 Results for RHS T-joint tests

From the plots obtained a relatively smooth M-Φ relationship is observed. Joints with greater initial stiffness generally failed at relatively low rotations whereas the joints having a lower initial stiffness exhibiting greater rotation before failure. In light of this trend it can be concluded that the lower the β value the greater the rotation obtained before ultimate failure. The only exception noted was with the CHS X50 joint and this could be attributed to the welds which may have had deeper penetration than was the case with the other CHS joints where a weld failure was the predominant failure mode. With the lower β values the initial stiffness of the joint becomes rather difficult to predict as the curve is quite flat.

The bird beak BB X38 joint as well as the CHS T-76 joints showed kinks in the graphs plotted. This error could be attributed to some readjustment that took place within the testing equipment while loading the joint or some readjustment in the measuring instruments. For the CHS joint the portion after the kink was used to determine initial stiffness as the kink occurred at a low rotation. For the BB X38 joint the kink occurs at a later stage hence the portion before the kink was used. Joint characteristics obtained from the M-Φ plots are presented in Table 10. The Bjorhovde scheme of joint classification is applied.

Table 10: Joint characteristics obtained from experimental tests

Joint Label	Initial Stiffness (kNm/rad)	Ult. Moment (kNm)	Joint Classification	
RHS				
X38	45.8	1.60	Semi-Rigid	Full -strength
X65	550.0	7.60	Semi-Rigid	Full -strength
X76	1476.0	12.4	Rigid	Full -strength
T38	16.7	0.75	Pinned	Partial -strength
T65	138.0	2.60	Semi-Rigid	Partial -strength
T76	336.0	4.51	Semi-Rigid	Full -strength
CHS				
X38	76.0	1.20	Semi-Rigid	Full -strength
X50	460.0	4.20	Rigid	Full -strength
X76	605.0	4.70	Rigid	Full -strength
T38	33.3	1.00	Semi-Rigid	Full -strength
T50	48.3	1.42	Semi-Rigid	Full -strength
T76	154.0	3.70	Semi-Rigid	Full -strength
BIRDBEAK				
BB X38	22.8	1.70	Pinned	Full -strength
BB X65	276.0	5.50	Semi-Rigid	Full -strength

In determining the ultimate moment most joints were found to fail before reaching the Yura deformation limit given by $80\,f_y/E$ which translates to a rotation of 0.136rad. Only the RHS T-joint and the bird beak X38 joints had excessive joint rotations such that the deformation limit had to be applied in order to determine the ultimate moment.

Most of the joints tested exhibit semi-rigid joint behaviour with full-strength achieved. Only the T38 RHS joint showed pinned behaviour and this is expected of a joint with low β value. Only three joints were classified as rigid and these all fell under the X-joint configuration; one being an RHS and the other two CHS joints. This suggests that X-joints exhibit greater stiffness than corresponding T-joints with similar geometry for brace and chord. This is further validated by the observation that initial stiffness values in the X-joints are higher than for corresponding T-joints. In comparing between RHS and CHS joints it was observed that the RHS joints have a greater initial stiffness for high β values whereas the CHS joints have higher initial stiffness for low β values.

The initial stiffness of the bird beak joints is generally higher than the corresponding RHS T-joints but lower than the RHS X-joints. Therefore the joint configuration of the bird bead joints tested gives an intermediate stiffness between that of the RHS X-joint and that of the RHS T-joint. In comparing with the CHS joints only one at low β value could be made. It is observed, as was the case with the RHS joints, that the CHS joint gives a higher initial stiffness.

4.6 Conclusion

The moment-rotation relationship for T and X-joints described in 4.1 has been presented and the joint properties from the specimens determined. A clear trend shows that for a given thickness of SHS the joint stiffness as well as ultimate strength is affected by the brace-chord ratio given by the parameter β. The joints are observed to predominantly exhibit semi-rigid behaviour. The Bjorhovde classification scheme has been used to classify the joints. A clear difference between the X and T-joint behaviour has also been observed. Because all the physical components of an actual joint are present in the specimens a clear picture of the joint failure modes is also obtained.

Only two joints were found to have sufficiently large rotations to employ the Yura deformation limits. The two joints both had low values of β. All other joints failed before reaching the deformation limit.

REFERENCES

British Standards Institute. (1987). *BS 18: Method for tensile testing of metals (including aerospace materials)*.

5. Finite Element Modelling

5.1 Introduction

Finite element (FE) modelling has grown into a very powerful and useful tool in contemporary research because of its capabilities and economy. Whereas experimental parametric tests are expensive to carry out, once a FE model is correctly calibrated large scale parametric tests can be carried out. Test conditions can usually be easily and correctly simulated in the FE model. However, to obtain accurate results a good understanding of finite element theory is required. Also key is knowledge on the capabilities as well as practical limitations of the software employed. In this study the general purpose analysis software ABAQUS (HKS, 2004) is used.

5.2 FE Modelling

Finite element modelling involves a number of operations which have to be carefully carried out in order to come up with a model that gives meaningful results. If anyone of these steps is not carried out with careful thought the accuracy of the solution may well be affected. The main steps involved are

- Generation and assembly of model
- Definition of material properties and analysis type
- Application of appropriate boundary conditions
- Specify load type and application method
- Discretisation and meshing
- Analysis
- Post-processing

The first step is where a 2D or 3D representation of the physical model is generated and this must represent to a great degree the geometry of the item being modelled or the separate parts to be later assembled in an assembly module of the software. Though ABAQUS is a powerful analysis software, model generation can be difficult as it does not have advanced draughting capability that would render easy generation of complex models or intricate features like 3D

welds. Researchers like Qian *et al* (2007) have used MSC Patran to generate the FE models which are then analysed using ABAQUS.

Material properties to be defined will usually depend on both the material of the model as well as the analysis type to be used. For instance for steel the modulus of elasticity, Poisson's ratio and yield stress are sufficient parameters for a linear analysis. In addition to these parameters an indication of plastic strains from the stress-strain relationship would be necessary to carry out an elastic-plastic analysis. Various types of linear and non-linear analyses are supported in ABAQUS.

Boundary conditions and loading types must simulate as much as possible the conditions that the model would be subjected to in its physical application or test condition. The model is then discretised to come up with a mesh density. Generally the more finely meshed the model the more accurate the result. However, the computational time also increases with increase in mesh density. Once the element type has been selected the model is then meshed. ABAQUS has an extensive element library that caters for, among others, solids and shell models. Elements typically have nodes where the boundary conditions are specified and loads can be applied. These nodes may also have various degrees of freedom. Mathematical computations from which results are derived are computed at integration points which in many cases lie on the nodes. The number of nodes on an element therefore has a significant bearing on the nature and accuracy of the results.

Once the analysis is done the right type of results output is required in order to have a correct interpretation. ABAQUS has options of printable tabulated output as well as a 'visualisation' module that allows output to be viewed in a graphical form.

5.3 FE Models

As stated in 5.1 the general purpose analysis software ABAQUS (HKS, 2004) is used for modelling the SHS joints. The different components of the joints were generated in the parts module of the software and assembled in the assembly module. The models were generated in 3D. 3D Welds were not modelled as they could not be generated in the parts generation module of the software. The components were therefore simply merged at the joints to

simulate the fusion that an ordinary weld would produce. The brace and chord therefore acted as though fused into one member. The ends of the brace members were given a rigid end cap to prevent loss of initial geometry at the brace ends due to instability phenomenon during the loading phase. This was also to simulate experimental conditions where the brace ends had end caps welded on.

Since a non-linear elastic-plastic analysis was used parameters for the material behaviour in both the elastic as well as plastic range had to be input in the software. Values of E = 200GPa, f_y = 340MPa and ν = 0.3 were used in the material property definition. Plastic strains in the plastic region ware entered as shown in Table 11 based on results from the tensile tests mentioned in 4.2.

Table 11: Plastic material properties used in FE models

Yield Stress (MPa)	**Plastic Strain**
340	0
385	0.07
435	0.152

The load was applied as a moment on the rigid end cap and the brace was restrained from sideways displacements so that only vertical movements were allowed in the brace member. The displacement of the brace was used to determine the rotation at the joint for the given loadings. The output of results was then obtained from the visualisation module after running the analysis.

Three different element types were employed in the analysis; solid, discrete rigid and shell elements. Solid elements typically used are the 8-noded linear brick element with reduced integration and hourglass control (C3D8R in the ABAQUS library). To a lesser extent the 20-node quadratic element C3D20R was also employed. This element is a higher order element and hence costly on computation time particularly with fine mesh. The C3D8 and C3D20, which are fully integrated elements, are shown in Fig. 45 with node configuration.

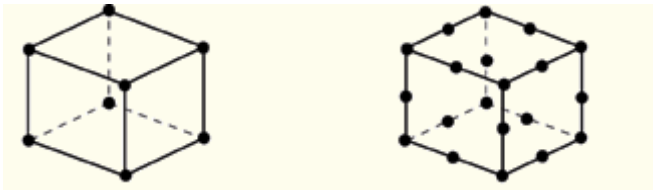

Fig. 45 C3D8 and C3D20 Solid elements
[Adapted from ABQUS (2004)]

The reduced integration elements have the same arrangement of nodes but use one fewer integration point in each direction.

Four node general purpose quadrilateral elements (S4R in the ABAQUS library) were employed for the shell models. This element is a general purpose shell element that can be applied with both thick and thin shells. Finite membrane strains as well as large rotations are accounted for. Shell elements typically model the mid-surface of the element, as shown in Fig. 46, and therefore the thickness of the element being modeled is input as a material property.

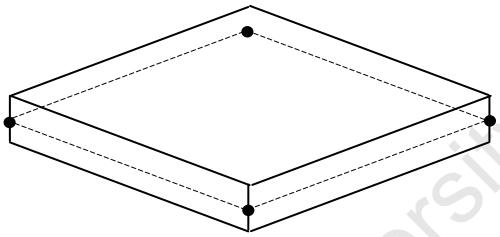

Fig. 46 Four node shell element representation showing nodes

Discrete rigid elements used for the end caps were four-node 3D quadrilateral elements (R3D4 in the ABAQUS library) shown in Fig. 47. These elements are unique from the others in that they have a unique rigid body reference node. The motion of the element is described using this unique reference. Boundary conditions are also prescribed at the reference node though the element interacts with other adjacent elements through its four nodes.

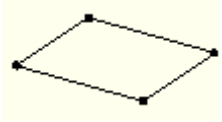

Fig. 47 Four node discrete rigid quadrilateral element

A relatively fine mesh was used for the models. No refinement of mesh was done at the joint as would be expected in a stress analysis. The deflection at the end of the brace was the

important parameter required to determine the overall race rotation for each applied moment. The model had to be run for each value of applied moment and a corresponding value of deflection obtained. Two FE models are shown in Fig. 48 and 49 for RHS and CHS respectively.

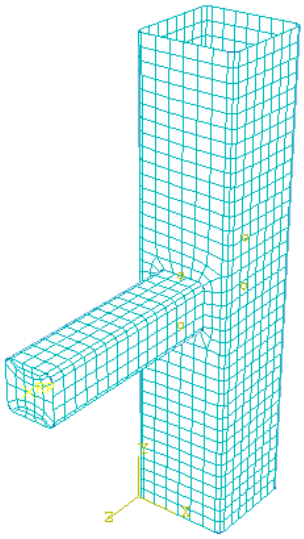

Fig. 48 RHS shell model

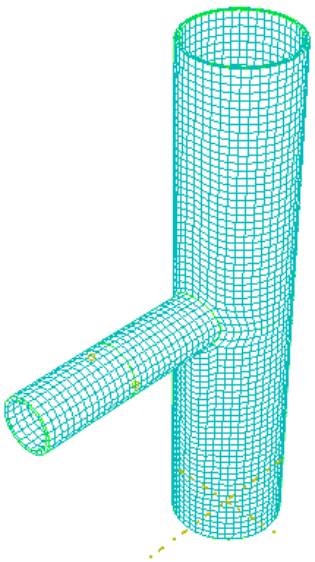

Fig. 49 Solid CHS model

5.3.1 Post processing

The rotation of the brace was determined from geometry after obtaining the vertical deflection at the end of the brace. In order to capture the brace deflection a point was defined as a 'set' on the rigid body reference node which had been defined at the midpoint of the rigid brace stiffener. The ***history output*** file was set to record the displacement of the defined point with each applied load so that its displacement could be tracked and the brace rotation determined. The results from the history output file were viewed in the 'visualisation' module of the program. From the results obtained the M-Φ curve was then plotted.

Fig.50 shows a typical representation of some results for a CHS joint as seen in the visualization module of ABAQUS. Although this particular view shows Von-Mises stresses in the joint the deflection of the brace is particularly apparent.

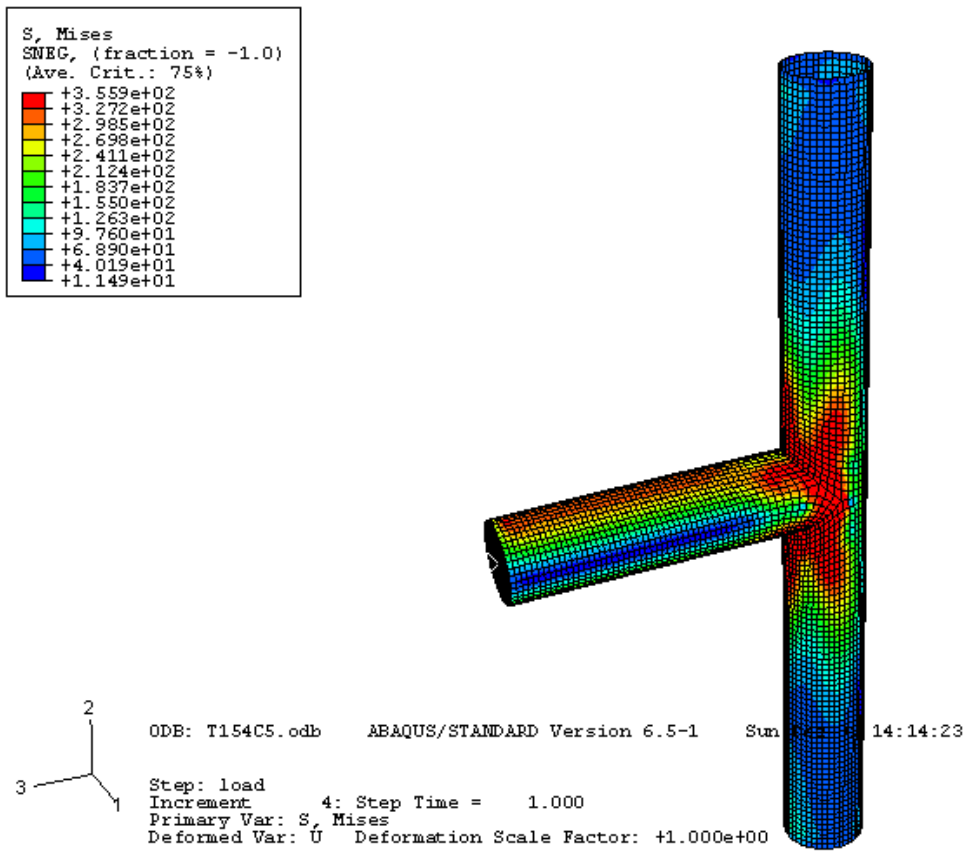

Fig. 50 CHS joint showing results in the post-processing 'visualization' module of ABAQUS

It is worth noting from the figure that the rotation of the brace results in high stresses at the joint and this would explain why weld failure occurs as one of the failure modes in some of the joints.

5.4 Calibration of model

Having already obtained the experimental results an effort was made to come up with FE models for the three different joint types used in the experimental work; CHS, RHS and RHS Birdbeak. For the RHS T-joint an attempt was made to employ a half-model that could take symmetry into account as well as a full model using solid 8-noded C3D8R elements. Both gave a crude estimation as can be seen in Fig.51 and 52 with the FEM model failing to reach the ultimate moment obtained in the experimental tests.

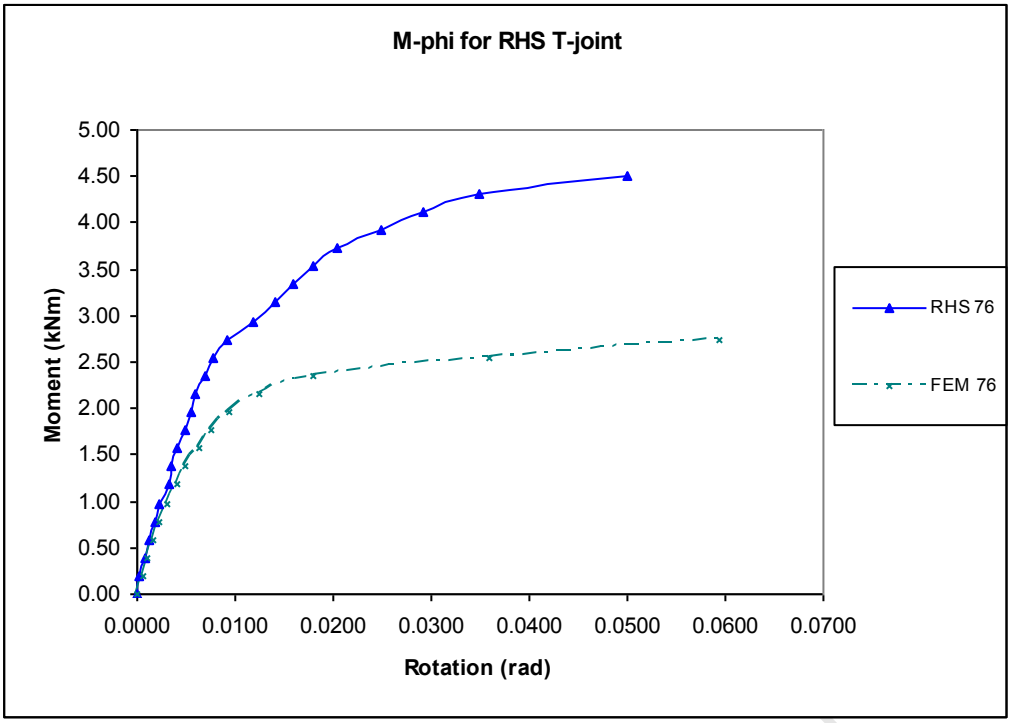

Fig. 51 Calibration of RHS T-joint using a half model employing solid elements

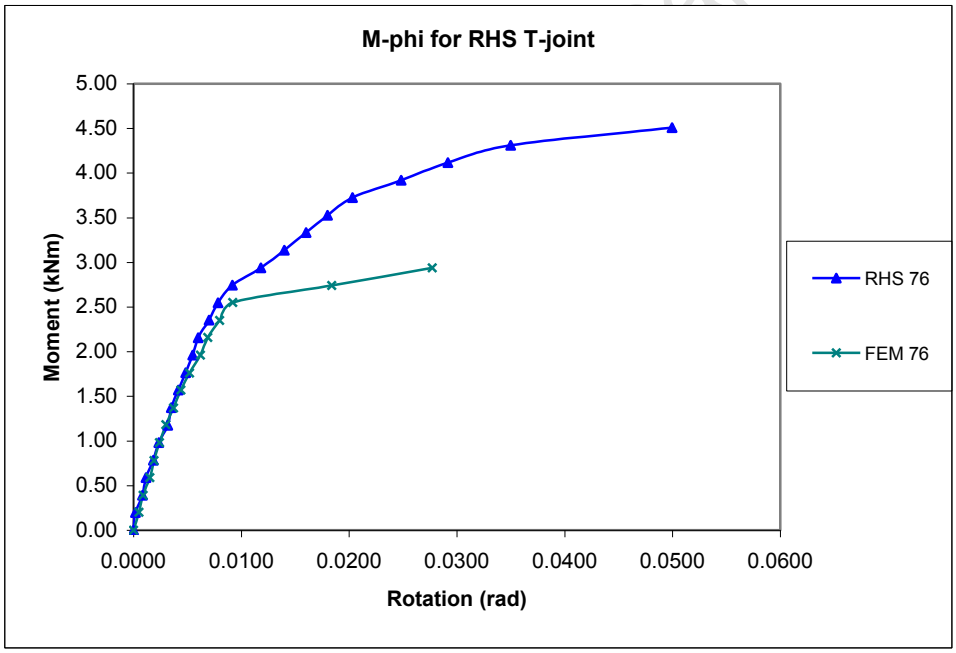

Fig. 52 Calibration of RHS T-joint using a full model employing solid elements

A full model for the CHS T-joints employing C3D8R elements gave a better correlation as seen in Fig. 53 with ultimate moments predicted fairly accurately by the models. It is likely that the kink on the T76C plot could be attributed to an error in the experimental procedure as the plot after the kink appears to follow a similar profile to that obtained from the FE model.

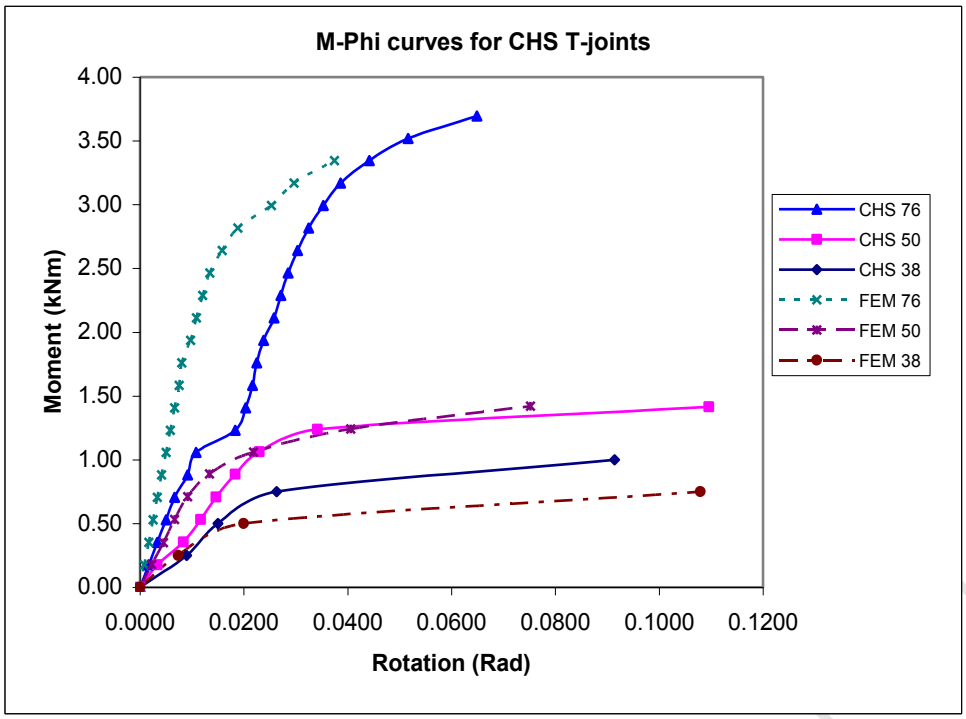

Fig. 53 Calibration of CHS T-joints using solid elements

A further calibration using full models and employing shell elements was undertaken for both RHS and CHS T-joints. The four noded quadrilateral element with reduced integration; S4R in the ABAQUS library, was employed. The results gave a better correlation as shown in Fig. 54 and 55.

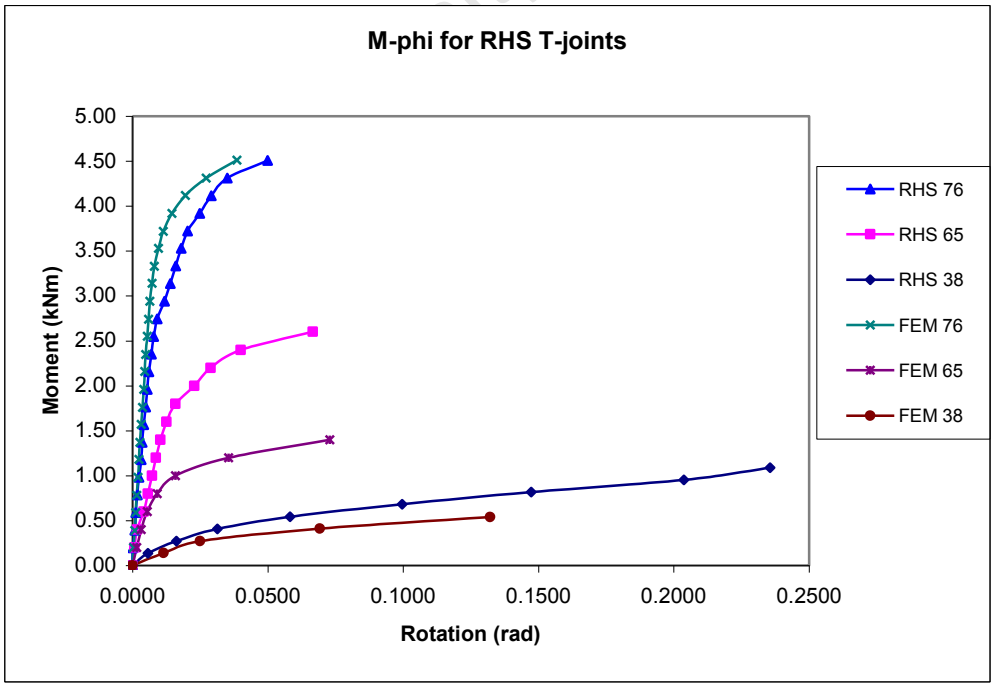

Fig. 54 Calibration of RHS T-joints using a full model employing shell elements

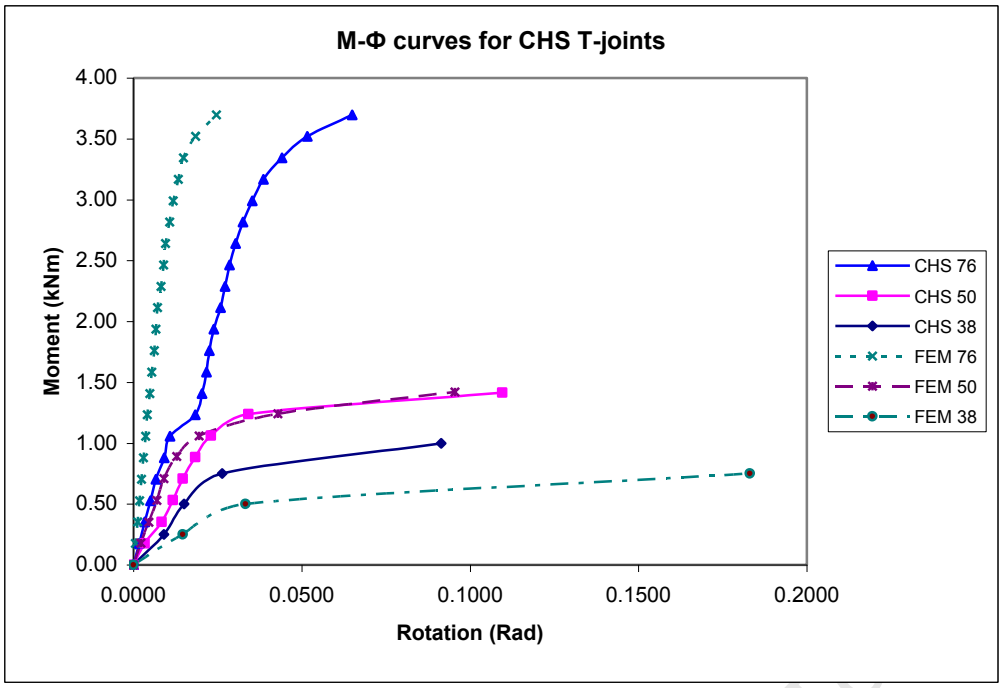

Fig. 55 Calibration of CHS T-joints using shell elements

The shell model was observed to produce smooth plots and hence was preferred to the solid model. However, since the RHS model did not predict the ultimate moment accurately for the T65 joint it was decided that a parametric analysis be carried out only for the CHS joints as the CHS model predicted the ultimate moments fairly accurately for all the T-joints. In addition the model was to be calibrated against work done by other researchers to ensure it was reliable.

The Bird beak X-joint model employing shell elements failed to capture the relationship obtained from the experimental results as can be seen in Fig. 56. This could be attributed to lack of 3D welds in the model which may have given the specimen additional initial stiffness in the experimental procedure.

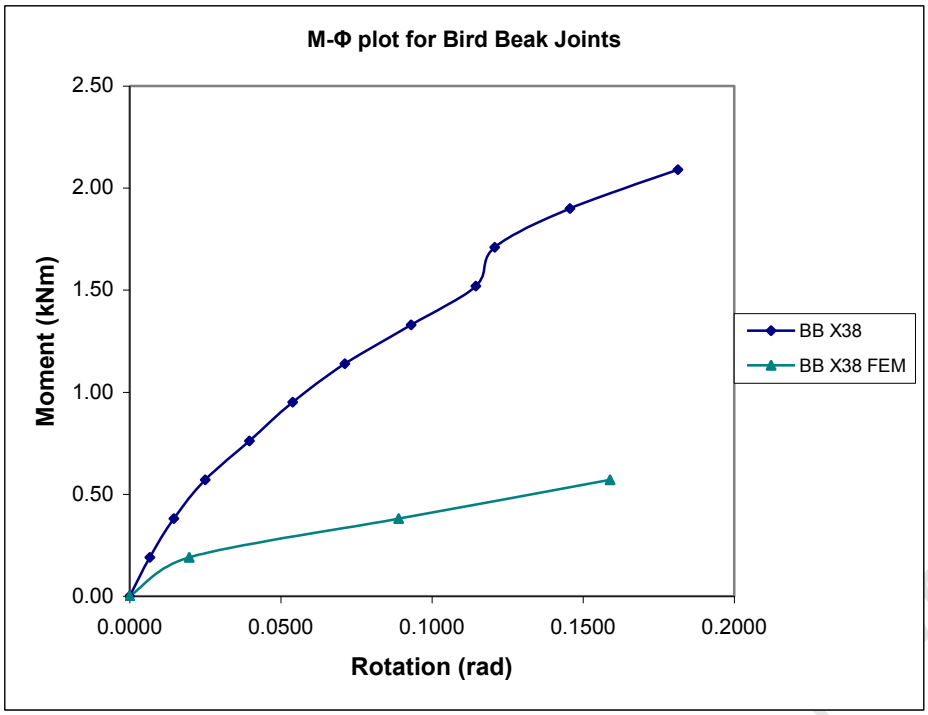

Fig. 56 Calibration of Bird beak X-joint using shell elements

Generally the inaccuracies in initial stiffness and ultimate moment for the RHS and Bird beak models could be attributed to the welds not being incorporated in the FE models. Owing to this only the CHS model was used to carry out the parametric analysis and develop an example design table for CHS joints.

For the CHS T-joint results it must be mentioned that although there was a slight difference in the initial stiffness obtained from the FEM and that from experimental results this could be attributed to inaccuracies in the experimental procedure as can be noticed from the kink on the CHS 76 curve obtained form the experimental test.

The CHS shell model was further calibrated against results for T-joints obtained by Jubran and Cofer (1995) who carried out numerical modelling of CHS tubular joints under moment loading. The only differences with the two models are that Jubran and Cofer (1995) used 20-noded and 15-noded solid elements to model the transition and welds respectively. The brace and chord were modelled from 8-node quadratic shell elements and the joints were named J&C after the two authors. The models developed for the calibration exercise had values of $\beta = 1$ and $\beta = 2$ and where compared with J&C 2T and J&C 3T which are corresponding joints with a similar β value. Results obtained from the calibration are shown in Fig. 57.

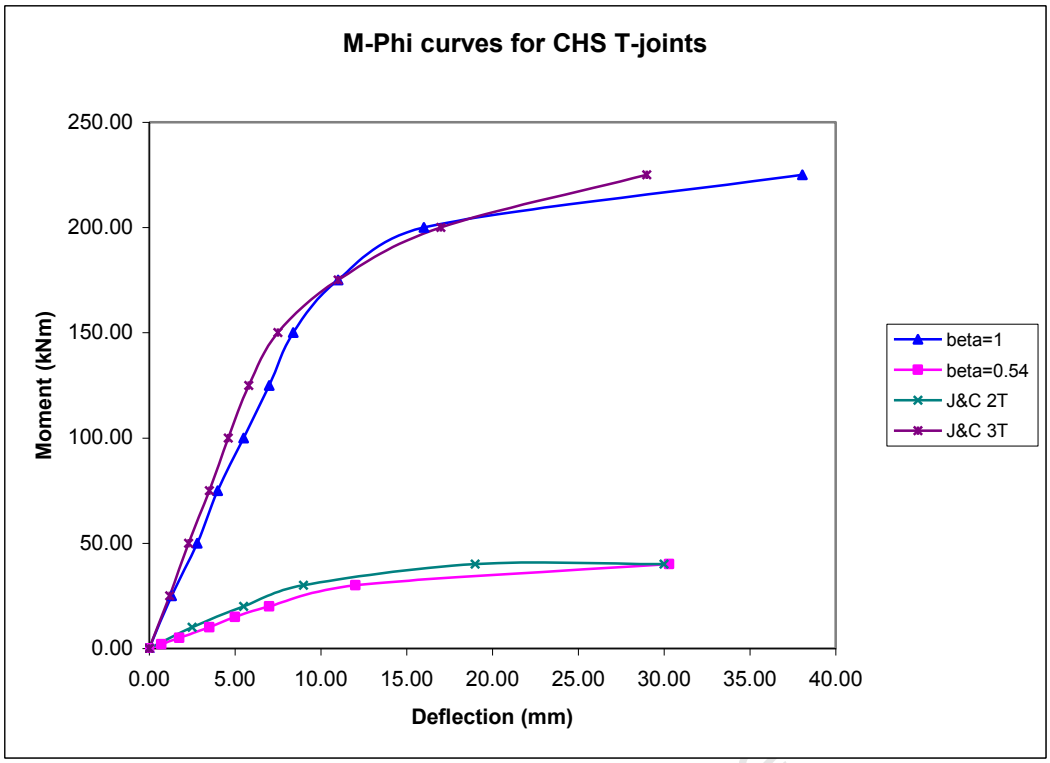

Fig. 57 Calibration against results obtained by Jubran & Cofer (1995) for CHS T-joints

The results obtained show close correlation hence the model was deemed accurate enough. In the parametric analyses that followed the parameters β and τ where varied for the different models and the effect of this observed in the numerical results.

5.5 Parametric Study

A parametric study was carried out for CHS T-joints in order to study their moment-rotation behaviour. The geometric parameters of the joints used in the study are given in Table 12 (2).

Table 12: Table of joint properties employed in the FE study

1. CHS Calibration		**Joint Parameters**						
Label	***β***	***γ***	***τ***	***α***	l_o	l_1	d_o	***Section Class***
T38C	0.5	15.24	1	9.45	360	154.2	76.2	1
T50C	0.66	15.24	1	9.45	360	218	76.2	1
T76C	1	15.24	1	9.45	360	195	76.2	1
2. Parametric Study		**Joint Parameters**						
Label	***β***	***γ***	***τ***	***α***	l_o	l_1	d_o	***Section Class***
(a) T100C	0.22	20.3	1	20	$10d_o$	$4d_1$	101.6	1
T127C	0.22	25.4	1	20	$10d_o$	$4d_1$	127.0	1
T154C	0.22	30.5	1	20	$10d_o$	$4d_1$	152.4	1
(b) T100C	1	20.3	1	20	$10d_o$	$3.5d_1$	101.6	2
T127C	1	25.4	1	20	$10d_o$	$3.5d_1$	127.0	3
T154C	1	30.5	1	20	$10d_o$	$3.5d_1$	152.4	3
(c) T100C	1	10.16	1	20	$10d_o$	$3.5d_1$	101.6	1
T127C	1	12.7	1	20	$10d_o$	$3.5d_1$	127.0	1
T154C	1	15.24	1	20	$10d_o$	$3.5d_1$	152.4	1
(d) T100C	1	8.47	0.833	20	$10d_o$	$3.5d_1$	101.6	1
T127C	1	10.58	0.833	20	$10d_o$	$3.5d_1$	127.0	1
T154C	1	12.70	0.833	20	$10d_o$	$3.5d_1$	152.4	1
(e) T100C	1	10.16	1.2	20	$10d_o$	$3.5d_1$	101.6	1
T127C	1	12.7	1.2	20	$10d_o$	$3.5d_1$	127.0	1
T154C	1	15.24	1.2	20	$10d_o$	$3.5d_1$	152.4	1

The shell model employing S4R elements was used for all the CHS T-joints in the parametric study. An attempt was made to restrict the section class of the specimens to Class 1 and 2 sections as these are considered able to achieve the full plastic moment; a parameter that is essential in the joint classification. The only exception is the joints in 2(b) which were kept that way in order to have a like-for-like comparison with joints in 2(a).

For the joints in 2(a) and 2(b) the value of β was different in order to confirm the effect that would have on the joint. For 2 (c), (d) and (e) the β value was kept constant but the thickness of the members were varied in different combinations. This approach was taken because much has been reported on the effects of β values to joint performance as opposed to effects of member thickness. The member thickness as well as value of τ was therefore varied in order to determine its effect on the joint performance. It must be noted that though the value of τ is the same in 2(b) and 2(c) the joints in the latter have a thickness of 5mm while those in the former have a thickness of 2.5mm. In 2(d) and (c) the thickness of the brace and chord are increased to 6mm respectively with the other connected member being 5mm in thickness.

Moment-rotation plots from the parametric study are presented in Fig. 58 to Fig. 62. Design tables derived from the results of the parametric study are presented in chapter 5.5.2.

5.5.1 Moment-Rotation plots from parametric study

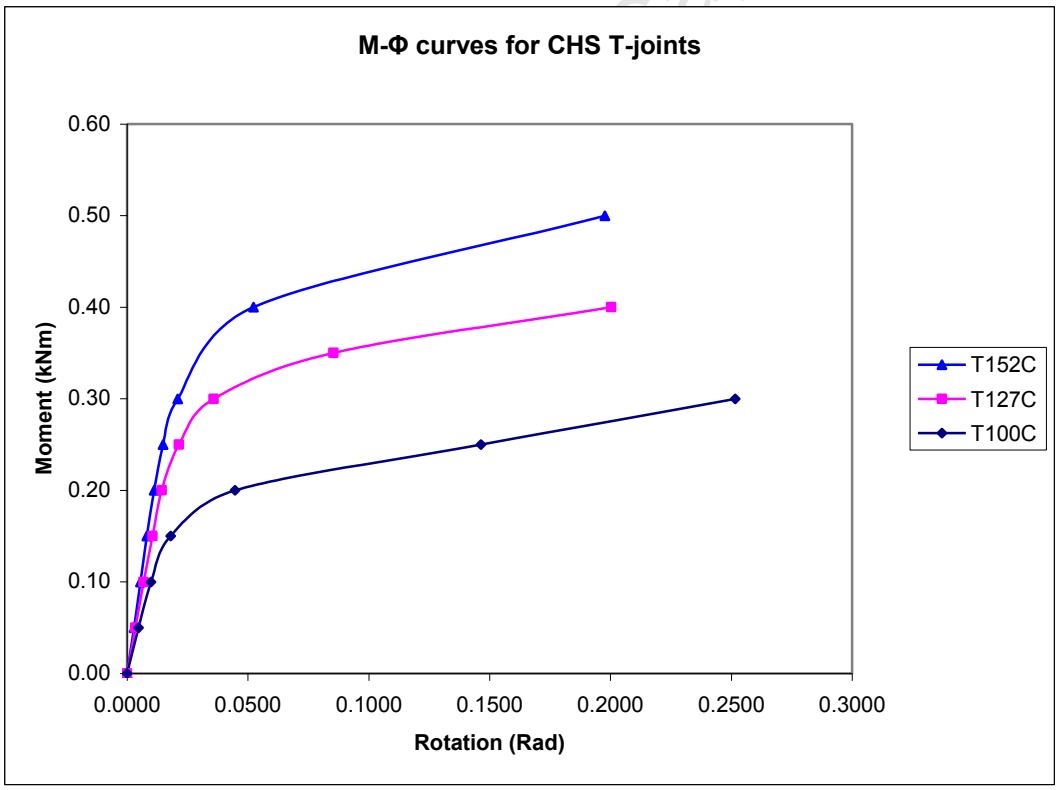

Fig. 58 M-Φ plots from finite element analysis for CHS T-joints with β =0.22 and τ =1

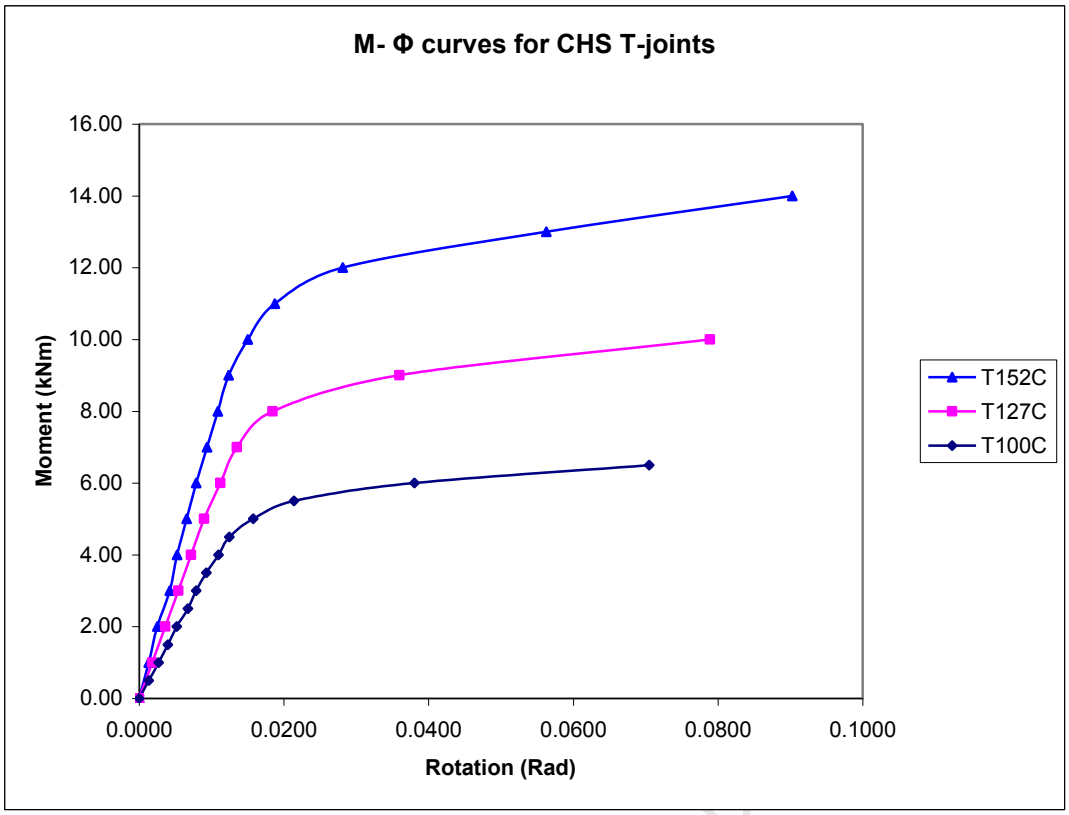

Fig. 59 M-Φ plots from finite element analysis for CHS T-joints with β =1 and τ =1

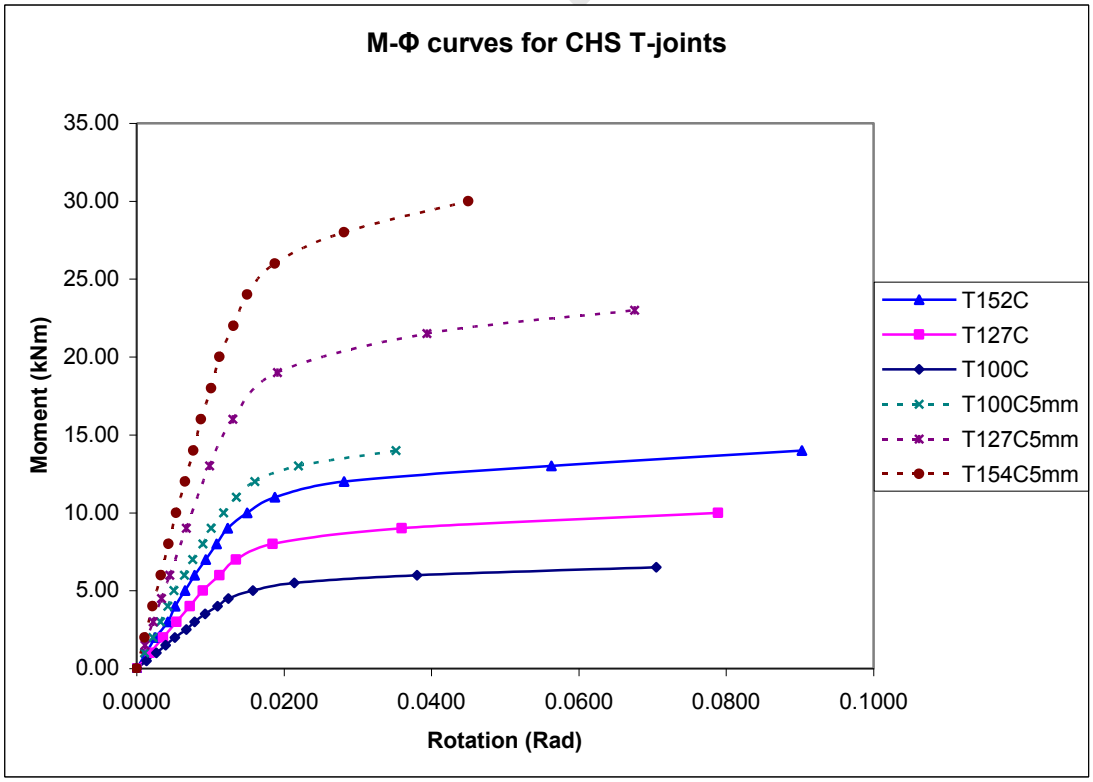

Fig. 60 M-Φ plots for comparison between 2.5mm and 5mm CHS T-joints with β=1 and τ=1

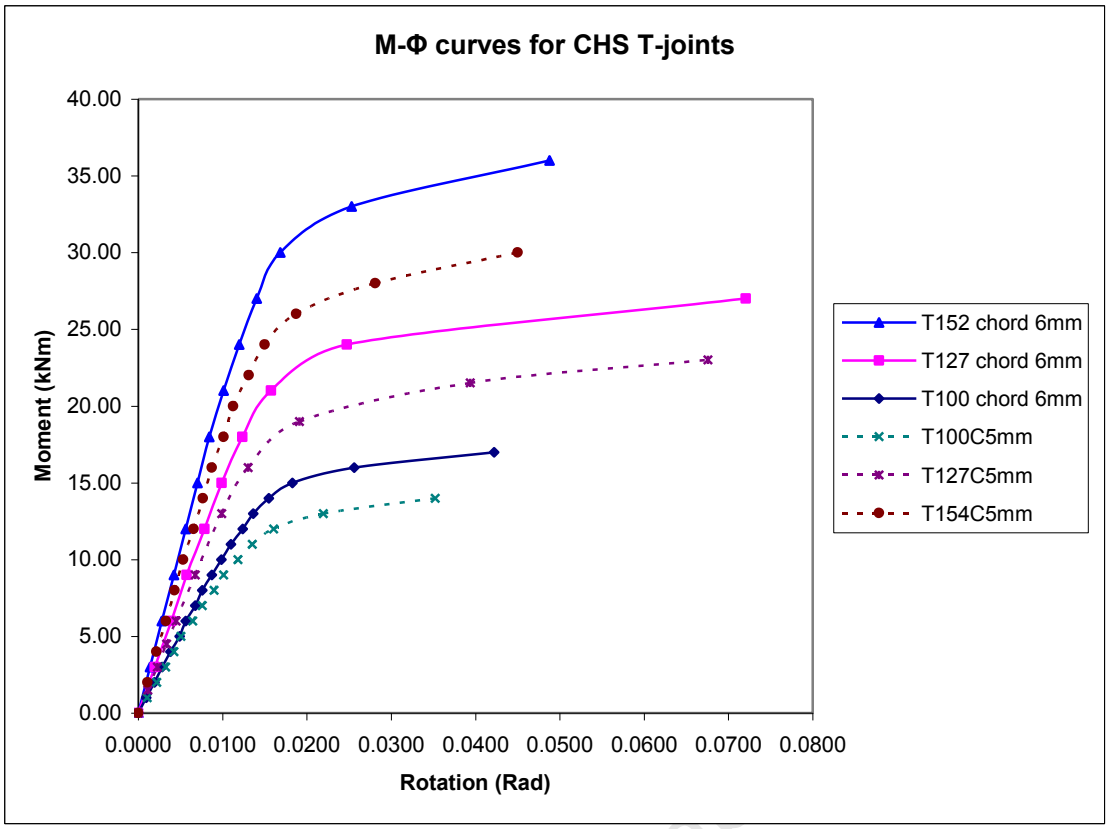

Fig. 61 M-Φ plots for comparison for 5mm CHS T-joints between τ =1and τ =0.833

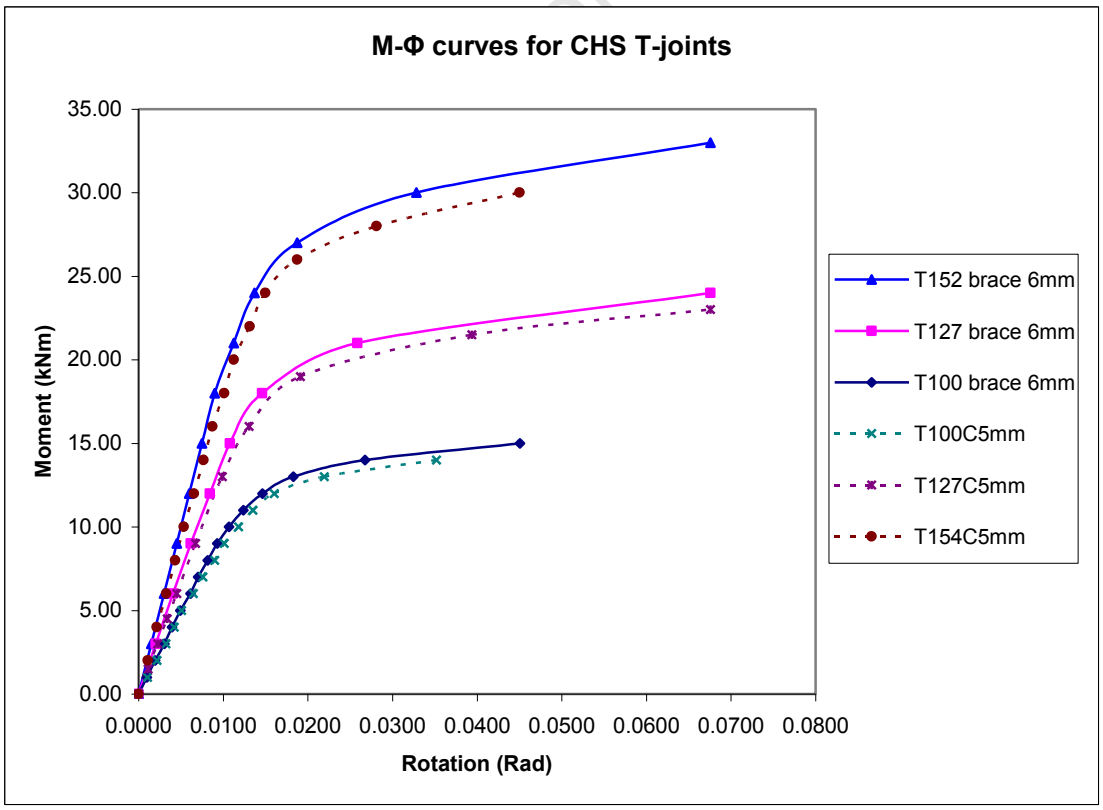

Fig. 62 M-Φ plots for comparison of 5mm CHS T-joints between τ =1and τ =1.2

The M-Φ plots obtained form the parametric analysis where all generally smooth plots, showing a well defined linear part from which the initial stiffness could be obtained, as well as a non-linear part with a distinct ultimate moment. The ultimate moment was typically characterized by convergence difficulty in FE solution due to the strains in the model exceeding fifty times that at initial yield.

5.5.2 Design Tables

The results obtained from the parametric study were used to develop design tables with information that a designer can use to undertake semi-rigid joint design or indeed to determine which joints can be used in semi-rigid design. The main parameters of initial joint stiffness, joint classification according to the Bjorhovde approach and ultimate moment are given in the design table. The design tables are presented in Tables 13 - 18.

Table 13: Design table 1 based on calibration in Table 12 (1)

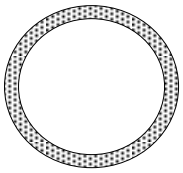			**CHS** $\tau = 1$		
Chord/Main Member (mm)	**Initial Stiffness ($S_{j,ini}$), kNm/Rad**	**β**	**Stiffness**	**Strength**	**M_{ult} kNm**
76.2 x 2.5	17	0.50	Pinned	Partial strength	0.75
76.2 x 2.5	78.9	0.66	Semi-rigid	Full strength	1.42
76.2 x 2.5	292.6	1	Semi-rigid	Full strength	3.70

Table 14: Design table 2 based on Table 12 (2(a))

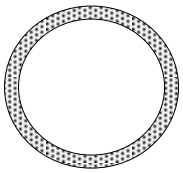		**CHS** *β = 0.22, τ = 1*		
Chord/Main Member (mm)	**Initial Stiffness ($S_{j,ini}$), kNm/Rad**	**Stiffness**	**Strength**	**M_{ult} kNm**
101.6 x 2.5	10.2	Semi-rigid	Full strength	0.25
127 x 2.5	14.3	Semi-rigid	Partial strength	0.38
152.4 x 2.5	17.9	Semi-rigid	Partial strength	0.48

Table 15: Design table 3 based on Table 12 (2(b))

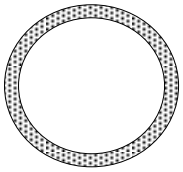		**CHS** *β = 1, τ = 1*		
Chord/Main Member (mm)	**Initial Stiffness ($S_{j,ini}$), kNm/Rad**	**Stiffness**	**Strength**	**M_{ult} kNm**
101.6 x 2.5	363.64	Semi-rigid	Full strength	6.5
127 x 2.5	535.71	Semi-rigid	Full strength	10
152.4 x 2.5	733.94	Semi-rigid	Full strength	14

Table 16: Design table 4 based on Table 12 (2(c))

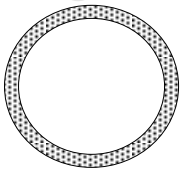		**CHS** *β = 1, τ = 1*		
Chord/Main Member (mm)	**Initial Stiffness ($S_{j,ini}$), kNm/Rad**	**Stiffness**	**Strength**	**M_{ult} kNm**
101.6 x 5	888.89	Semi-rigid	Full strength	14
127 x 5	1343.30	Semi-rigid	Full strength	23
152.4 x 5	1818.20	Semi-rigid	Full strength	30

Table 17: Design table 5 based on Table 12 (2(d))

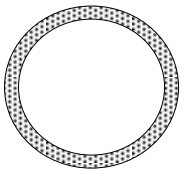		**CHS** $\beta = 1, \tau = 0.833$		
Chord/Main Member (mm)	**Initial Stiffness ($S_{j,ini}$), kNm/Rad**	**Stiffness**	**Strength**	**M_{ult} kNm**
101.6 x 5	1034.5	Semi-rigid	Full strength	17
127 x 5	1519.0	Semi-rigid	Full strength	27
152.4 x 5	2142.9	Semi-rigid	Full strength	36

Table 18: Design table 6 based on Table 12 (2(e))

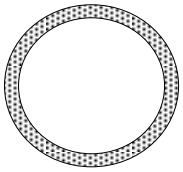		**CHS** $\beta = 1, \tau = 1.2$		
Chord/Main Member (mm)	**Initial Stiffness ($S_{j,ini}$), kNm/Rad**	**Stiffness**	**Strength**	**M_{ult} kNm**
101.6 x 5	1000.0	Semi-rigid	Full strength	15
127 x 5	1428.6	Semi-rigid	Full strength	24
152.4 x 5	2000.0	Semi-rigid	Full strength	33

The design tables summarize the important joint parameters of initial joint stiffness, joint classification and ultimate moment for each joint combination. As can be seen the pinned joint is associated with low values of initial stiffness and ultimate moment, and it can be seen that this occurs at a β value of less than 1 (Table 12). The rest of the joints all fell into the class of semi-rigid joints and show a wide range of values for both initial stiffness and ultimate moment.

Chord thickness appears to have a greater effect on joint performance than does brace thickness. In comparing 2(d) and 2(e) it was noticed that an increase in chord thickness gave a stiffer and stronger joint than the case of a similar increase in thickness of the brace

member only. A design guide would essentially have lots of these tables in various combinations of member sizes, β, and τ.

5.6 Conclusion

Although there is an endless number of possibilities for combinations of β and τ design tables for the most preferable sections or combination of sections can be drawn and used for the purpose of design. A procedure for the development of these design charts from a parametric study has been shown. It has also been shown that not only does the ratio of connecting members have an effect on the joint performance, the joint thicknesses of the connected members also do. Although previous research has clearly shown the effect of β on joint performance the current research has also shown how sensitive the joint performance can be to changes in thickness of the connected members.

The failure mode observed in the experimental tests of weld failure could not be reproduced or observed in the FE models. This is because the approach taken in the model generation and analysis does not account for development of cracks in the joint. A more rigorous and complex model generation procedure is required for that. The excessive deflection at failure could however be observed from the FE models as was seen with the experimental test results.

REFERENCES

Hibbit, Karlsson & Soresen Inc. (HKS). (2004). ABAQUS, version 6.5-1.

Jubran, S.J. Cofer, W.F. 1995. Finite-Element Modeling of Tubular Joints. I: Numerical Results. *Journal of Structural Engineering*. **121** (3), pp. 496-508.

Qian,X.,D. Choo, Y.S. Liew, J.Y.R. 2007. Static strength of thick-walled CHS X-joints subjected to brace moment loadings. *Journal of Structural Engineering*. **133** (9), pp. 1278-1287.

6 DISCUSSION

6.1 Introduction

Results from the experimental work have been presented in Chapter 4 and those from the finite element analysis have been presented in Chapter 5. Although the models developed for the finite element analysis have been calibrated such that they model as close as possible what was obtained from the experimental tests it is clear that the FE models did not produce a spot on correlation. This could be attributed to several factors such as the fact that welds were not modelled in the FE model and there could have been some slight inaccuracies in the experimental tests as the number of tests carried out also represents only a small sample. Confidence in the CHS model developed was gained by the close correlation to the results of Jubran & coffer (1995). The M-Φ relationships obtained from the shell model show smooth plots from which the initial stiffness and ultimate moments were easily obtained. The two sets or results are further discussed in 6.2 and 6.3.

6.2 Experimental results

The two predominant failure modes observed in the experimental results were local buckling failure in the chord as well as weld failure at the joints. Generally larger rotations in the joints were obtained with the lower β values; suggesting that as a joint moves from rigid to pinned the rotations at the joint increase. This observed trend is expected as it is supported from theory and the literature. As observed from results presented in Table 9 most of the joints exhibit semi-rigid behaviour with only the RHS X76, CHS X76 and CHS X50 exhibiting rigid behaviour. The T38 was the only joint that was observed to show a pinned joint behaviour. A comparison between the RHS and CHS joints shows that RHS joints have a lower initial stiffness at low β value but higher initial stiffness at higher β values than the corresponding CHS joints. However when compared to the birdbeak joints the RHS in all cases shows a higher initial stiffness than the birdbeak joints. This would suggest that the birdbeak joint configuration used in this study has less strength than the corresponding RHS joint.

6.3 Finite Element results

The calibration of FE models against experimental data did not give a perfect correlation though in the case of the CHS model the ultimate moment was predicted accurately. It was therefore decided to use the CHS model in the parametric analysis. In comparing the joint characteristics for CHS T-joints between those obtained from the experimental and those from the FE analysis it was observed that the T50 and T76 were classified as semi-rigid, full-strength joints in both cases with differences only in the initial stiffness. The T38 joint gave a pinned, partial-strength joint in the FE analysis and semi-rigid, full-strength joint in the experimental test thus highlighting the slight difference in results from the two. In the calibration against results obtained by Jubran and Coffer (1995) both the joint behaviour and ultimate strength showed good correlation.

In the parametric analysis the CHS model good results with smooth M-Φ plots. All the joints in the parametric analysis showed semi-rigid behaviour and were classified as full-strength except for two joints of $\beta = 0.22$ which were classified as partial-strength. The effect of changing the member thickness while keeping β and τ constant was to give a joint with higher initial stiffness and ultimate moment. When the value of τ was varied by changing the chord or brace thickness it was noted that the joint is more sensitive for a change in chord thickness than for a change in brace thickness. For instance looking at the 101.6 x 5mm joint, a 1mm increment in chord thickness gives an initial joint stiffness increment of 16.4% as compared to a 12.5% increment in joint stiffness for a 1mm increment in brace thickness.

6.4 Conclusion

The moment-rotation behaviour of the SHS joints has been presented for both cases of experimental investigation and finite element analysis. The failure modes as observed in the experimental tests have also been reported. As the experimental tests where limited to the geometry of tested specimens only a parametric analysis has been carried out using finite element modeling and this has given an understanding on how the joint behavior is ultimately affected by changes in some geometric parameters. The results have been further used to develop some design tables.

7 CONCLUSION AND RECOMMENDATION

7.1 Introduction

In developing the design tables for the CHS joints a procedure based on sound theory has been developed and has the potential to aid designers in easily carrying out semi-rigid joint design. The only limitation is that that there is an unlimited number of possibilities with regards hollow section type, tube thickness and combination of brace and chord. One approach therefore would be to determine the most prevalent hollow section seizes and preferred size combinations at joints and develop design tables for those cases. A tailor made approach for each project can also be made using the model developed to come up with the required joint parameters for the semi-rigid analysis and design to be carried out..

The design tables presented can be used much in the same way as the design charts presented in Eurocode 3 for the semi-rigid design of open sections. Eurocode looks at different connection types for open sections and presents the designer with the basic information required without having to carry out a cumbersome analytical procedure or having to develop a finite element model. Software has further been developed to go with the Eurocode tables for semi-rigid design of open section joints. The software requires only the selection of members being connected as well as the connection type with corresponding joint properties of initial stiffness and ultimate moment as read from the design table. The same approach can be used for SHS joints. This makes semi-rigid design a less complicated undertaking; something the design community would really appreciate.

7.2 Conclusion

Welded hollow section joints predominantly exhibit semi-rigid joint behaviour. The moment-rotation plots are typically characterized by a linear followed by a non-linear behaviour before ultimate failure. It has been established from the study carried out that the brace to chord ratio (β), member thickness and thickness ratio of brace to chord (τ) all have an effect on the performance of hollow section joints in relation to the moment-rotation behaviour. The effects of varying the member thickness have different sensitivity depending on whether the brace or chord thickness is adjusted. It has also been shown that employing shell elements in

the finite element models gives smooth plots and predicts the joint behaviour fairly accurately.

Although in most joints the plastic behavior was characterized by large rotations as compared to the linear elastic part most of the joints did not reach the Yura deformation limit. This suggests that most of the joints do not exhibit excessive joint rotation. The only exception was with an RHS and a bird beak joint, both having a low β value.

7.3 Recommendations

Whereas the CHS joint model has been successfully developed and calibrated there is need to further develop accurate and reliable FE models for the RHS and Birdbeak joints and further develop design tables for these joint types as well. Further parametric studies can also be done to determine the joint behaviour in cases or scenarios that have not previously been simulated or tested. The development of a model with welds simulated would give a greater understanding to the effect of the welds in the global behaviour of the joint in a FE analysis. It may also give better results for the joint cases where the FE model could not accurately predict the joint behaviour as obtained from the experimental testing.

7.4 Summary

In accordance with the aims of the research, the moment-rotation behaviour of different hollow section joints has been investigated through a process of experimental testing as well as finite element modeling. A parametric study has been carried out on CHS T-joints and the results used to develop design tables based on the Bjorhovde classification scheme. This presents a procedure that can be used to develop design tables for SHS joints particularly for application in semi-rigid design.

Moment-rotation behaviour of bolted tubular steel joints

K. Mudenda, A. Zingoni, A. Masarira
Department of Civil Engineering, University of Cape Town
Rondebosch 7701, Cape Town, South Africa

Keywords: Hollow steel joints, Square hollow section, Moment-rotation behaviour, Joint rotational stiffness, Semi-rigid joints, Joint collapse, Steel structures.

ABSTRACT: A programme of experimental research has been undertaken to investigate the moment-rotation behaviour of hollow joints of tubular steel members, which find application as lightweight construction for large trusses and frames. The initial focus is on structural configurations in which 2-dimensional effects dominate, hence out-of-plane member incidences and torsional effects on joints will be ignored. The joint construction of interest in this study is one in which the primary member at a joint is bolted to one or more secondary members via an extended end plate attached onto the secondary member(s). This construction of joints is intended to minimize the costly operations of welding on site. It is desired to establish the rotational stiffness of the joints within the elastic regime of material behaviour, and also to investigate the collapse behaviour of such joints. The cross joint as well as T configurations have been chosen for study. Parameters of interest are the dimensions of secondary members relative to those of the primary member, and number of bolts. In the paper, we present preliminary results of the experimental tests, augmented with some FEM results of the numerical modeling of the T-joint.

1 INTRODUCTION

Rectangular hollow sections (RHS) have found wide application in plane truss and space-truss structures, as well as concrete-filled columns and beams in steel frame systems. Closed sections offer many advantages in performance as well as aesthetics over the traditional open sections. However, the greatest challenge has been the difficulty of connecting them, as they can only be accessed from one side; the outer surface. Direct connection of members by means of welding has for a long time been the most popular method for joining such sections. However, welding requires a good degree of workmanship in order to obtain reliable joints. When stiffening is required to increase joint strength, fabrication costs are likely to increase further. Site welding usually involves difficulties in quality and cost control, which makes bolting a more attractive alternative for connecting members on site. Steel sub-assemblies can be fabricated in a workshop, transported to site and simply bolted together. Bolting is a less specialised operation than welding; semi-skilled and even unskilled labour can easily and accurately perform the operation on site.

However, the structural mechanics of bolted RHS steel connections is not yet fully understood particularly with regard to moment-rotation behaviour of these joints. Much research on steel joints has focused on beam-column connections involving open sections as well as splice joints subjected to axial loads. With regard to hollow joints, Dutta (2002) considered some joint configurations for square hollow sections (SHS) that have been previously investigated and noted that the two main connection techniques used have been: (i) plates welded to both connected members and bolted; (ii) ‘blind’ bolting, which involves bolting through only one face of the member where the connecting plate sits. The former is costly as it involves a lot of fabrication, while the latter is patented and requires specialised labour and equipment. This paper presents an investigation of a different configuration of bolted SHS joints with particular focus on their moment-rotation characteristics. The bolting method investigated is that of ‘through’ bolting, which involves bolting through both opposing faces of the member and not just through one face. Two possible configurations are shown in Fig.1 (a) and (b). The paper presents the preliminary results on the experimental testing of

such joints, and also presents some results of finite element (FE) modelling of one of the joints. The results obtained from the FE model are compared with the laboratory test results.

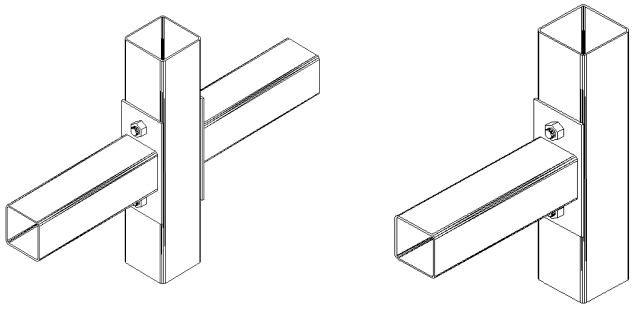

(a) Cross-joint configuration (b) T-joint configuration

Fig.1 Through bolted joint configurations for RHS connections

2 LITERATURE REVIEW

2.1 *Experimental Tests*

Moment-rotation behaviour of joints is essential in the design of structural connections using the semi-rigid approach. This approach recognises the deformation capacity of the joint as well as its load carrying capacity. Therefore moment-rotation behaviour gives a more accurate picture of joint behaviour in a structure when loaded. Experimental tests to determine moment rotation behaviour of bolted RHS connections have been carried out by Wilkinson et al (2000) and Wheeler et al (1997). Wheeler et al (2000) further presents a finite element (FE) model of the moment end plate connections that were investigated in the experimental tests. Wilkinson et al (2000) carried out an investigation into the plastic behaviour of knee joints under both opening and closing moment loading. The knee bolted connection involved welding plates to both connecting members and bolting through the plates. The joint reached a moment greater than the plastic moment; M_p of the RHS connected members. Wheeler et al (1997) studied tubular section end plate connections with eight and four bolts, which can be used as splices as well as beam-column connections. The joints were subjected to pure flexure. Three modes of failure were observed; tensile bolt failure, punching shear in tensile weld zone and excessive plate deformation. Joints with eight bolts were found to be rigid while those with four bolts were found to be semi-rigid. The Bjorhovde et al (1990) method of joint classification was used.

Whereas Wheeler et al (1997) observed that plate thickness and bolt location had more profound effect on joint behaviour than material property, Wilkinson et al (2000) observed that material property plays a profound role in joint behaviour. Lindner (1993) investigated an RHS fish plate connection that employed a 'through' bolting concept in conjunction with spacer tubes welded to the RHS walls to take in the bolts. The joint was found to be expensive and not practicable. It had been tested for axial load cases. Korol et al (1993) studied the moment resistance of a joint incorporating an open section welded onto an end plate and bolted to a RHS column using 'blind' high strength bolting techniques. The joint was found to have promising potential in structural applications.

2.2 *Finite element models*

Finite element models are a convenient method of carrying out large scale parametric analyses that would prove otherwise expensive with experimental testing. The FE models need only be calibrated by reliable test results. Lee (1999) presents a summary of different finite element modeling techniques and approaches used to model offshore tubular joints. The modeling of bolted connections is a very complex task and many researches have attempted to come up with accurate models of bolted joint behavior. Also in the recent past, software manufacturers have developed elements that are more adept at simulating the complex contact simulations and non-linear behavior associated with bolted connections. Krishnamurthy and Graddy (1976) are considered by many to have pioneered research into the modeling of bolted connections. Wheeler et al (2000) carried out modeling for a four-bolt moment end plate connection using the ABAQUS (HKS 2002) finite element package and employing linear elements. Results were compared to test data they had previously obtained (Wheeler et al, 1997). The two results compared well and it was concluded that the model could be used for a parametric study. Razavi et al (2007) developed an inelastic bolt model concept for bolt modeling. The model makes use of algorithms which save computing time by eliminating the need to model a real bolt. It was found to accurately predict behavior of bolted connections.

3 SPECIMEN CONFIGURATION AND PREPARATION

Experimental testing was carried out to determine the rotational stiffness of the cross-joint configuration, henceforth referred to as the X-joint, as well as the T-joint. A total of 14 specimens were assembled and tested in order to determine the moment-rotation behaviour of the joints.

A tensile test was first carried out on flat strips of the RHS members, as well as the gusset plate, to determine the strength properties of the material. A 200kN capacity Zwick machine was used. The maximum elongation as well as yield strength and ultimate strength obtained are shown in Table 1.

Table 1 material property of the joint components

Component	$\sigma_{0.2\ (MPa)}$	$\sigma_{u\ (MPa)}$	Elongation
Gusset plate	283	385	49%
RHS plate	338	370	33%

A gusset plate was then perpendicularly welded onto one end of each secondary member. The X-joint assembly was achieved when two plate-bearing ends of secondary members where placed against opposite faces of the primary member and secured together through bolts (Fig. 1(a)). In the case of the T-joint, the joint assembly is achieved by fixing only one plate-bearing end onto the primary member and securing with through bolts (Fig. 1(b)). The number of bolts on either side of the secondary member was varied to study its effect. The cross-sectional dimensions of the primary member were kept constant at 76.2mm x 76.2mm square and 2.5mm thickness; the specimens being of constant length 360mm. Joint specimens were assembled with different sizes of secondary members, the combinations being indicated in Table 2. The specimen label starts with the joint configuration, followed by the nominal size of the secondary member and the number of bolts used to hold the end plate on either side of the secondary member.

Table 2 Test specimen dimensions (secondary members)

Specimen Label	Secondary Member Size (mm)	Length of secondary member (mm)
X76-1, T76-1 X76-2, T76-2	76.2 x 76.2 x 2.5	305
X65-1, T65-1 X65-2, X65-3,	63.5 x 63.5 x 2.5	229
X38-1, T38-1 X38-2, T38-2 X38-3, T38-3	38.1 x 38.1 x 2.5	152

Fabrication details were as follows: The RHS members as well as plates were first cut to required sizes. The main member as well as extended plates was drilled with 14mm diameter holes at the appropriate locations to take in the M12 bolts. The secondary members were then welded onto the plate by a 5mm fillet weld using metal inert gas (MIG) welding. The plates employed were of varying dimensions to accommodate the different size RHS members. A general guideline for the spacing of the holes from the welds and edges was adapted from Dutta (2002).

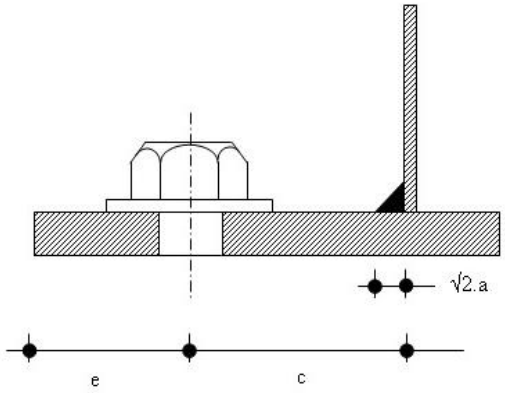

Fig.2 Convention for bolt hole location

The parameter c was calculated using (1) Dutta (2002):

$$c = \sqrt{2}.a + \frac{\Theta N}{2} - t \quad (1)$$

Where,
c = distance of bolt hole centre from weld
a = weld thickness
ΘN = outer diameter of socket wrench
t = thickness of supporting disk
e = end distance

The distance c was calculated as approximately 20mm and bolt spacing where applicable, was taken as 30mm. An end distance of 30mm was used. Plates of width 100mm were used to accommodate the 76.2mm RHS members while 76.2mm wide plates were used to accommodate the 63.5mm and 38.1mm members, giving a flush contact interface between the plate and the primary member.

The X-joint specimens were tested in an Amsler hydraulic loading machine. The loading on the secondary member was applied through two steel members equidistant from the centre of the connection. The T-joints were tested in a Denison loading machine. Deflections were measured using dial gauges.

4 EXPERIMENTAL RESULTS

Moment-rotation (M-Φ) curves obtained from the experimental testing are shown in Fig.3 to Fig.7. The predominant failure mode was excessive deformation of the gusset plate as well as weld failure on the tension side corners of the hollow section profile. The failure mode of the T-joint is shown in Fig.8. The T65-1 joint was tested to generate data for comparison with the FE model.

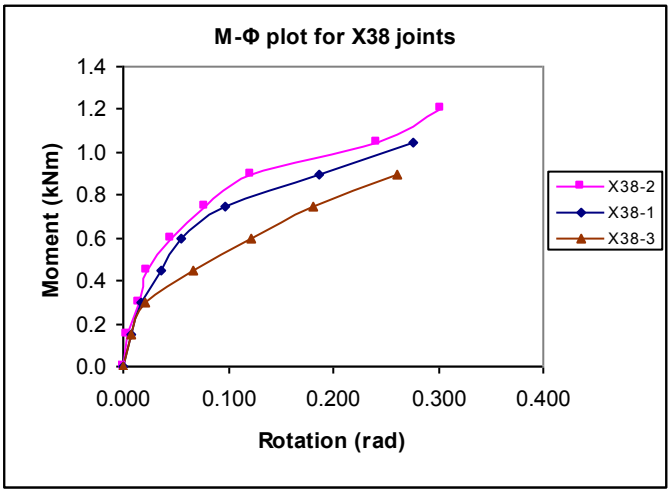

Fig.3 Moment rotation curves for X38 joints

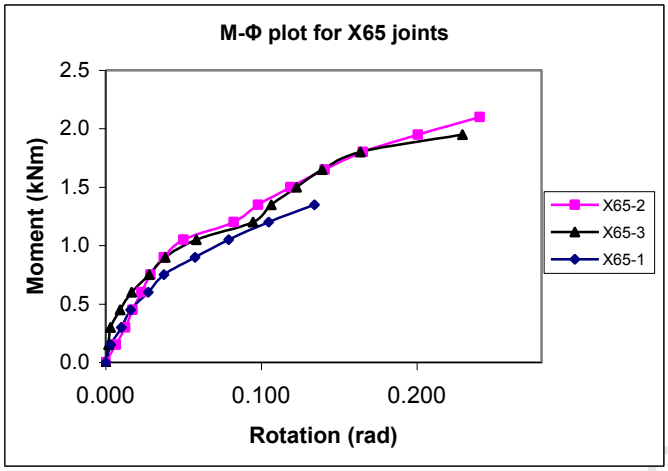

Fig.4 Moment-rotation curves for X65 joints

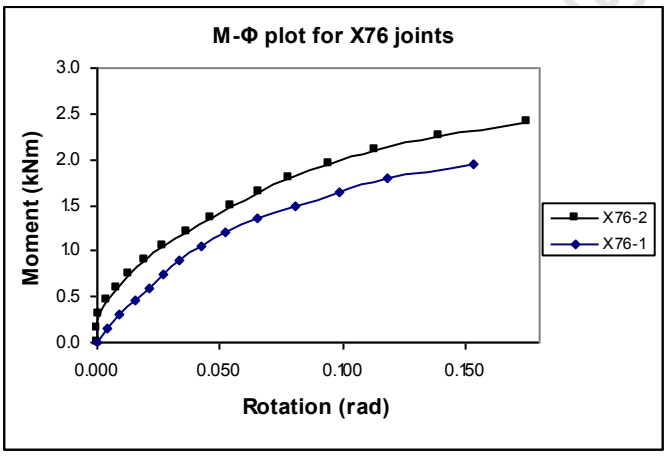

Fig.5 Moment-rotation curves for X76 joints

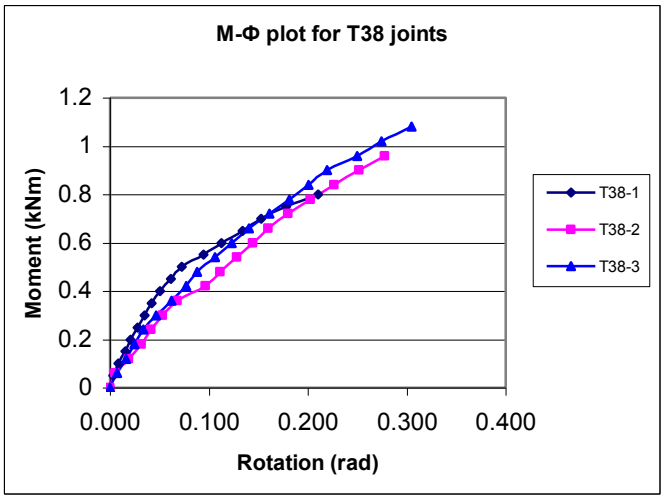

Fig.6 Moment-rotation curves for T38 joints

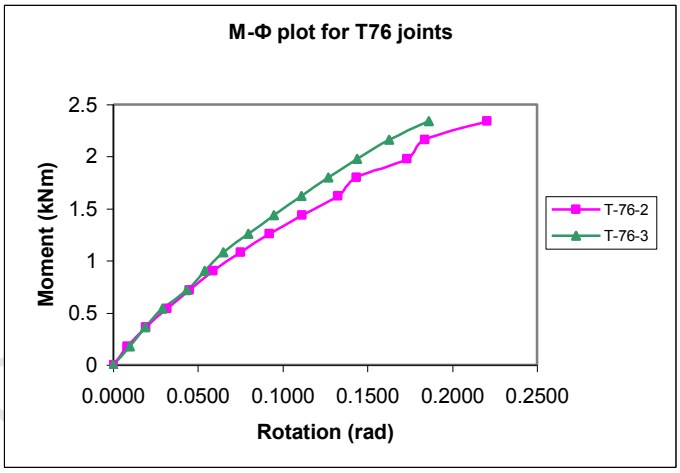

Fig.7 Moment-rotation curves for T76 joints

The X38-3 joint appears to have failed prematurely. This may be attributed to loss of the initial bolt pre-stress in one or more bolts.

Fig.8 Failure mode of the T-joint

5 FINITE ELEMENT ANALYSIS

The finite element (FE) model was generated using the commercially available ABAQUS (HKS 2002) software package. 3D geometrically nonlinear analysis was employed. As there are multiple contact interactions within the model, complex contact simulation was carried out with the aid of a step procedure. Linear 8 node elements with reduced integration (C3D8R) were employed. Welds were not modelled. Material property was incorporated for the nonlinear analysis using a plot of true stress and logarithmetic plastic strain. The FE model for a T-joint is shown in Fig.7 below. Only half of the joint was modelled in the analysis due to symmetry.

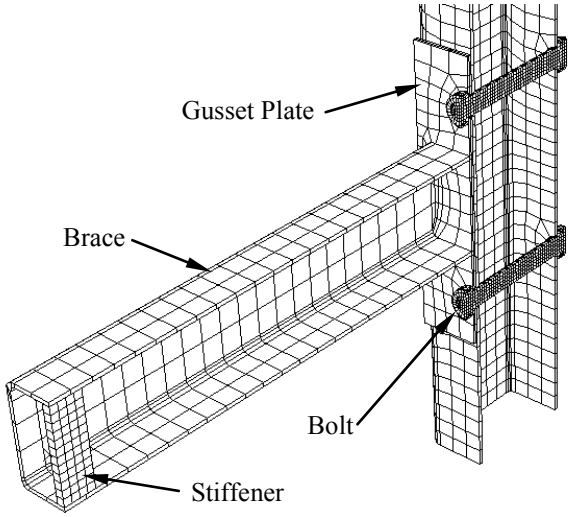

Fig.7 T-Joint model

As observed with the experimental tests failure is associated with excessive deflection of the extended plate.

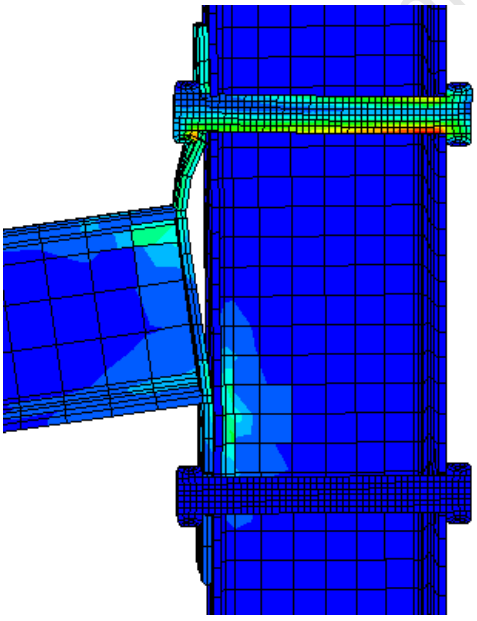

Fig.9 Failure mode of the T-joint from the FE analysis

The model showed high stresses at the tension side corners of the hollow section-plate connection which would explain the weld failure observed in the experimental tests. The failure mode from the FE model compares well with that observed from the experimental tests. However, the FE model gives a higher initial stiffness than that obtained from the experimental tests. A comparison for the T65-1 joint is given in Fig.10

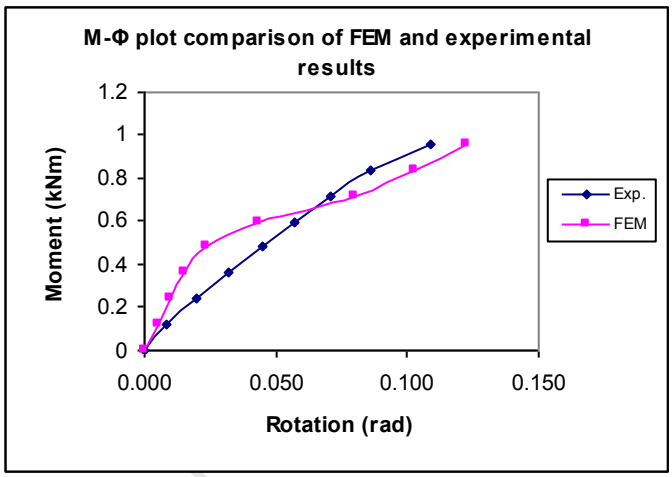

Fig.10 Comparison of FEM and experimental test results for the T65-1 joint

6 DISCUSSION

For the X38 and X65 joints the initial stiffness appears to be in the same range suggesting that the number of bolts used has a marginal effect on the overall behaviour of the joint. However for the X76 joint the number of bolts appears to have considerable effect on both the stiffness as well as moment capacity of the joint.

A comparison of the initial joint stiffness as well as moment corresponding to the Yura deformation limit given by (2) is shown in Table 3.

$$\frac{80\,fy}{E} \qquad (2)$$

The moment capacity as determined from (2) is seen to increase with increase in the size of the secondary member. Therefore as the ratio of secondary to primary tends to unity there is an increase in joint strength.

Table 3. Comparison of specimen joint properties

Specimen Label	Initial Stiffness (KNm/rad)	Moment capacity (KNm) at Yura limit
X38-1	16	0.79
X65-1	25	1.25
X76-1	30	1.95

7 CONCLUSION AND RECOMMENDATIONS

A bolted connection for square hollow sections has been studied and its moment rotation behaviour determined through an experimental testing program on the X- and T-joint configurations. The secondary member size was varied and the effect of the number of bolts employed for the joints was determined. Experimental results are presented and discussed.

A 3D finite element model was developed using the ABAQUS finite element package and was able to simulate the complex contact interactions of the joint. However, the model gives a slightly higher initial stiffness than what was obtained from the experimental tests.

The joint offers an alternative to site welded joints for tubular members. Since not much research has been reported in the area of bolted end plate joints for tubular joints, more research needs to be carried out and design guidelines developed. Research into other joint configurations is also required. Though the finite element model correctly simulates the failure mode it needs to be refined in order to come up with a model that gives very close correlation with experimental results. This can then be used for large scale parametric studies that save on costs associated with experimental testing.

REFERENCES

Bjorhovde, R., Brozzetti, J., Colson, A., 1990. A classification system for beam to column connections. *Journal of Structural Engineering,* 116 (11): 3059-3076

Dutta, D., 2002. *Structures with Hollow Sections.* Berlin: Ernst & Sohn Verlag für Architektur und technische Wissenschaften GmbH.

HKS. 2002. *ABAQUS Theory manual*, Version 6.3, Hibbit, Karlsson and Sorensen Inc., USA.

Korol, R.M., Ghobarah, A., Mourad, S., 1993. Blind Bolting W-Shape to HSS Columns. *Journal of Structural Engineering*, 119 (12): 3463-3481

Krishnamurthy, N., Graddy, D., 1976. Correlation between 2- and 3- dimensional finite element analysis of steel bolted end-plate connections. *Computers and Structures*, 6: 381-389

Lee, M.M.K., 1999. Strength, stress and fracture analyses of offshore tubular joints using finite elements. *Journal of Constructional steel Research*, 51: 265-286

Linder, J., 1993. Bolted connections to hollow sections with through bolts. *Proceedings of the fifth international symposium on tubular structures,* Nottingham, United Kingdom, E & FN Spon, London

Razavi, H., Abolmaali, A., Ghassemieh, M., 2006. Invisible elastic bolt model concept for finite element analysis of bolted connections. *Journal of Constructional Steel Research*, 63: 647-657

Wheeler, A.T., Clarke, M.J., Hancock, G.J., 1997. Bending tests of bolted end plate connections in cold formed rectangular hollow sections. *Research Report r736, The University of Sydney.* [Online]. Available from: http://www.civil.usyd.edu.au/publications/r736.pdf.[Cited 6th February 2007]

Wheeler, A.T., Clarke, M.J., Hancock, G.J., 2000. FE modelling of four-bolt, tubular moment end-plate connections. *Journal of structural Engineering*, 126 (7): 816-822

Wilkinson, T., Hancock, G.J., 2000. Tests to examine plastic behaviour of knee joints in cold-formed RHS. *Journal of Structural Engineering*, 126 (3): 297-305